575

Benchmark Systems for Network Integration of Renewable and Distributed Energy Resources

Task Force C6.04

April 2014

Benchmark Systems for Network Integration of Renewable and Distributed Energy Resources

Task Force
C6.04.02

Members

Kai Strunz (DE) – (Convener), Ehsan Abbasi (DE), Chad Abbey (CA), Christophe Andrieu (FR), Udaya Annakkage (CA), Stefano Barsali (IT), Ryan C. Campbell (US), Robert Fletcher (US), Feng Gao (CN), Trevor Gaunt (ZA), Ani Gole (CA), Nikos Hatziargyriou (GR), Reza Iravani (CA), Géza Joos (CA), Hiroo Konishi (JP), Maren Kuschke (DE), Erkki Lakervi (FI), Chen-Ching Liu (US), Jean Mahseredjian (CA), Farid Mosallat (CA), Dharshana Muthumuni (CA), Antje Orths (DK), Stavros Papathanassiou (GR), Krzysztof Rudion (DE), Zbigniew Styczynski (DE), Suresh C. Verma (JP)

ISBN: 978-285-873-270-8:

Contents

List of Figures

List of Tables

Nomenclature

Variables

a	Distance in transmission line or cable geometry
B'_{ph}	Susceptance per phase per unit length
B'_0	Zero sequence susceptance per unit length
b	Distance in transmission line or cable geometry
C	Capacitance
C_0	Zero sequence capacitance
c	Distance in transmission line or cable geometry
CF	Coincidence Factor
D_{e}	Equivalent distance between overhead conductors and their fictitious earth return conductors
$D_{\text{n}i\text{p}i}$	Distance between concentric neutrals of one conductor and adjacent phase conductor
$D_{\text{p}i\text{n}i}$	Distance between the phase conductor and its own tape shield or its own concentric neutrals
D_{AB}	Distance between conductors of phases A and B
$D_{\text{BA}'}$	Distance between conductors of phase B and the image of phase A
d	Distance in transmission line or cable geometry
d_{c}	Diameter of conductor
d_{ns}	Diameter of natural strands
d_{ov}	Overall diameter of cable, including insulation, shield, and jacket
E	Voltage
e	Distance in transmission line or cable geometry
f	Frequency
$f_{\text{full load}}$	Full load frequency
$f_{\text{no load}}$	No load frequency
GMD	Geometric mean distance
GMD_{pn}	GMD between phase conductor and neutral
GMD_{pp}	GMD between phase conductors
GMR	Geometric mean radius
GMR_{bundle}	Effective geometric mean radius of a bundle
GMR_{ns}	Geometric mean radius of neutral strand

g	Distance in transmission line or cable geometry
H	Normalized generator inertia constant
I	Current
I_{base}	Base current
I_{DC}	DC current
I_{inv}	Inverter output current
I_{max}	Maximum current
I_{th}	Threshold current
i_{d}	Direct component of current
i_{q}	Quadrature component of current
K_{SD}	Speed droop feedback gain
K_{i}	Integral gain
k	Number of neutral strands
L	Inductance
L_{G}	Inductance of grid equivalent
L_0	Zero sequence inductance
l	Line length
$\dot{m}_{\text{H}}$	Mass flow to hydrogen infrastructure
N_{ld}	Number of loads in a subnetwork
P	Active power
P_{EL}	Input active power of electrolyser
P_{ES}	Output active power of storage
P_{eq}	Equivalent active power
P_{FC}	Output active power of fuel cell
P_{G}	Active power to electricity infrastructure
P_{ii}	Element *ii* of potential coefficient matrix
P_{ij}	Element *ij* of potential coefficient matrix
P_{max}	Maximum active power
P_{out}	Output active power
P_{S}	Output active power of substation
P_{SMES}	Output active power of SMES
P_{MES}	Input active power to multiple energy storage

P_{W}	Output active power of generator-side converter of WECS
pf	Power factor
pf_{eq}	Equivalent power factor
pf_k	Power factor of individual load
Q	Reactive power
Q_{eq}	Equivalent reactive power
Q_{max}	Maximum reactive power
Q_{out}	Output reactive power
Q_{W}	Output reactive power of generator-side converter of WECS
R_{G}	Resistance of grid equivalent
R_{tr}	Transformer resistance
R'	Resistance of conductor per unit length
R'_{ac}	AC resistance per unit length
R'_{dc}	DC resistance per unit length
R'_{earth}	Mutual resistance due to image conductance in the earth per unit length
R'_i	Resistance of individual conductor per unit length
R'_{n}	Equivalent resistance of concentric neutrals per unit length
R'_{ph}	Resistance per phase per unit length
R'_{ns}	Resistance of single neutral strand per unit length
R'_0	Zero sequence resistance per unit length
S	Apparent power
S_{base}	Base value of apparent power
S_{CF}	Apparent power according to coincidence factor
S_k	Apparent power of individual load
S_{rated}	Rated apparent power
S_{SC}	Short circuit apparent power
T'_{d0}	Transient open-circuit time constant, direct component
T''_{d0}	Sub-transient open-circuit time constant, direct component
T''_{q0}	Sub-transient open-circuit time constant, quadrature component
t_{i}	Thickness of insulation
t_{j}	Thickness of outer jacket
t_{ts}	Thickness of tape shield

V_{base}	Base voltage
V_{DC}	DC voltage
V_{d}	Direct component of voltage
$V_{d,cc}$	Direct component of current control voltage
$V_{ES\text{-}a,b,c}$	Phase voltages of energy storage system
V_{G}	Voltage of grid equivalent
V_{q}	Quadrature component of voltage
$V_{q,cc}$	Quadrature component of current control voltage
V_{ref}	Reference voltage
V_{1}	Rated voltage of transformer primary
V_{2}	Rated voltage of transformer secondary
W_{ES}	Energy stored in energy storage system
W_{H}	Energy stored in hydrogen tank
W_{SMES}	Energy stored in SMES
X_{d}	Generator synchronous reactance, direct component
X_{q}	Generator synchronous reactance, quadrature component
X_{tr}	Transformer leakage reactance
X'_{d}	Generator transient reactance, direct component
X'_{ph}	Inductive reactance per phase per unit length
X'_{q}	Generator transient reactance, quadrature component
X'_{0}	Zero sequence reactance per unit length
X''_{d}	Generator sub-transient reactance, direct component
X''_{q}	Generator sub-transient reactance, quadrature component
x	Line length
Z_{base}	Base impedance
Z_{G}	Line impedance of grid equivalent
Z_{gnd}	Ground impedance
Z_{pole}	Grounding impedance of pole
Z_{tr}	Transformer impedance
Z_{tx}	Grounding impedance of transformer
Z'_{ii}	Self-impedance of conductor i per unit length
Z'_{ij}	Mutual impedance between conductors i and j per unit length

Z'_{m}	Mutual impedance of line per unit length
Z'_{s}	Self-impedance of line per unit length
Z'_{00}	Zero sequence impedance of line per unit length
Z'_{11}	Positive sequence impedance of line per unit length
Δ	Difference operator
α_{l}	Temperature coefficient of resistance at TC_{l}
δ	Damping coefficient
θ	Phase angle provided by PLL
ϑ	Temperature of conductor
φ_{E}	Phase angle of voltage E
φ_{V}	Phase angle of voltage V
ω_{ref}	Reference angular frequency
ω_{s}	Angular frequency of system

Acronyms, Abbreviations, Constants, and Units

AAC	All Aluminum Conductor
ABC to dq	Park Transformation
Al	Aluminum
AC	Alternating Current
ACSR	Aluminum Conductor Steel Reinforced
AGC	Automatic Generation Control
AWG	American Wire Gauge
A1	Aluminum, hard-drawn (per IEC standard)
A1/S1A	Aluminum, hard-drawn with Steel, regular strength (per IEC standard)
cm	centimeter
cmil	circular mil (the area of a circle with diameter of 1 mil; equal to 0.0005067 mm^2)
cw	Conductor Wire
cw'	Sub-conductor Wire
Cu	Copper
CB	Circuit Breaker
CHP	Combined Heat and Power
DC	Direct Current
DEMS	Decentralized Energy Management System
DER	Distributed Energy Resource
DFIG	Doubly-Fed Induction Generator
DG	Distributed Generation
DIN	Deutsches Institut für Normung (German Institute for Standardization)
EHV	Extra-High Voltage
EMTDC	Electro-Magnetic Transients including DC
EMTP	Electro-Magnetic Transients Program
ESS	Energy Storage System
gw	Ground Wire
GMD	Geometric Mean Distance
GMR	Geometric Mean Radius
HV	High Voltage
HVDC	High Voltage Direct Current
Hz	Hertz
IACS	International Annealed Copper Standard
ID	Identifier
IEC	International Electrotechnical Commission
j	Imaginary unit
kcmil	Thousand circular mils (equal to 0.5067 mm^2)
km	kilometer
kA	kilo Ampere
kV	kilo Volt
kVA	kilo Volt-Ampere
kVAr	kilo Volt-Ampere reactive
ln	Log base e
LL	Line-to-Line
LN	Line-to-Neutral
LV	Low Voltage
LVRT	Low Voltage Ride Through

mil	One-thousandth of an inch (equal to 0.00254 cm)
mm	millimeter
ms	millisecond
MV	Medium Voltage
MVA	Mega Volt-Ampere
MW	Mega Watt
nw	Neutral Wire
NA2XS2Y	Underground cable designation (per the German DIN VDE standards): N = DIN VDE; A = aluminum conductor; 2X = XLPE insulation; S = copper tape shielded; 2Y = polyethylene jacket
N/A	Not Applicable
OH	Overhead
p.u.	per unit
PLL	Phase Locked Loop
PSCAD	Power System Computer Aided Design
PWM	Pulse-Width-Modulated
REA	Rural Electrification Administration
RM	Round conductor, Multiple strands (per IEC standard)
rms	root-mean-square
S	Switch
s	second
SC	Service Cable
SESAM	Stochastic Energy Source Access Management
SMES	Super-conducting Magnetic Energy Storage
S1A	Regular-strength steel (per IEC standard)
S2A	High-strength steel (per IEC standard)
TB	Technical Brochure
TF	Task Force
UG	Underground
VDE	Verband der Elektrotechnik, Elektronik und Informationstechnik (German Association for Electrical, Electronic and Information Technology)
VSI	Voltage Source Inverter
V2G	Vehicle-to-grid
WECS	Wind Energy Conversion System
WT	Wind Turbine
XLPE	Cross-Linked Polyethylene
Y-Y	Wye-Wye Transformer Connection
Δ-Y	Delta-Wye Transformer Connection
Ω	Ohm
1-ph	Single-phase
3-ph	Three-phase
#	Number or quantity

1. Introduction

It is widely accepted that the transition towards the widespread use of renewable and distributed energy resources (DER) is one of the key challenges in the 21st century. The success of this transition heavily relies on the availability of methods and techniques that enable the economic, robust, and environmentally responsible integration of DER. Industry, universities, and research institutes all over the world are actively engaged in developing these methods and techniques. What is missing, however, are test systems that facilitate the analysis and validation of the developed methods and techniques. This deficiency has been addressed by CIGRE Task Force (TF) C6.04.02. A common basis for testing has been developed and is presented in this report.

Establishing a common basis for testing the integration of DER and Smart Grid technology is a significant challenge because distributed energy systems are diverse by themselves. TF C6.04.02 has taken care of this issue by developing a distinctive benchmark modeling methodology that covers the spectrum of DER integration issues in a mutually exclusive and collectively exhaustive manner. Following this principle, a comprehensive set of complementary reference systems has been developed to facilitate the analysis of DER integration at high voltage, medium voltage, and low voltage levels and at the desired degree of detail.

This Technical Brochure (TB) is organized as described in the following. The benchmark modeling methodology is introduced in Chapter 2. An overview of the scope of application of the benchmarks for practical studies is given in Chapter 3. In Chapter 4, the so-called resource-side benchmark aimed at the study of source-side solutions to DER network integration is introduced. The high voltage (HV) transmission network benchmark for wind farm integration is developed in Chapter 5. The medium voltage (MV) distribution network benchmark for DER integration is described in Chapter 6. The low voltage (LV) distribution network benchmark for DER integration is elaborated upon in Chapter 7. In Chapter 8, case studies illustrate the application of the benchmarks. The appendix is devoted to more in-depth background information.

For each of the benchmark networks, versions for North American style 60 Hz and European style 50 Hz were developed. It may be observed that many other parts of the world also use 50 Hz power systems and 60 Hz power systems. Users are encouraged to use these benchmarks with their own regional and national requirements in mind, and to adapt them to their best use based on sound engineering practices.

2. Benchmarking Methodology

In [1] the CIGRE HVDC (high voltage direct current) benchmark model was presented as a common reference for HVDC control studies. While the topology of an HVDC system is relatively well-defined, renewable and distributed energy systems are much more diverse. For integration studies of DER and wind farms, it is therefore not possible to define one single benchmark configuration that fits all needs. To cover the spectrum of studies pertinent to the integration of DER and renewable energy resources, a comprehensive set of benchmarks was developed.

Central to the methodology is the hierarchical structure of four levels depicted in Figure 2.1. A generalization-specialization hierarchy exists between any two levels. Starting from the highest level, i.e. the electric power system, divisions are performed until all levels of detail that are of interest for the evaluation of the integration of renewable and distributed energy resources are reached.

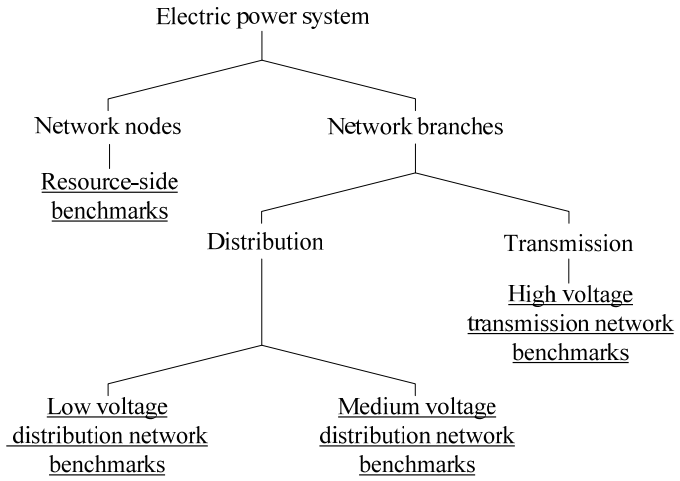

Figure 2.1: Hierarchy for identifying benchmarks

An electric power system is described by its underlying network structure and the resources connected to its nodes. A network equivalent connected to a DER is by itself a suitable candidate for a benchmark since many of the techniques for the integration of renewable resources and DER rely on resource-side control and power electronic conversion. Further specialization is needed on the network side since very diverse types of networks exist. In this context, it is sensible to distinguish transmission networks and distribution networks. The latter can vary significantly in their characteristics depending on voltage level and local preferences. Together, high voltage (HV) transmission, medium voltage (MV) distribution, and low voltage (LV) distribution networks represent a suitable set of candidates for benchmarking the network side.

The DER integration benchmarks are thus derived according to the hierarchy of Figure 2.1, in which the underlined items indicate the benchmarks. Each benchmark is then further specified through European and North American versions.

3. Benchmark Application Matrix

Generally, the benchmarks serve the analysis, design, and validation of methods for the network integration of renewable and distributed energy resources. In what follows, the applications are detailed illustrating the wide spectrum of studies that can be performed.

3.1 Application of Resource-side Benchmark

As the term suggests, the resource-side benchmark introduced in Chapter 4 is devoted to resource-side solutions for the integration of renewable and distributed energy resources. As illustrated in Table 3.1, this concerns major areas such as operation and control, planning and design, power quality, protection, and stability. For each of these areas, various issues exist. Within operation and control, energy management on the resource-side is of interest. An example is the management of local storage to compensate for intermittency. Power electronic control is another key issue. Here, the evaluation of techniques of maximum power tracking is an important example.

Table 3.1: Application matrix for resource-side benchmark

Context	Issue	Example study
Operation and control	Energy management	Managing local storage
	Power electronic control	Maximum power tracking
Planning and design	Converter selection	Impact of multi-level inverters
	Sizing	Design of filters for DER interfaces
Power quality	Harmonics	Measuring harmonics
Protection	Fault current	Assessing fault current contributions of DER
	Fault voltage	Impact of terminal overvoltage on DG
Stability	Low voltage ride through	Impact of terminal short circuit on DC bus voltage

In planning, selection of converters and design of filters for DG interfaces are of interest. Within planning and design, an important issue is the selection of an appropriate power electronic interface for the DER. The area of power quality is a major one due to the issue of harmonics. An example for a study challenge related to this issue concerns the impact of different types of power electronic converters on the harmonics measured at the point of common coupling. The area of protection is important and covers the issues of faults. Study examples include the impact of terminal overvoltages on the DG or the assessment of fault current contributions of DG. Finally, belonging to the broader area of stability is the issue of low voltage ride through (LVRT).

3.2 Application of Network Benchmarks

The application of the high voltage, medium voltage, and low voltage network benchmarks is summarized in Table 3.2. Operation and control has long been an area of strong importance but now requires a fresh look in the wake of DER integration. In the presence of DER and large-scale intermittent renewable energy, this includes optimal power flow, unit commitment, energy management, security, frequency control, and voltage control. New issues that attract increasing attention in the area of operation and control are vehicle-to-grid, demand side response, and emissions displacement. In the area of planning and design, issues include network extension, siting of DER, and the evaluation of investment decisions. It is here of

interest to evaluate the impact of installing DER versus large power plants or investing into line extension.

Table 3.2: Application matrix for network benchmarks

Context	Issue	Example study
Operation and control	Demand side response	Quantifying the benefit of demand side response
	Energy management	Managing storage for wind energy conversion
	Emissions displacement	Value of renewable energy sources for emissions displacement
	Frequency control	Keeping the power balance in a microgrid
	Optimal power flow	Optimizing losses in the presence of DG
	Security	Self-healing network algorithms
	Vehicle-to-grid	Designing V2G controls
	Voltage control	Impact of DG on control of distribution and transmission
	Unit commitment	Optimized and secure scheduling in the presence of DER and large-scale intermittent renewable energy
Planning and design	DER siting	DER siting for congestion mitigation
	Distribution reinforcement	Ratings in the presence of DER
	Investment decision	Quantify value of DG versus line investment
	Network extension	Transmission planning for wind interconnections
Power quality	Ferroresonance	Risk of ferroresonance in transformers connecting DG
	Flicker	Effect of distributed wind on flicker
	Harmonics	Effect of DG on harmonics in networks
	Motor starting	Providing starting currents with DER
	Service interruption	System average interruption duration and frequency indices
	Unbalance	Impact of single-phase DG connections
	Voltage profile	Reactive power management with DG
Protection	Coordination of devices	Coordinating devices such as reclosers
	Fault current	Desensitization of relays through DG
	Fault voltage	Voltage support through DG
	Grounding	Comparing different strategies
	Insulation coordination	Testing for overvoltages
	Relay tripping	Impact of DG on unwanted tripping
Stability	Islanding	Enhancing stability with controlled islanding
	Low voltage ride through	Impact of LVRT profile on system stability
	Small-signal angle stability	Angle stability in networks with off-shore wind farms
	Stabilizer design	Testing stabilizers for DG in real-time hardware-in-the-loop
	Transient stability	Response of DER subject to large disturbances
	Voltage stability	Voltage collapse assessment

Also strong attention in the context of the integration of renewable energy and DER is attributed to the area of power quality. Important issues here are voltage profile, flicker, harmonics, service interruption, unbalance of three-phase quantities, ferroresonance, and the starting of motors. The development of new methods and techniques is also required within the area of protection. Issues include relay tripping, coordination of devices, the evaluation of fault currents and voltages, insulation coordination, and grounding. The different approaches to grounding are visible when comparing the North American and European versions of the network benchmarks. Example studies related to the protection issues are the impact of DG on unwanted tripping of relays, the coordination of reclosers in the presence of downstream

DG, the desensitization of relays because of the influence of DG on fault currents, and grounding. Also affected by the integration of renewable energy and DER are issues of stability such as small-signal angle stability, transient stability, voltage stability, and the design of stabilizers. Emerging attention is particularly devoted to the issues of low voltage ride through and islanding.

4. Resource-side Benchmark

This benchmark was developed in order to study the effects of interconnecting renewable and distributed energy resources with electric power systems and for detailed analyses of specific resource-side topologies and control strategies. For this purpose, a single benchmark configuration is desirable. This configuration can be adjusted using the recommended data to study resources with power ratings ranging from a few kW on low voltage distribution systems to hundreds of MW on high voltage transmission systems.

4.1 Configuration

The resource-side benchmark is shown in Figure 4.1. It consists of an AC bus tied to a grid equivalent. The DER and local load modules connect to the AC bus through switches S1 and S2, which allow for different configurations and tests to be performed. The grid equivalent is connected through switch S3 that enables islanding of the DER and loads. A more detailed example of a DER is depicted in DER module 2, where a system of source, complementary storage and load modules are tied to a DC bus [2], and a power electronic converter module then interfaces the system with the AC bus. Additional DER modules can also be added to study the effects of paralleling DER. Note that voltage step-up or isolation transformers may be needed within the DER modules depending on the voltage levels, power levels, and local utility requirements.

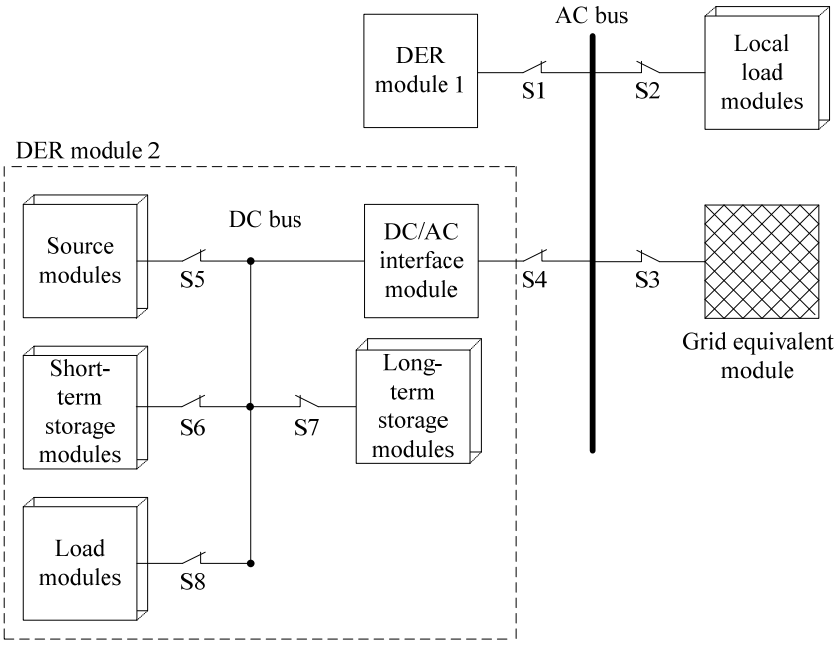

Figure 4.1: Resource-side benchmark

The grid equivalent for interconnection with the DER modules is shown in Figure 4.2. It consists of a voltage source behind a series impedance. The voltage source is specified by its voltage level, V_G, and short-circuit power, S_{SC}, and the impedance is specified as Z_L. Values for the parameters for the grid equivalent vary depending on the voltage level to which the DER modules are connected. Typical values for these parameters are given below in Section 4.2 for North American systems and in Section 4.3 for European systems.

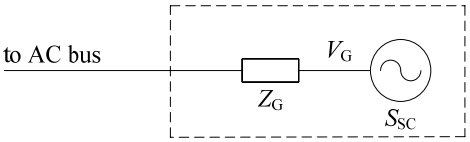

Figure 4.2: Grid equivalent for resource-side benchmark

4.2 North American Grid Equivalent Data

The system frequency for the North American grid equivalent is 60 Hz. Different voltage levels can be selected depending on the desired network connection. The power transfer limits of networks restrict the power ratings of the renewable and distributed resources that can be connected to a given power system. Table 4.1 gives typical values for the necessary parameters of the North American grid equivalent. The grid voltage values given are typical of the North American low, medium, and high voltage levels. Note that three values of LV grid voltage are given in the table; these correspond to the three differing types of LV systems found in North American systems: residential, commercial, and industrial, respectively. Short-circuit power, S_{SC}, is given as a range to provide flexibility for considering the impact of resources on system voltage: large values of S_{SC} correspond to stiff networks, while small values of S_{SC} correspond to weak networks.

Table 4.1: Parameters of North American grid equivalent of resource-side benchmark

Voltage level	Grid voltage, V_G [kV, rms LL]	Short circuit power, S_{SC} [MVA]	R/X Ratio
Low voltage	0.12 / 0.208 / 0.48†	1 to 10	0.70 to 11.00
Medium voltage	12.47	100 to 1000	0.40 to 2.00
High voltage	230	5000 to 20000	0.07 to 0.60

† 0.12 kV is line-to-neutral voltage of single-phase residential subnetwork; 0.208 kV is of commercial subnetwork; 0.48 kV is of industrial subnetwork

4.3 European Grid Equivalent Data

The system frequency for the European grid equivalent is 50 Hz. Different voltage levels can be selected depending on the desired network connection. Table 4.2 gives typical values for the necessary parameters of the European grid equivalent. The grid voltage values given are typical of the European low, medium and high voltage levels. As in Section 4.2, short-circuit power, S_{SC}, is given as a range to provide flexibility for considering the impact of DER on system voltage.

Table 4.2: Parameters of European grid equivalent of resource-side benchmark

Voltage level	Grid voltage, V_G [kV, rms LL]	Short circuit power, S_{SC} [MVA]	R/X Ratio
Low voltage	0.4	1 to 10	0.70 to 11.00
Medium voltage	20	100 to 1000	0.40 to 2.00
High voltage	220	5000 to 20000	0.07 to 0.60

4.4 Flexibility

Benchmark parameters may be modified. Some guidelines on how to change those parameters are given in the following subsections.

4.4.1 Voltage

The recommended grid voltage can be changed within the requirements of the study to be performed. It is preferable for the chosen value to be a commonly installed voltage. For instance in the North American case typical voltage values at the high voltage level are 115 kV, 230 kV, 345 kV, 500 kV, and 765 kV line-to-line (LL). At the medium voltage level they are 4.6 kV, 12.0 kV, 12.47 kV, 13.2 kV, 13.8 kV, 21.6 kV, 22 kV, 24.9 kV, 34.5 kV, and 69 kV LL; and at the low voltage level for single-phase they are 120 V line-to-neutral (LN) and 240 V LL, and for three-phase they are 208 V and 480 V LL. For the European case, typical high voltage levels are 110 kV, 132 kV, 150 kV, 220 kV, 225 kV, 380 kV, and 400 kV LL; typical medium voltage levels are 6.6 kV, 10 kV, 11 kV, 12 kV, 15 kV, 20 kV, and 36 kV; and typical low voltage levels are 380 V, 400 V, and 415 V LL.

4.4.2 Frequency

It is possible to perturb the values of grid frequency. This is of interest when testing for the response to abnormal frequency conditions.

4.5 Application Study: Cache Control

An example application of the resource-side benchmark was presented in [3], in which several DER technologies were interconnected through a DC bus in an energy storage and management system. A summary of this example of the resource-side benchmark, using the European grid-equivalent, is given below.

4.5.1 System Specification

The main function is to compensate for stochastic fluctuations of renewable power sources within the DER module, in order to provide a scheduled power output to the grid. In this example, a DC-AC converter is used for interconnection to the AC bus of the external electric power system as shown in the top right quadrant of Figure 4.3. Here the European LV grid equivalent is used, in which the grid voltage, V_G, is 400 V, and the system frequency is 50 Hz. The grid-interface transformer and equivalent grid impedance are represented by a lumped series resistance and inductance: $R_G = 0.02\ \Omega$ and $L_G = 0.04$ mH. The DC-AC converter is of the voltage source inverter (VSI) type; it operates in current mode control. The control aims to keep the DC voltage constant and therefore the active power over the grid interface is the power flow coming from the renewable stochastic source, P_W, minus the power flow to the storage, P_{ST}. The reactive power set-point is controlled through regulation of the output AC voltage magnitude.

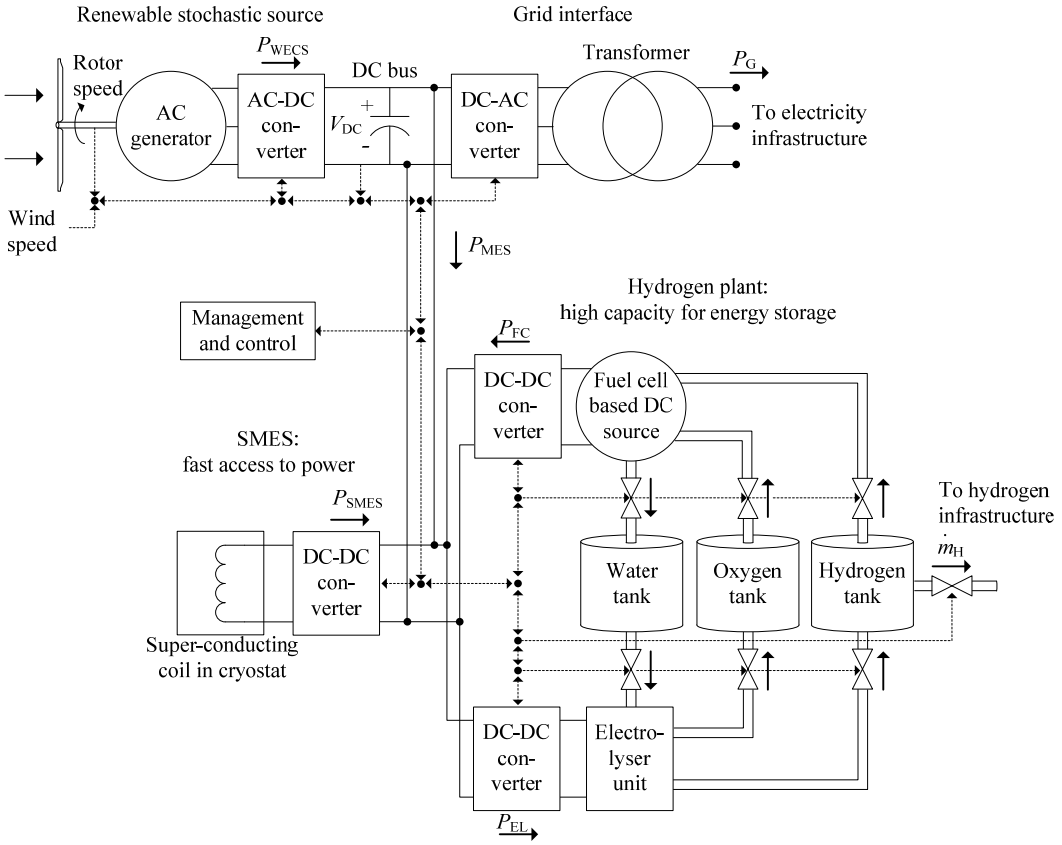

Figure 4.3: Resource-side benchmark application example: model

The renewable stochastic power source shown in the upper left quadrant of Figure 4.3 is a wind turbine modeled as a permanent magnet synchronous machine. It is connected to the DC-bus through an AC-DC power electronic controlled rectifier. Actual wind-speed measurements from the National Wind Technology Center meteorological tower near Boulder, Colorado were used as the input to this source. All power electronic converters were represented by averaged models in this example.

The bottom right quadrant of Figure 4.3 shows a hydrogen storage system for large capacity long-term energy storage. This capacity-oriented hydrogen plant stores energy using an electrolyser to create hydrogen, which then becomes available to produce electricity using a fuel cell. Hydrogen exchange with a hydrogen infrastructure, such as a hydrogen fuel station for hydrogen-powered vehicles is possible through the hydrogen infrastructure interface.

The bottom left quadrant of Figure 4.3 shows the short-term energy storage module as a 600 H super-conducting magnetic energy storage (SMES) device, which provides a fast response to power fluctuations. This access-oriented SMES module is needed to compensate for fast power fluctuations of the stochastic source module. As the SMES can react quickly, it can provide cache control to the larger long-term energy storage [3].

4.5.2 Simulation

Simulation results for an example scenario covering a 24 hour period are shown in Figure 4.4. The power generated by the stochastic wind turbine, P_W, is shown in the top graph. The SESAM controller is tasked with supplying a scheduled variable rate of electricity to the grid during the day, as shown in the second graph, and a fixed rate of hydrogen to the hydrogen infrastructure during the night, as shown in the third graph. The fourth graph shows total electric power to the two storage modules, and the fifth graph shows the total energy held in storage.

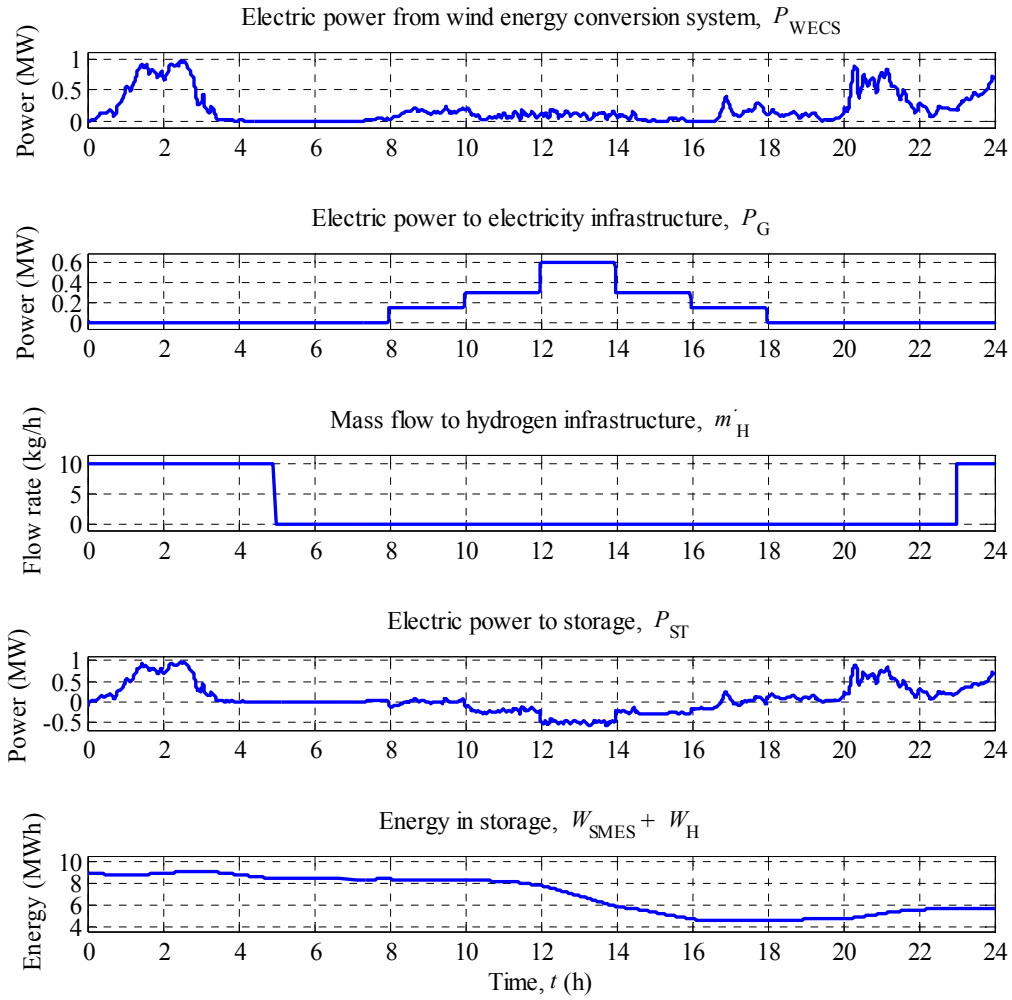

Figure 4.4: Resource-side benchmark application example: power flow in SESAM system

5. High Voltage Transmission Network Benchmark

The high voltage (HV) transmission network benchmark is based on a physical HV network in North America covering areas of Manitoba, North Dakota, and Minnesota. Compared with the original network, the number of nodes has been reduced such that the essential characteristics are maintained, while the model is also suitable for simulation with EMTP-type programs. The model developed here is adapted from prior work on the validation of flexible AC transmission models [4]. It incorporates three areas: one with surplus generation, one with excess load, and an intermediate area that is weakly connected to the remaining system.

The remainder of the chapter is organized as follows: Sections 5.1 and 5.2 describe the North American and European versions of the benchmark, respectively, providing all the necessary data including topology, line parameters, tower geometry, conductor data, transformer parameters, load values, generator parameters, and shunt capacitor values. Section 5.3 describes the flexibility of the benchmark, suggesting possible modifications to the network depending on the studies of interest. Section 5.4 provides an example of the benchmark's use in the form of a wind farm case study.

5.1 North American Configuration

Structure: The network transmission voltages used are 230 kV and 345 kV, which are typical in North American transmission systems. Generation bus voltages are 22 kV, and the system frequency is 60 Hz.

Symmetry: This is a balanced three-phase HV transmission network. Ideal line transposition is assumed.

Line types: Overhead lines are constructed with stranded aluminum conductors reinforced with a steel core, i.e. ACSR. The 230 kV lines have one conductor per bundle, and the 345 kV line has two conductors per bundle. A standard overhead transmission line tower structure is used. It provides sufficient clearance from ground and between conductors to ensure adequate immunity to switching over-voltages while attempting to minimize the line inductances.

Grounding: It is assumed that ground wires are solidly grounded.

5.1.1 Topology

The HV transmission network benchmark is shown in Figure 5.1. The network consists of 13 buses and covers three geographical areas, referred to as Areas 1, 2, and 3, separated by dashed lines. Area 1 is predominantly a generation center with most of its generation coming from hydro power. Area 2, situated about 500 km from Area 1, has a load center with a small amount of thermal generation available. Area 3 is situated between the main generation area 1 and the main load center area 2. Area 1 is representative of Manitoba, Area 2 is a representation of Minnesota, and Area 3 is representative of North Dakota.

Three voltage levels exist in the network: generation bus voltage of 22 kV, primary transmission high voltage of 230 kV, and a long line connecting Areas 1 and 2 at the extra-high voltage (EHV) level of 345 kV. Bus 6a in Area 3 is a suitable location for studying the incorporation of large-scale renewable energy sources such as wind energy conversion systems (WECS). A transmission line connects this bus from the HV side of the WECS plant transformer between Busses 6b and 12. This link represents the infrastructure for

transmission of power from the WECS station to the grid. The length and installation type of the transmission line, i.e. overhead or underground, can be chosen depending on study objectives.

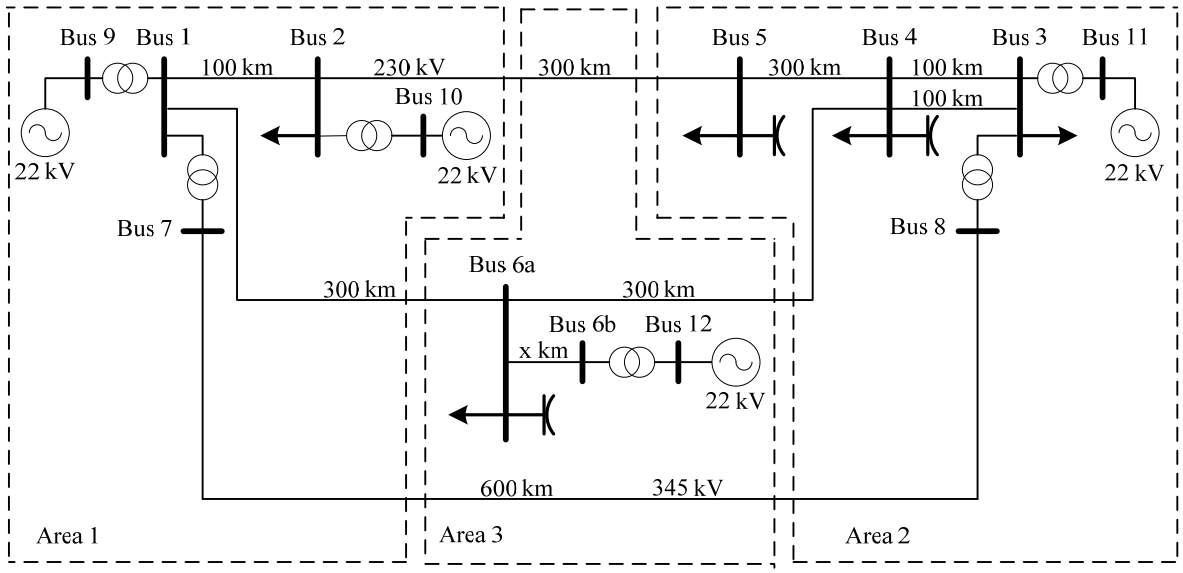

Figure 5.1: Topology of North American HV transmission network benchmark

5.1.2 Network Data

In this subsection, benchmark network data are organized into a number of tables. In Table 5.1, the base values for the per unit system used are provided. The given base power applies to all three phases and the base voltage is a line-to-line voltage. Figure 5.2 in conjunction with Table 5.2 gives the tower geometry from which line parameters can be derived. The types of conductors used in this benchmark are assigned a conductor identifier (Conductor ID) and the associated conductor parameters are provided in Table 5.3. Table 5.4 gives the resistance, reactance, and susceptance values of the transmission lines, as calculated in the Appendix 9.3.1 from the given geometries and conductor data. The data for the transformers are given in Table 5.5.

Line segment 9 is optional with user-definable geometrical configuration, length and installation type; however the voltage of the line should be retained at 230 kV. A base case power flow has been performed with the length of line segment 9 equal to zero, i.e. bus 6a merges with bus 6b. The results of this base case power flow are given in the Appendix 9.2.1. In the absence of further data, the data for the other 230 kV lines given in Table 5.2, Table 5.3, and Table 5.4 could be used to specify an overhead transmission line for segment 9 with user-defined length.

Table 5.1: Per unit system base values of North American HV transmission network benchmark

No. of phases	S_{base}	V_{base}	I_{base}	Z_{base}
	[MVA]	[kV]	[kA]	[Ω]
3	100	230	0.251	529.00
3	100	345	0.167	1190.25

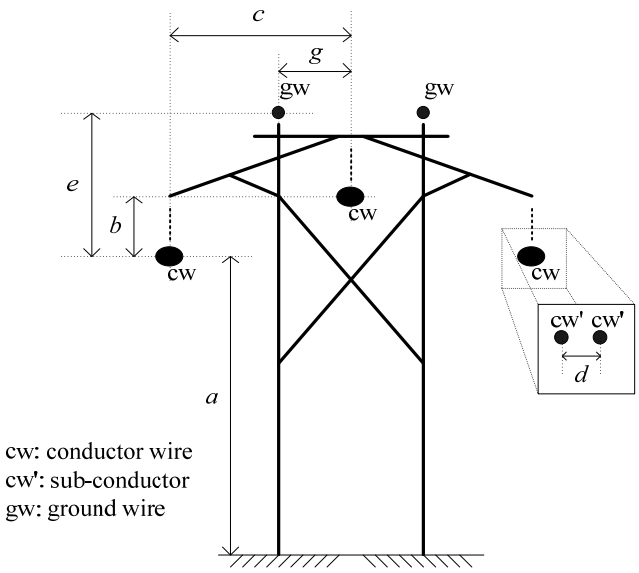

Figure 5.2: Geometry of overhead lines of North American HV transmission network benchmark

Table 5.2: Geometry of overhead lines of North American HV transmission network benchmark

Voltage	*a*	*b*	*c*	Sag	# Sub-cond./ bundle	*d*	# of gw	*e*	*g*	Sag of gw
[kV]	[m]	[m]	[m]	[m]		[m]		[m]	[m]	[m]
230	14.40	1.22	5.49	5.94	1	N/A	2	3.81	3.05	4.45
345	17.50	3.50	7.93	7.25	2	0.46	2	5.00	4.65	7.25

Table 5.3: Conductor parameters of North American HV transmission network benchmark

Conductor ID	Function	Type	Stranding	Size	d_c	*GMR*	R'_{dc} at 20 ºC	R'_{ac} at 50 ºC
				[kcmil]	[cm]	[cm]	[Ω/km]	[Ω/km]
1	conductor wire	ACSR "Cardinal"	54/7	954	3.04	1.231	0.0587	0.0671
2	conductor wire	ACSR "Tern"	45/7	795	2.70	1.073	0.0710	0.0808
3	ground wire	1/2-inch high-strength steel	7	190.6	1.26	0.457	2.1000	2.3900

Note: Conductor type is designated using customary North American notation; see Nomenclature Section for definitions of abbreviations. R'_{ac} varies with temperature as shown in Appendix 9.3.1 and with current flow due to core magnetization in steel cables; for the ACSR in this table, the given values are approximate and do not account for magnetic effects. Values of d_c, *GMR*, R'_{dc} and R'_{ac} for conductor wire obtained from Aluminum Electrical Conductors Manual [5]; values of d_c, R'_{dc} and R'_{ac} for ground wires obtained from [6] with R'_{ac} given at 70 A and *GMR* calculated by multiplying $d_c/2$ by GMR-factor 0.7256 per Table 2.6 of [16].

Table 5.4: Connections and line parameters of North American HV transmission network benchmark [S_{base}=100 MVA]

Line segment	Node from	Node to	Conductor ID	R'_{ph}	X'_{ph}	B'_{ph}	R'_0	X'_0	B'_0	l	Voltage	S_{rated}
				[p.u./km]	[p.u./km]	[p.u./km]	[p.u./km]	[p.u./km]	[p.u./km]	[km]	[kV]	[MVA]
1	1	2	1,3	1.27E-4	9.05E-4	1.81E-3	4.63E-4	2.96E-3	1.05E-3	100	230	250
2	1	6a	1,3	1.27E-4	9.05E-4	1.81E-3	4.63E-4	2.96E-3	1.05E-3	300	230	250
3	2	5	1,3	1.27E-4	9.05E-4	1.81E-3	4.63E-4	2.96E-3	1.05E-3	300	230	250
4	3	4	1,3	1.27E-4	9.05E-4	1.81E-3	4.63E-4	2.96E-3	1.05E-3	100	230	250
5	3	4	1,3	1.27E-4	9.05E-4	1.81E-3	4.63E-4	2.96E-3	1.05E-3	100	230	250
6	4	5	1,3	1.27E-4	9.05E-4	1.81E-3	4.63E-4	2.96E-3	1.05E-3	300	230	250
7	4	6a	1,3	1.27E-4	9.05E-4	1.81E-3	4.63E-4	2.96E-3	1.05E-3	300	230	250
8	7	8	2,3	3.39E-5	3.18E-4	5.09E-3	1.83E-4	1.15E-3	3.57E-3	600	345	500
9	6b	6a	-	-	-	-	-	-	-	optional	230	optional

Table 5.5: Transformer parameters of North American HV transmission network benchmark [S_{base}=100 MVA]

Node from	Node to	Connection	Primary rated voltage, V_1	Secondary rated voltage, V_2	Leakage reactance, X_{tr}	Grounding impedance, Z_{gnd}	S_{rated}
			[kV]	[kV]	[p.u.]	[Ω]	[MVA]
1	7	3-ph YNyn0	230	345	0.01	3	1000
9	1	3-ph YNd11	22	230	0.01	3	1000
10	2	3-ph YNd11	22	230	0.01	3	1000
3	8	3-ph YNyn0	230	345	0.01	3	1000
11	3	3-ph YNd11	22	230	0.01	3	1000
12	6b	3-ph YNd11	22	230	0.02	3	500

5.1.3 Load Data

In Table 5.6, the parameters of the loads at each node are expressed in the per unit system. The values given in the table represent maximum active and reactive powers at each bus. No loads are connected to buses 1, 7, 8, 9, 10, 11, 12, and 6b.

Table 5.6: Load parameters of North American HV transmission network benchmark [S_{base}=100 MVA]

Node	P_{max}	Q_{max}
	[p.u.]	[p.u.]
1	0	0
2	2.85	2.00
3	3.25	2.44
4	3.26	2.44
5	1.03	0.62
6a	4.35	2.96
7	0	0
8	0	0
9	0	0
10	0	0
11	0	0
12	0	0
6b	0	0

5.1.4 Generator Data

Parameters of the generator model and operation data are presented in Table 5.7, and Table 5.8 identifies the system reference bus. All generators are rated at 22 kV, 60 Hz. Exciters of the synchronous generators have been modeled as first-order transfer functions. Typical values for the parameters of the exciters are provided in the example of section 5.4.

Table 5.7: Generator parameters and operation data of North American HV transmission network benchmark [S_{base}=100 MVA]

Generator	Node	H	δ	X_d	X'_d	X''_d	T'_{d0}	T''_{d0}	X_q	X''_q	T''_{q0}	S_{rated}	P_{out}	V_{out}
		[s]	[p.u.]	[p.u.]	[p.u.]	[p.u.]	[s]	[s]	[p.u.]	[p.u.]	[s]	[MVA]	[MW]	[p.u.]
1	10	5.0	1.0	1.5	0.4	0.35	5.0	0.002	1.2	0.35	0.002	700	500	1.03
2	11	3.0	0.0	1.4	0.3	0.28	6.0	0.002	1.35	0.27	0.002	500	200	1.03
3	12	5.0	1.0	1.5	0.4	0.35	5.0	0.002	1.2	0.35	0.002	500	300	1.03
Slack	9	See Table 5.8												

Table 5.8: Reference bus of North American HV transmission network benchmark

Bus voltage angle	Bus voltage magnitude
[deg]	[p.u.]
0	1.03

5.1.5 Shunt Capacitor Data

Fixed capacitor banks provide voltage support at buses 4, 5 and 6a. Reactive power injection occurs at the rated voltage for each of those buses and is counted positive when injected into the buses is given in Table 5.9.

Table 5.9: Shunt Capacitive Compensation of North American HV transmission network benchmark [S_{base}=100 MVA]

Node	Q
	[p.u.]
4	1.6
5	0.8
6a	1.8

5.2 European Configuration

Structure: The network transmission voltages used are 220 kV and 380 kV, which are typical in European transmission systems. Generation bus voltages are 22 kV, and the system frequency is 50 Hz.

Symmetry: This is a balanced three-phase HV transmission network. Ideal line transposition is assumed.

Line types: Overhead lines are constructed with stranded aluminum conductors reinforced with a steel core, i.e. ACSR. The 220 kV lines have one conductor per bundle and the 380 kV line has two conductors per bundle. A standard overhead transmission line tower structure is used. It provides sufficient clearance from ground and between conductors to ensure adequate immunity to switching over-voltages while attempting to minimize the line inductances.

Grounding: It is assumed that ground wires are solidly grounded.

5.2.1 Topology

The topology of the European HV transmission network benchmark matches the North American counterpart and is repeated for convenience in Figure 5.3. The network consists of 13 buses and covers three geographical areas, referred to as Areas 1, 2, and 3, marked by dashed lines. Area 1 is predominantly a generation center. Area 2, situated about 500 km from Area 1, is a load center with a small amount of generation available. Area 3 is situated between the main generation Area 1 and the main load center Area 2.

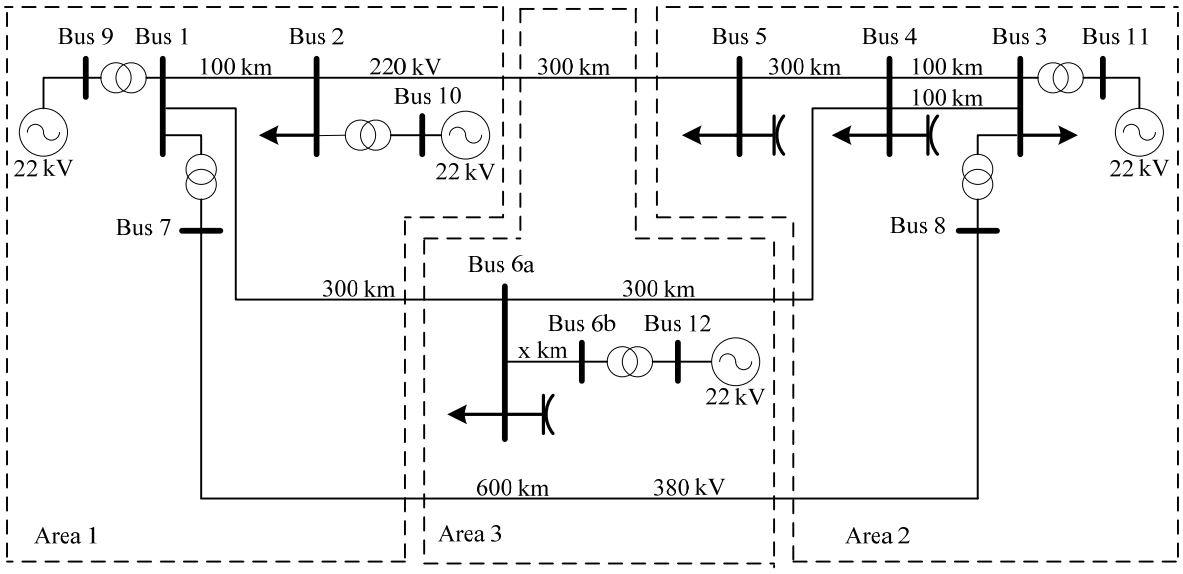

Figure 5.3: Topology of European HV transmission network benchmark

Three voltage levels exist in the network: generation bus voltage of 22 kV, primary transmission high voltage of 220 kV, and a long line connecting Areas 1 and 2 at the extra-high voltage (EHV) level of 380 kV. Bus 6a in Area 3 is a suitable location for studying the incorporation of large-scale renewable energy sources such as wind energy conversion systems (WECS). A transmission line separates this bus from the HV side of the WECS plant transformer that is between Bus 6b and Bus 12. This link represents the infrastructure for transmission of power from the WECS station to the grid. The length and installation type, i.e. overhead or underground, should be determined as a function of the particular study theme.

5.2.2 Network Data

In this subsection, benchmark network data are again organized into a number of tables. In Table 5.10, the base values for the per unit system used are provided. The given base power applies to all three phases and the base voltage is a line-to-line voltage. Figure 5.4, in conjunction with Table 5.11 gives the tower geometry from which line parameters can be derived. The types of conductors used in this benchmark are assigned a Conductor ID and the associated conductor parameters are provided in Table 5.12. Table 5.13 gives the resistance, reactance, and susceptance values of the transmission lines, as calculated in Appendix 9.3.1. The data for the transformers are given in Table 5.14.

Table 5.10: Per unit system base values of European HV transmission network benchmark

No. of phases	S_{base}	V_{base}	I_{base}	Z_{base}
	[MVA]	[kV]	[kA]	[Ω]
3	100	220	0.262	484
3	100	380	0.152	1444

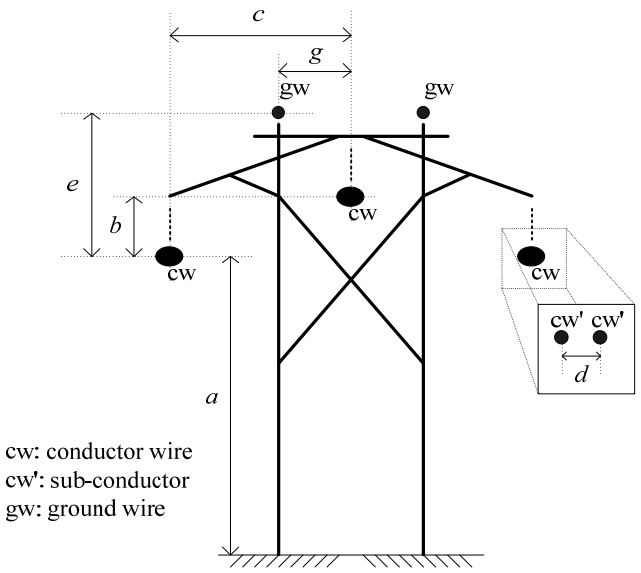

Figure 5.4: Geometry of overhead lines of European HV transmission network benchmark

Table 5.11: Geometry of overhead lines of European HV transmission network benchmark

Voltage	*a*	*b*	*c*	Sag	# Sub-cond./ bundle	*d*	# of gw	*e*	*g*	Sag of gw
[kV]	[m]	[m]	[m]	[m]		[m]		[m]	[m]	[m]
220	14.40	1.22	5.49	5.94	1	N/A	2	3.81	3.05	4.45
380	17.50	3.50	7.93	7.25	2	0.46	2	5.00	4.65	7.25

Table 5.12: Conductor parameters of European HV transmission network benchmark

Conductor ID	Function	Type	Stranding (Aluminum/ Steel)	Cross-sectional Area	d_c	*GMR*	R'_{dc} at 20 ºC	R'_{ac} at 50 ºC
				[mm^2]	[cm]	[cm]	[Ω/km]	[Ω/km]
1	conductor wire	A1/S1A	54/7	500	3.09	1.251	0.0587	0.0659
2	conductor wire	A1/S1A	45/7	450	2.85	1.131	0.0642	0.0732
3	ground wire	S2A	7	95	1.26	0.457	2.1000	2.3900

Note: Conductor type is designated using IEC notation as specified in IEC61089 [7]; see Nomenclature Section for definitions of abbreviations. R'_{ac} varies with temperature as shown in Appendix 9.3.1 and with current flow due to core magnetization in steel cables; for the A1/S1A in this table, the given values are approximate and do not account for magnetic effects. Values of d_c, *GMR*, R'_{dc} and R'_{ac} for conductor wires obtained from IEC61597 [8]; values of d_c, R'_{dc} and R'_{ac} for ground wires obtained from [6] with R'_{ac} given at 70 A and *GMR* calculated by multiplying d_c/2 by GMR-factor 0.7256 per Table 2.6 of [16].

Table 5.13: Connections and line parameters of European HV transmission network benchmark [S_{base}=100 MVA]

Line seg-ment	Node from	Node to	Cond-uctor ID	R'_{ph}	X'_{ph}	B'_{ph}	R'_0	X'_0	B'_0	l	Voltage	S_{rated}
				[p.u./km]	[p.u./km]	[p.u./km]	[p.u./km]	[p.u./km]	[p.u./km]	[km]	[kV]	[MVA]
1	1	2	1,3	1.35E-4	8.22E-4	1.38E-3	4.41E-4	2.72E-3	8.06E-4	100	220	250
2	1	6a	1,3	1.35E-4	8.22E-4	1.38E-3	4.41E-4	2.72E-3	8.06E-4	300	220	250
3	2	5	1,3	1.35E-4	8.22E-4	1.38E-3	4.41E-4	2.72E-3	8.06E-4	300	220	250
4	3	4	1,3	1.35E-4	8.22E-4	1.38E-3	4.41E-4	2.72E-3	8.06E-4	100	220	250
5	3	4	1,3	1.35E-4	8.22E-4	1.38E-3	4.41E-4	2.72E-3	8.06E-4	100	220	250
6	4	5	1,3	1.35E-4	8.22E-4	1.38E-3	4.41E-4	2.72E-3	8.06E-4	300	220	250
7	4	6a	1,3	1.35E-4	8.22E-4	1.38E-3	4.41E-4	2.72E-3	8.06E-4	300	220	250
8	7	8	2,3	2.27E-5	2.16E-4	5.21E-3	1.25E-4	8.00E-4	3.64E-3	600	380	500
9	6b	6a	-	-	-	-	-	-	-	optional	220	optional

Table 5.14: Transformer parameters of European HV transmission network benchmark [S_{base}=100 MVA]

Node from	Node to	Connection	Primary rated voltage, V_1	Secondary rated voltage, V_2	Leakage reactance, X_{tr}	Grounding impedance, Z_{gnd}	S_{rated}
			[kV]	[kV]	[p.u.]	[Ω]	[MVA]
1	7	3-ph YNyn0	220	380	0.013	3	1000
9	1	3-ph YNd11	22	220	0.013	3	1000
10	2	3-ph YNd11	22	220	0.013	3	1000
3	8	3-ph YNyn0	220	380	0.013	3	1000
11	3	3-ph YNd11	22	220	0.013	3	1000
12	6b	3-ph YNd11	22	220	0.026	3	500

Line Segment 9 is an optional line with user-definable geometrical configuration, length and installation type; however the voltage of the line should be retained at 220 kV. A base case power flow has been performed with the length of line segment 9 equal to zero, i.e. bus 6a merges with bus 6b, the results for which are given in Appendix 9.2.2. In the absence of further data, the data for the other 220 kV lines given in Table 5.11, Table 5.12, and Table 5.13 could be used to specify an overhead transmission line for line segment 9 with a similar configuration as the other lines in the network, but with user-defined length.

5.2.3 Load Data

In Table 5.15, the parameters of the loads at each node are expressed in the per unit system. The values given in the table represent maximum active and reactive powers at each bus. No loads are connected to buses 1, 7, 8, 9, 10, 11, 12, and 6b.

Table 5.15: Load parameters of European HV transmission network benchmark [S_{base}=100 MVA]

Node	P_{max}	Q_{max}
	[p.u.]	[p.u.]
1	0	0
2	2.85	2.00
3	3.25	2.44
4	3.26	2.44
5	1.03	0.62
6a	4.35	2.96
7	0	0
8	0	0
9	0	0
10	0	0
11	0	0
12	0	0
6b	0	0

5.2.4 Generator Data

Parameters of the generator model and operation data are presented in Table 5.16 and Table 5.17 identifies the system reference bus. All generators are rated at 22 kV, 50 Hz. Exciters of the synchronous generators have been modeled as first-order transfer functions.

Table 5.16: Generator parameters and operation data of European HV transmission network benchmark [S_{base}=100 MVA]

Generator	Node	H	δ	X_d	X'_d	X''_d	T'_{d0}	T''_{d0}	X_q	X''_q	T''_{q0}	S_{rated}	P_{out}	V_{out}
		[s]	[p.u.]	[p.u.]	[p.u.]	[p.u.]	[s]	[s]	[p.u.]	[p.u.]	[s]	[MVA]	[MW]	[p.u.]
1	10	5.0	1.0	1.25	0.333	0.292	5.0	0.002	1.0	0.292	0.002	700	500	1.03
2	11	3.0	0.0	1.667	0.25	0.233	6.0	0.002	1.125	0.225	0.002	500	200	1.03
3	12	5.0	1.0	1.25	0.333	0.292	5.0	0.002	1	0.292	0.002	500	300	1.03
Slack	9	See Table 5.17												

Table 5.17: Reference bus of European HV transmission network benchmark

Bus voltage angle	Bus voltage magnitude
[deg]	[p.u.]
0	1.03

5.2.5 Shunt Capacitor Data

Fixed capacitor banks provide voltage support at buses 4, 5 and 6a. Reactive power injection at the rated voltage for each of those buses is given in Table 5.18.

Table 5.18: Shunt capacitive compensation of European HV transmission network benchmark [S_{base}=100 MVA]

Node	Q
	[p.u.]
4	1.6
5	0.8
6a	1.8

5.3 Flexibility

For some studies, it may be of interest to evaluate the impact of a WECS or similar under different network conditions. Some guidelines on how to change various benchmark parameters are given in the following subsections.

5.3.1 Voltage

The nominal base voltage of the HV transmission network benchmarks are 230 kV for the North American and 220 kV for the European case. Other voltages are possible, but the conductors, conductor spacing, tower configurations, transformers, etc. would all have to be modified appropriately. With this in mind, the base voltages may be modified to study different voltage levels as long as the chosen values are realistic. Section 4.4.1 suggested some appropriate voltages.

5.3.2 Line Lengths

As the WECS may be geographically located far from a nearby busbar, it is usually necessary to construct additional network infrastructure in order to link the generation plant to the grid. For example, a transmission line or cable may have to be constructed from existing bus 6a to the WECS location at bus 12. The transmission line that connects bus 6a to bus 6b represents the link associated with the WECS. The length of this line can be varied to investigate concerns such as low voltage ride-through (LVRT) capability and maximum power that can reliably be transmitted over lines of different lengths.

5.3.3 Line Types and Parameters

In the provided benchmark system, the branch connecting buses 6a and 6b has been represented by an overhead transmission line. It is possible to replace this branch with a cable link. In this way, cases such as connection of offshore wind farms to the grid through underwater cables can be explored. It would then be necessary to modify the line parameters in accordance with information supplied by cable manufacturers.

The provided benchmark utilizes AC lines for transmission of the power generated by the WECS from bus 12 to bus 6a. DC schemes, including the line-commutated HVDC and the pulse-width-modulated (PWM) voltage-source inverter based technologies, can replace the AC link in order to examine enhancement of system performance introduced by DC transmission.

5.3.4 Loads

Load values can be modified as necessary. Also, MV and LV network benchmarks from the subsequent chapters of this document may be inserted at the load points if more detailed representations are of interest to the study. If such a combination of the network

benchmarks is desired, a means of matching the HV and MV voltage levels is needed. While this could be done with a single transformer, as described later in Section 6.3.5, a more common occurrence would involve some representation of a subtransmission network. A simple subtransmission model is thus recommended hereafter.

Figure 5.5 shows a simplified subtransmission network, which, in conjunction with the MV network benchmark described in the following chapter, may be inserted in place of a load in the HV network benchmark.

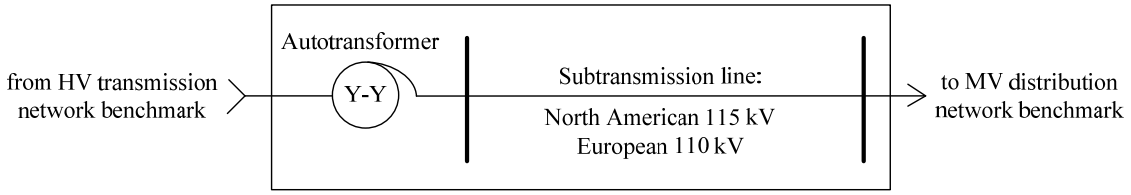

Figure 5.5: Topology of HV-MV subtransmission network benchmark integration

The parameters for the two-winding autotransformer are specified in Table 5.19. Improved realism could be attained by two modifications. First, a delta-connected tertiary winding could be added to the autotransformer to suppress triple harmonics. Second, tap changers may be added to the autotransformer as follows:

- At the primary side that corresponds to the transmission voltage level, ±5 % in 2.5 % increment no-load taps;
- At the secondary that corresponds to the subtransmission voltage level: ±10 % in 0.625 % increment load changing taps.

The line parameters and associated constants for tower geometries in Figure 5.2 or Figure 5.4 are specified in Table 5.20. The types of conductors used are given in Table 5.21. Table 5.22 gives the resistance, reactance, and susceptance values of the subtransmission line, as calculated in the Appendix 9.3.1. Note that the p.u. values of Table 5.22 are calculated using 115 kV and 110 kV as base voltages of North American and European subtransmission networks, respectively. For apparent power, base value of 100 MVA is used.

Table 5.19: Autotransformer parameters of subtransmission network benchmark

Network Benchmark	Connection	V_1	V_2	Z_{tr}†	S_{rated}
		[kV]	[kV]	[p.u.]	[MVA]
North American	3-ph YNYn0	230	115	0.01 + j0.12	150
European	3-ph YNYn0	220	110	0.01 + j0.12	150

† based on lowest MVA rating

Table 5.20: Geometry of overhead lines of subtransmission network benchmark

Network Benchmark	*a*	*b*	*c*	Sag	# Sub-cond./ bundle	*d*	# of gw	*e*	*g*
	[m]	[m]	[m]	[m]		[m]		[m]	[m]
North American	10.00	0.35	1.90	1.80	1	-	2	1.50	1.40
European	10.00	0.35	1.90	1.80	1	-	2	1.50	1.40

Table 5.21: Conductor parameters of subtransmission network benchmark

Network Benchmark	Function	Type	Stranding	Cross-sectional area	d_c	GMR	R'_{dc} at 20 ºC	R'_{ac} at 50 ºC
					[cm]	[cm]	[Ω/km]	[Ω/km]
North American	conductor wire	AAC	37	795.0 kcmil	2.61	1.000	0.0713	0.0814
	ground wire	1/2-inch high-strength steel	7	190.6 kcmil	1.26	0.457	2.1000	2.3900
European	conductor wire	A1	37	400 mm^2	2.60	0.998	0.0721	0.0819
	ground wire	S2A	7	95 mm^2	1.26	0.457	2.1000	2.3900

See notes at bottom of Table 5.3 for North American and Table 5.12 for European.

Table 5.22: Line parameters of subtransmission network benchmark [S_{base}=100 MVA]

Network Benchmark	R'_{ph}	X'_{ph}	B'_{ph}	R'_0	X'_0	B'_0	l	Voltage	S_{rated}
	[p.u./km]	[p.u./km]	[p.u./km]	[p.u./km]	[p.u./km]	[p.u./km]	[km]	[kV]	[MVA]
North American	6.16E-4	3.13E-3	5.31E-4	1.96E-3	1.32E-2	2.39E-4	50	115	150
European	6.77E-3	2.85E-3	4.05E-4	1.90E-3	1.21E-2	1.82E-4	50	110	150

5.4 Application Study: Ride-Through Testing of Wind Energy Conversion System

The example presented in this section shows how the proposed HV transmission system benchmark can be used for verification of low voltage ride-through (LVRT) capability of a wind farm and for studying line congestion in the network affected by a reduction in the wind power generation.

5.4.1 System Specification

The wind farm in this study represented a wind farm connected via an underground cable and employing variable-speed wind turbines with doubly-fed induction generators. The study was targeted at control and protection strategy investigation, which provided LVRT capability to the WECS plant. The wind farm substituted the generator located at bus 12 in the original North American benchmark system. The overhead transmission line between buses 6b and 6a was also replaced by a submersible cable with compensation reactors installed at both ends, as depicted in Figure 5.6. A summary of the wind farm specifications is given in Table 5.23, and data for the underground cable are given in Table 5.24.

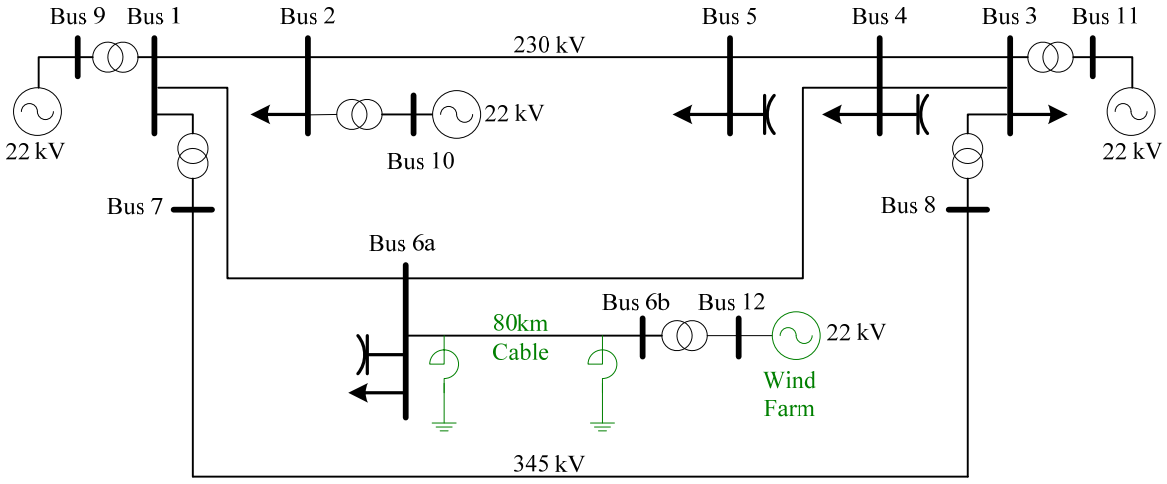

Figure 5.6: HV transmission network benchmark application example: model

Table 5.23: HV transmission network benchmark application example: wind farm parameters

Rated power	350 MVA
Wind farm bus voltage	22 kV
Wind turbine type	Variable-speed DFIG
Control scheme	Maximum power tracking strategy with LVRT capability
Cable link length	80 km
Cable link voltage	230 kV

Table 5.24: HV transmission network benchmark application example: underground cable parameters [S_{base}=100 MVA]

Node from	Node to	R'_{ph}	X'_{ph}	B'_{ph}	R'_0	X'_0	B'_0	l	Voltage
		[p.u./km]	[p.u./km]	[p.u./km]	[p.u./km]	[p.u./km]	[p.u./km]	[km]	[kV]
6a	6b	2.85E-4	1.47E-3	1.59E-3	7.17E-4	2.51E-3	1.26E-3	80	230

5.4.2 Simulation

Simulation was carried out on the North American configuration, using the PSCAD/EMTDC [9] simulation tool. It was simulated at a time step of 20 µs, but the waveforms were plotted at 1000 µs intervals. The simulation ran for 10 seconds. The modeled wind farm represents a lumped variable-speed wind turbine with a doubly-fed induction generator (DFIG). The DFIG is controlled through a power electronic converter, which connects the rotor of the induction generator to the grid at bus 12 and is comprised of two voltage-source inverters linked together at their DC sides via a DC-link capacitor. The grid-side converter regulates the active and reactive power outputs of the equivalent wind turbine, while the generator-side converter adjusts DC bus voltage and reactive power flow through the machine's rotor. In the simulation case, the DFIG converter is simulated using detailed switching models of the power electronics and control system

[10]. The VSI uses a pulse-width-modulated (PWM) switching technique and operates at a switching frequency of 1 kHz.

In the simulation, the following assumptions have been made:

- Wind power is delivered by a lumped wind turbine.
- Transmission lines have been represented by the Bergeron model.
- All loads have been represented by constant R and L elements.
- Exciters of the synchronous generators have been modeled as first-order transfer functions with a gain of 20 and a time constant of 0.05 s.
- Generators are supplied with constant mechanical torques. As mentioned before, the generation plant located at bus 9 is a slack bus, which is modeled here by an ideal voltage source.
- Magnetic saturation is ignored in synchronous machines and transformers.
- Each machine shaft is modeled as a single rotating mass.
- Each synchronous generator has been considered to include only one amortisseur winding on its q-axis.

Wind farms must be able to sustain generation after clearance of under-voltages as low as zero p.u. with durations up to 9 cycles [11]. This feature was tested by applying a solid 3-phase-to-ground fault at bus 12. Figure 5.7 indicates successful recovery of the DFIG after the 150 ms fault was cleared. Wind farm voltage, V_{12}, active and reactive power generation of the wind farm, P_W and Q_W, respectively, and the voltage at bus 6a, V_{6a}, before, during and after the fault are shown in the same figure.

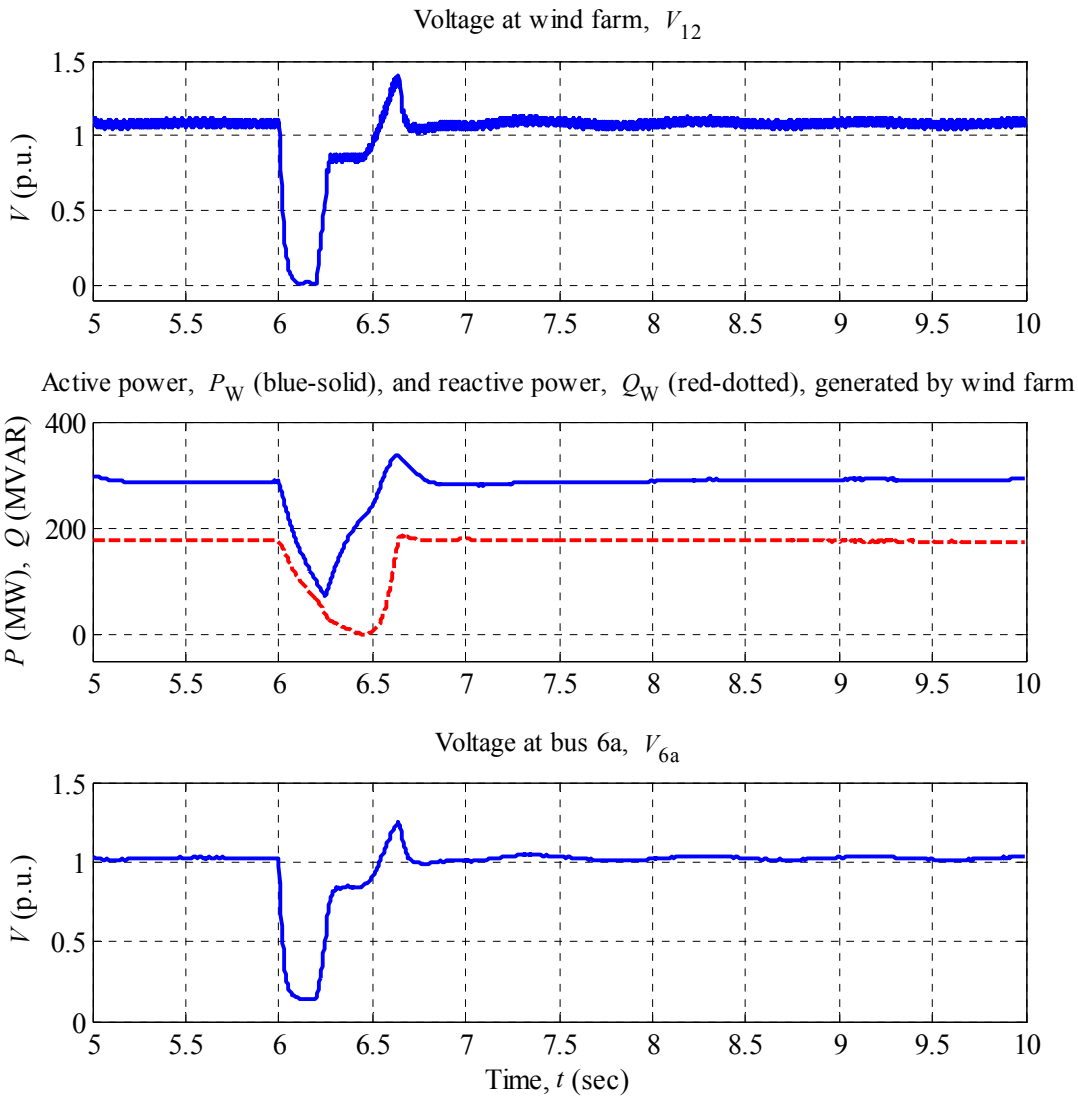

Figure 5.7: HV transmission network benchmark application example: low voltage ride through response of tested wind farm

6. Medium Voltage Distribution Network Benchmark

The medium voltage (MV) distribution network benchmark is derived from a physical MV network in southern Germany, which supplies a small town and the surrounding rural area. Compared with this original network, the number of nodes for the benchmark network was reduced to enhance user friendliness and flexibility while fully maintaining the realistic character of the network. The benchmark network in this chapter is representative of physical MV networks typical of North America and Europe. It is to be noted that distribution network design approaches and installation common practices vary greatly between North America and Europe; a discussion of these differences is given in Appendix 9.1.

6.1 North American Configuration

Structure: North American MV distribution feeders are three-phase and either of meshed or radial structure, with the latter dominating rural installations. The benchmark allows flexibility to model both meshed and radial structures. Each feeder includes numerous laterals at which MV/LV transformers would be connected. In North America, radial structures are prevalent, and single-phase MV lines are included as subnetworks off the three-phase main lines. The nominal voltage on the three-phase sections is 12.47 kV, and on the single-phase sections the line-to-neutral voltage is 7.2 kV. The system frequency is 60 Hz.

Symmetry: Due to the existence of single-phase laterals, the North American MV network configuration is inherently unbalanced. Although effort to balance the loading is made, a balanced three-phase network should not be assumed, particularly for voltage drop calculations.

Line types: Overhead lines are used with bare conductors made of aluminum with or without steel reinforcement, i.e. AAC and ACSR.

Grounding: The grounding of the MV network largely depends on regional preferences. The majority of North American networks are solidly grounded.

6.1.1 Topology

The topology of the North American version of the MV network benchmark is shown in Figure 6.1. Framed by dashed lines are Feeders 1 and 2. Both feeders operate at 12.47 kV and are fed via separate transformers from the 115 kV subtransmission system. Either feeder alone or both feeders can be used for studies of DER integration. Further variety may be introduced by means of configuration switches S1, S2, and S3. If these switches are open, then both feeders are radial. Closing S2 and S3 in feeder 1 would create a loop or mesh. With the given location of S1, it can either be assumed that both feeders are fed by the same substation or by different substations. Closing S1 interconnects the two feeders through a distribution line. If different substations are assumed, then 115 kV subtransmission lines, such as those given in Section 5.3.4 should be used to connect the HV grid equivalent to each of the transformers.

In addition to three-phase lines, MV networks in North America contain single-phase lines. For these cases the single-phase subnetwork shown in Figure 6.2 was developed. It is inserted into the MV network at the locations indicated in Figure 6.1 and connected to the given phase.

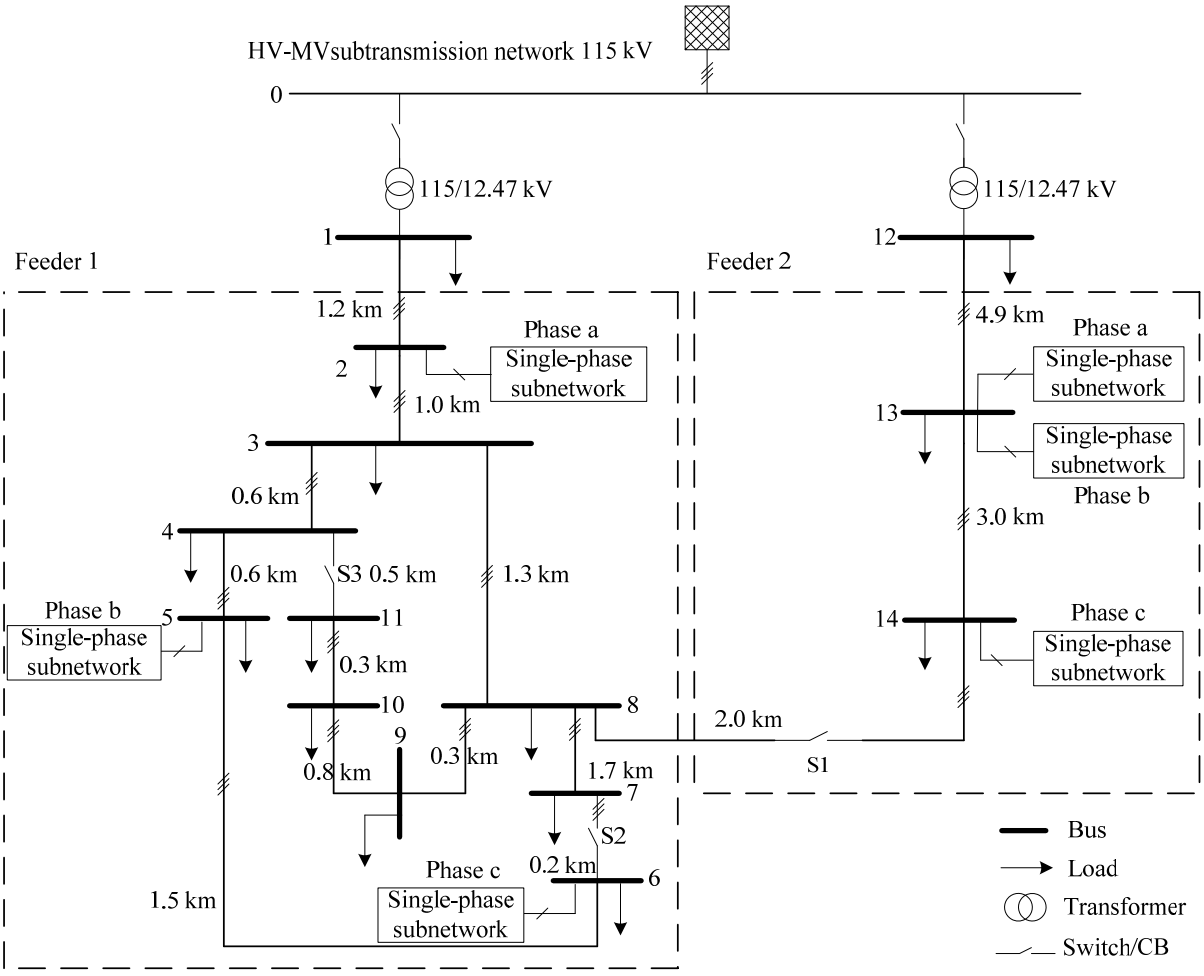

Figure 6.1: Geometry of overhead lines of three-phase sections of North American MV distribution network benchmark

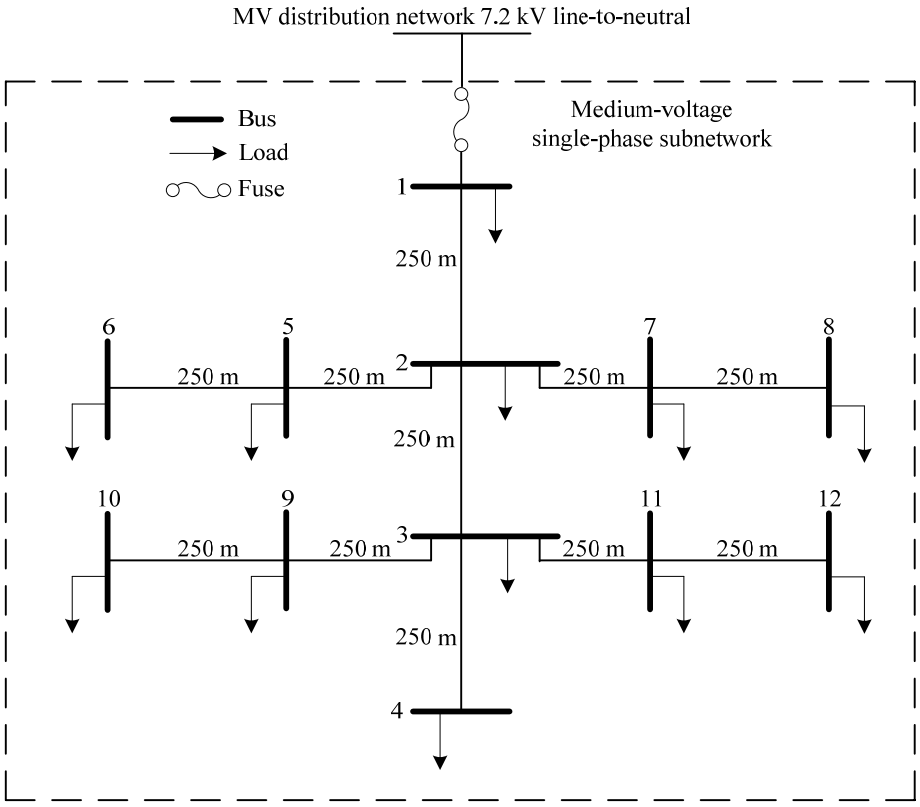

Figure 6.2: Topology of single-phase sections of North American MV distribution network benchmark

6.1.2 Network Data

In the North American version, conductors are mounted on towers as overhead lines. Neutral wires are available in three-phase and single-phase sections as shown. Figure 6.3 and Table 6.1 give the tower geometries for both the three-phase and single-phase lines. The types of conductors used in this benchmark are designated by the Conductor ID. The associated conductor parameters are provided in Table 6.2.

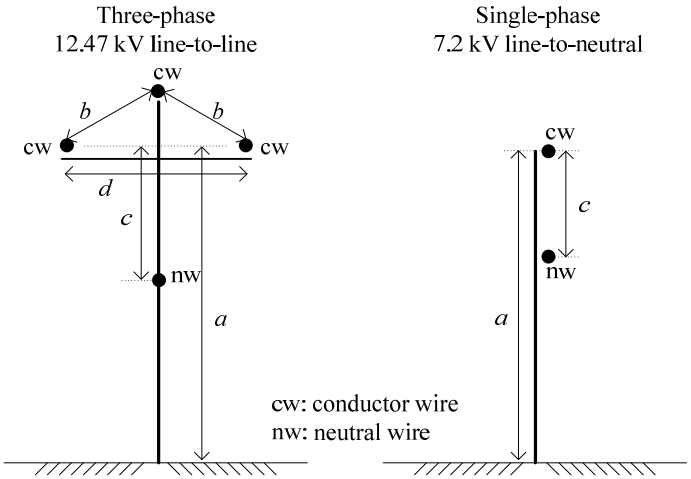

Figure 6.3: Geometry of overhead lines of North American MV distribution network benchmark

Table 6.1: Geometry of overhead lines of North American MV distribution network benchmark

Tower	*a*	*b*	*c*	*d*
	[m]	[m]	[m]	[m]
Three-phase	13.7	1.64	2.13	3.05
Single-phase	13.7	N/A	2.13	N/A

Table 6.2: Conductor parameters of North American MV distribution network benchmark

Conductor ID	Function	Type	Stranding	Size	d_c	*GMR*	R'_{dc} at 20 ºC	R'_{ac} at 50 ºC
				[kcmil or AWG]	[cm]	[cm]	[Ω/km]	[Ω/km]
1	conductor wire	AAC "Tulip"	19	336.4	1.69	0.640	0.168	0.190
2	neutral wire	AAC "Phlox"	7	3/0	1.18	0.427	0.338	0.380
3	conductor & neutral	ACSR "Sparrow"	6/1	2	0.80	0.140	0.832	1.010

Note: Conductor type is designated using customary North American notation. R'_{ac} varies with temperature and current flow due to core magnetization in steel cables; for the ACSR in this table, the given values are approximate and account for magnetic effects assuming a current flow of 146 A. Values of d_c, *GMR*, R'_{dc}, and R'_{ac} obtained from Aluminum Electrical Conductors Manual [5], with *GMR* for the ACSR obtained from Table 2.3 of [16].

Table 6.3 defines the network topology, line lengths of the three-phase sections of Figure 6.1, and installation type. It also provides the phase and zero sequence resistance, reactance and susceptance values of the lines, as calculated in Appendix 9.3.1. In Table 6.4, the single-phase sections are described similarly.

Table 6.3: Connections and line parameters of three-phase sections of North American MV distribution network benchmark

Line segment	Node from	Node to	Conductor ID	R'_{ph}	X'_{ph}	B'_{Ph}	R'_0	X'_0	B'_0	*l*	Installation
				[Ω/km]	[Ω/km]	[µS/km]	[Ω/km]	[Ω/km]	[µS/km]	[km]	
1	1	2	1,2	0.282	0.703	3.193	0.466	1.243	1.826	1.20	overhead
2	2	3	1,2	0.282	0.703	3.193	0.466	1.243	1.826	1.00	overhead
3	3	4	1,2	0.282	0.703	3.193	0.466	1.243	1.826	0.61	overhead
4	4	5	1,2	0.282	0.703	3.193	0.466	1.243	1.826	0.56	overhead
5	5	6	1,2	0.282	0.703	3.193	0.466	1.243	1.826	1.54	overhead
6	6	7	1,2	0.282	0.703	3.193	0.466	1.243	1.826	0.24	overhead
7	7	8	1,2	0.282	0.703	3.193	0.466	1.243	1.826	1.67	overhead
8	8	9	1,2	0.282	0.703	3.193	0.466	1.243	1.826	0.32	overhead
9	9	10	1,2	0.282	0.703	3.193	0.466	1.243	1.826	0.77	overhead
10	10	11	1,2	0.282	0.703	3.193	0.466	1.243	1.826	0.33	overhead
11	11	4	1,2	0.282	0.703	3.193	0.466	1.243	1.826	0.49	overhead
12	3	8	1,2	0.282	0.703	3.193	0.466	1.243	1.826	1.30	overhead
13	12	13	1,2	0.282	0.703	3.193	0.466	1.243	1.826	4.89	overhead
14	13	14	1,2	0.282	0.703	3.193	0.466	1.243	1.826	2.99	overhead
15	14	8	1,2	0.282	0.703	3.193	0.466	1.243	1.826	2.00	overhead

Table 6.4: Connections and line parameters of single-phase sections of North American MV distribution network benchmark

Line segment	Node from	Node to	Conductor ID	R'_{ph} [Ω/km]	X'_{ph} [Ω/km]	B'_{ph} [μS/km]	l [m]	Installation
1	1	2	3	1.144	0.884	2.374	250	overhead
2	2	3	3	1.144	0.884	2.374	250	overhead
3	3	4	3	1.144	0.884	2.374	250	overhead
4	2	5	3	1.144	0.884	2.374	250	overhead
5	5	6	3	1.144	0.884	2.374	250	overhead
6	2	9	3	1.144	0.884	2.374	250	overhead
7	9	8	3	1.144	0.884	2.374	250	overhead
8	8	7	3	1.144	0.884	2.374	250	overhead
9	9	10	3	1.144	0.884	2.374	250	overhead
10	10	11	3	1.144	0.884	2.374	250	overhead
11	9	12	3	1.144	0.884	2.374	250	overhead

In Table 6.5, the transformer parameters are given. Delta to grounded-wye transformers are most commonly used in North America with phase angle of the delta leading that of the wye. The three MVA rating values indicate the power ratings for the cases of natural cooling, fan cooling with a single fan, and fan cooling with dual fans, respectively. The impedances were calculated based on the lowest MVA rating and referred to the low voltage side, as described in Appendix 9.3.3.

Table 6.5: Transformer parameters of North American MV distribution network benchmark

Node from	Node to	Connection	V_1 [kV]	V_2 [kV]	Z_{tr}† [Ω]	S_{rated} [MVA]
0	1	3-ph Dyn1	115	12.47	0.010 + j1.24	15
0	12	3-ph Dyn1	115	12.47	0.013 + j1.55	12

† refers to V_2 side

To achieve power flows with acceptable voltages at each bus, tap changers are essential. The power flow results given in Appendix 9.2.3 make use of the following suggested specifications for a tap changing transformer:

- Primary: ±5 % in 2.5 % increment no-load taps.
- Secondary: ±10 % in 0.625 % increment load changing taps.

Table 6.6 gives the parameters of the equivalent HV network connected at the high voltage side of the substation transformers.

Table 6.6: HV-MV subtransmission equivalent network parameters of North American MV distribution network benchmark

Nominal system voltage [kV]	Short circuit power, S_{SC} [MVA]	R/X ratio
115	5000	0.1

6.1.3 Load Data

Load Data Table 6.7 gives the values of the coincident peak loads per phase for each node of the three-phase sections. Table 6.8 provides coincident peak load values for the residential single-phase subnetworks separately. Note that the appropriate coincidence factor is applied in Table 6.7. The coincidence factor is a function of the number of customers served. The use of coincidence factors is described in Appendix 9.3.4. Coincidence factors should also be used when the single-phase subnetworks are not modeled in detail but are instead reduced to a single equivalent load.

The load values given for nodes 1 and 12 are much larger than those given for the other nodes. These loads represent additional feeders served by the transformer and are not actually part of the feeder that is modeled in detail. This is made clear by the topology in Figure 6.1. Daily load profiles for residential and commercial or industrial loads are given in Figure 6.4.

Table 6.7: Load parameters of three-phase sections of North American MV distribution network benchmark

Node	Apparent Power, *S* [kVA]						Power Factor, *pf*	
	Phase A		Phase B		Phase C			
	Residential	Commercial or Industrial	Residential	Commercial or Industrial	Residential	Commercial or Industrial	Residential	Commercial or Industrial
1	5010	3070	4910	2570	3860	3520	0.93	0.87
2	100 + Subnetwork	200	50	300	200	300	0.95	0.85
3	---	80	200	80	50	80	0.90	0.80
4	200	---	100	---	100	---	0.90	---
5	200	50	Subnetwork	200	---	50	0.95	0.85
6	50	---	100	---	Subnetwork	---	0.95	---
7	---	100	100	100	---	100	0.95	0.95
8	100	---	150	---	---	200	0.90	0.90
9	100	---	150	---	100	---	0.95	---
10	150	---	100	---	250	---	0.90	---
11	50	150	50	150	---	150	0.95	0.85
12	1060	1260	1060	1260	1060	1260	0.90	0.87
13	Subnetwork	225	Subnetwork	225	---	225	0.95	0.85
14	---	90	---	90	Subnetwork	90	0.90	0.90

Table 6.8: Load parameters of single-phase sections of North American MV distribution network benchmark

Node	Apparent Power, *S* [kVA]	Power Factor, *pf*
1	15	0.90
2	15	0.95
3	15	0.90
4	15	0.90
5	10	0.95
6	50	0.95
7	50	0.95
8	10	0.95

Node	Apparent Power, S [kVA]	Power Factor, pf
9	50	0.95
10	15	0.90
11	10	0.95
12	10	0.95

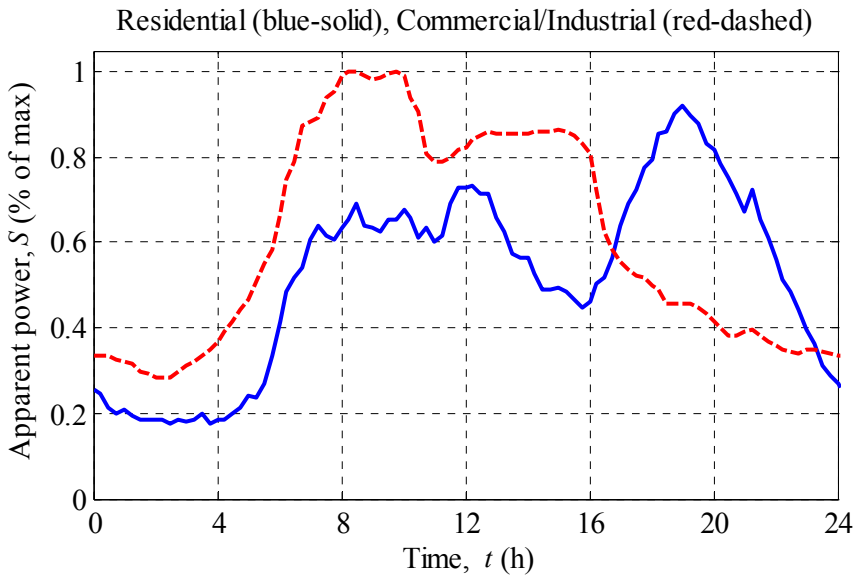

Figure 6.4: Daily load profiles of MV distribution network benchmark

6.2 European Configuration

Structure: European MV distribution feeders are three-phase and either of meshed or radial structure, with the latter dominating rural installations. The benchmark allows flexibility to model both meshed and radial structures. Each feeder includes numerous laterals at which MV/LV transformers would be connected. The nominal voltage is 20 kV. The system frequency is 50 Hz.

Symmetry: Efforts are typically made to balance the various low voltage laterals along the MV lines, but some unbalances are still typically experienced in practice. Unbalance is not explicitly included in the European benchmark, but it can be introduced if desired. Section 6.3 on flexibility provides further information.

Line types: Overhead lines are used with bare conductors made of aluminum with or without steel reinforcement, i.e. A1 or A1/S1A. Underground cables are XLPE with round, stranded aluminum conductors and copper tape shields.

Grounding: The grounding of the MV network largely depends on regional preferences. European networks are typically ungrounded or impedance-grounded.

6.2.1 Topology

The topology of the European version of the MV distribution network benchmark is shown in Figure 6.5. Framed by dashed lines are Feeders 1 and 2. Both feeders operate at 20 kV and

are fed via separate transformers from the 110 kV subtransmission network. Either feeder alone or both feeders can be used for studies of DER integration. Further variety can be introduced by means of configuration switches S1, S2, and S3. If these switches are open, then both feeders are radial. Closing S2 and S3 in feeder 1 creates a loop or mesh. With the given location of S1, it can either be assumed that both feeders are fed by the same substation or by different substations and closing S1 interconnects the two feeders through a distribution line. If different substations are assumed, then 110 kV subtransmission lines, such as those given in Section 5.3.4, should be used to connect the HV grid equivalent to each of the transformers.

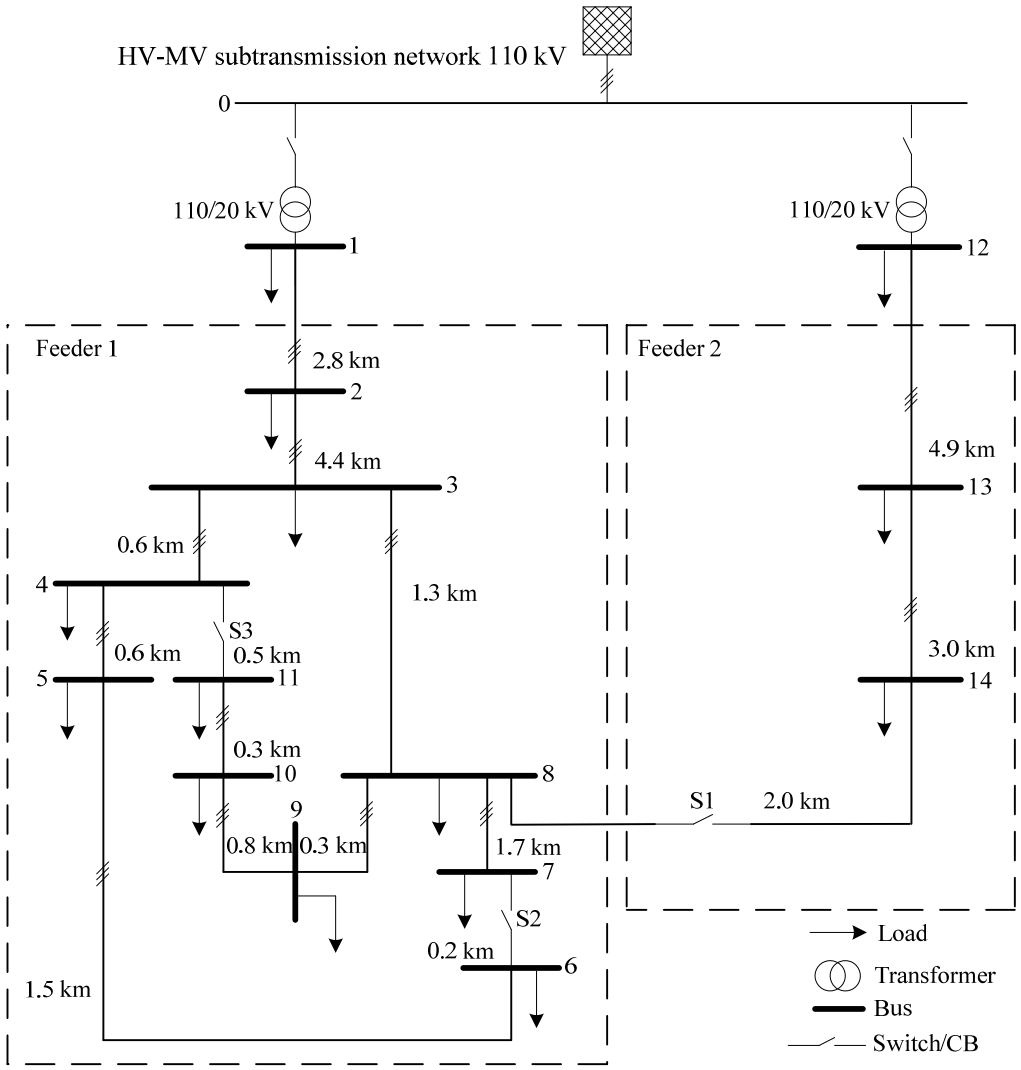

Figure 6.5: Topology of European MV distribution network benchmark

6.2.2 Network Data

In the European version of the benchmark, overhead lines are mounted on towers without neutral wires, and underground cables are tape-shielded and buried in back-filled trenches with a protective plate. Figure 6.6 and Table 6.9 give the geometries for the overhead lines and underground cables, from which line parameters can be derived. The types of conductors used in this benchmark are designated by the Conductor ID. The associated conductor parameters are provided in Table 6.10 for overhead and Table 6.11 for underground.

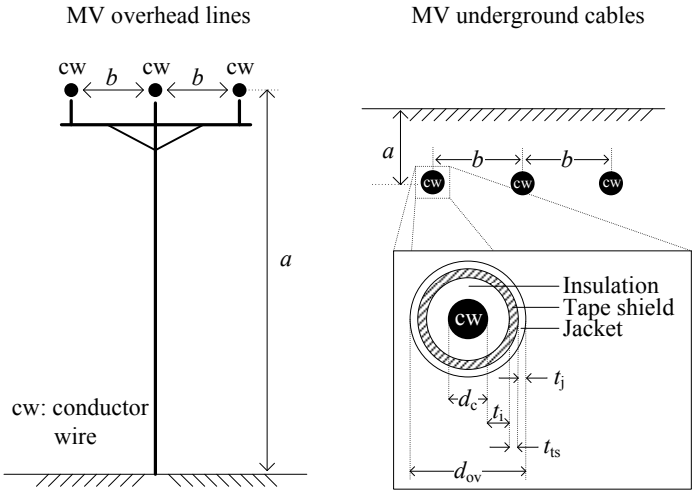

Figure 6.6: Geometry of overhead and underground lines of European MV distribution network benchmark

Table 6.9: Geometry of overhead and underground lines in European MV distribution network benchmark

Installation	*a*	*b*
	[m]	[m]
Overhead	9.5	1.0
Underground	0.7	0.3

Table 6.10: Conductor parameters of overhead lines of European MV distribution network benchmark

Conductor ID	Type	Stranding	Cross-sectional Area	d_c	*GMR*	R'_{dc} at 20 ºC	R'_{ac} at 50 ºC
			[mm^2]	[cm]	[cm]	[Ω/km]	[Ω/km]
1	A1	7	63	1.02	0.370	0.4545	0.5100

Note: Conductor type is designated using IEC notation as specified in IEC61089 [7].
Values of d_c, *GMR*, R'_{dc}, and R'_{ac} obtained from IEC61597 [8].

Table 6.11: Conductor parameters of underground lines of European MV distribution network benchmark

Conductor ID	Type	Stranding	Cross-sectional Area	d_c	*GMR*	R'_{dc} at 20 ºC	R'_{ac} at 90 ºC	t_i	t_j	t_{ts}	d_{ov}
			[mm^2]	[cm]	[cm]	[Ω/km]	[Ω/km]	[mm]	[mm]	[mm]	[mm]
2	NA2XS2Y	19	120	1.24	0.480	0.253	0.338	5.5	2.5	0.2	34.2

Note: Conductor type is designated using the German DIN VDE notation for underground cables. Values of d_c, R'_{dc}, R'_{ac}, t_i, t_j, t_{ts}, and d_{ov} obtained from Table 5.6.6b of [12] with stranding and *GMR* from Tables 3.6 and 3.12 of [16].

Table 6.12 lists the network topology and line lengths of the network of Figure 6.5 and provides the positive and zero sequence resistance, reactance and susceptance values of the lines, as calculated in Appendices 9.3.1 and 9.3.2.

Table 6.12: Connections and line parameters of European MV distribution network benchmark

Line segment	Node from	Node to	Conductor ID	R'_{ph} [Ω/km]	X'_{ph} [Ω/km]	B'_{ph} [μS/km]	R'_0 [Ω/km]	X'_0 [Ω/km]	B'_0 [μS/km]	l [km]	Installation
1	1	2	2	0.501	0.716	47.493	0.817	1.598	47.493	2.82	underground
2	2	3	2	0.501	0.716	47.493	0.817	1.598	47.493	4.42	underground
3	3	4	2	0.501	0.716	47.493	0.817	1.598	47.493	0.61	underground
4	4	5	2	0.501	0.716	47.493	0.817	1.598	47.493	0.56	underground
5	5	6	2	0.501	0.716	47.493	0.817	1.598	47.493	1.54	underground
6	6	7	2	0.501	0.716	47.493	0.817	1.598	47.493	0.24	underground
7	7	8	2	0.501	0.716	47.493	0.817	1.598	47.493	1.67	underground
8	8	9	2	0.501	0.716	47.493	0.817	1.598	47.493	0.32	underground
9	9	10	2	0.501	0.716	47.493	0.817	1.598	47.493	0.77	underground
10	10	11	2	0.501	0.716	47.493	0.817	1.598	47.493	0.33	underground
11	11	4	2	0.501	0.716	47.493	0.817	1.598	47.493	0.49	underground
12	3	8	2	0.501	0.716	47.493	0.817	1.598	47.493	1.30	underground
13	12	13	1	0.510	0.366	3.172	0.658	1.611	1.280	4.89	overhead
14	13	14	1	0.510	0.366	3.172	0.658	1.611	1.280	2.99	overhead
15	14	8	1	0.510	0.366	3.172	0.658	1.611	1.280	2.00	overhead

Table 6.13 gives the transformer parameters. The impedances calculated are referred to the secondary side, as described in Appendix 9.3.3.

Table 6.13: Transformer parameters of European MV distribution network benchmark

Node from	Node to	Connection	V_1 [kV]	V_2 [kV]	Z_{tr}† [Ω]	S_{rated} [MVA]
0	1	3-ph Dyn1	110	20	0.016+j1.92	25
0	12	3-ph Dyn1	110	20	0.016+j1.92	25

† refers to V_2 side

To achieve power flows with acceptable voltages at each bus, tap changers are essential. The power flow results given in Appendix 9.2.4 make use of the following suggested specifications for a tap changing transformer:

- Primary: ±5 % in 2.5 % increment no-load taps.
- Secondary: ±10 % in 0.625 % increment load changing taps.

Table 6.14 gives the parameters of the equivalent HV network connected at the high voltage side of the substation transformers.

Table 6.14: HV-MV subtransmission equivalent network parameters of European MV distribution network benchmark

Nominal system voltage [kV]	Short circuit power, S_{SC} [MVA]	R/X ratio
110	5000	0.1

6.2.3 Load Data

Table 6.15 gives the values of the coincident peak loads for each node of the benchmark. It is assumed that in the European version of the benchmark the loads are symmetric and therefore equal in all three phases. Note that the appropriate coincidence factor is applied in Table 6.15. The coincidence factor is a function of the number of customers served. The use of coincidence factors is described in Appendix 9.3.4.

Note that the load values given for nodes 1 and 12 are much larger than those given for the other nodes. These loads represent additional feeders served by the transformer and are not actually part of the feeder that is modeled in detail. This is made clear by the topology in Figure 6.5. Daily load profiles are given in Figure 6.4.

Table 6.15: Load parameters of European MV distribution network benchmark

Node	Apparent Power, *S* [kVA]		Power Factor, *pf*	
	Residential	Commercial / Industrial	Residential	Commercial / Industrial
1	15300	5100	0.98	0.95
2	---	---	---	---
3	285	265	0.97	0.85
4	445	---	0.97	---
5	750	---	0.97	---
6	565	---	0.97	---
7	---	90	---	0.85
8	605	---	0.97	---
9	---	675	---	0.85
10	490	80	0.97	0.85
11	340	---	0.97	---
12	15300	5280	0.98	0.95
13	---	40	---	0.85
14	215	390	0.97	0.85

6.3 Flexibility

For some studies, it may be of interest to evaluate the impact of a DER under different network conditions. Some guidelines on how to change various benchmark parameters are given in the following subsections. Interesting reference material may also be found in [13].

6.3.1 Voltage

The nominal base voltage of the MV benchmark networks are 12.47 kV for the North American and 20 kV for the European versions. Other voltages are possible, but the conductors, conductor spacing, tower configurations, transformers, etc. may all need to be adjusted appropriately. With this in mind, the base voltages may be modified to study different voltage levels as long as the chosen values are realistic.

6.3.2 Line Lengths

The line lengths as given in Table 6.3, Table 6.4, and Table 6.12 can be modified as long as voltage drops do not become excessive and a reasonable MV distribution network character is retained.

6.3.3 Line Types and Parameters

The MV distribution network benchmark uses overhead lines. It is also possible to use sections of underground cable or even to use an entire underground network. It would then be necessary to modify the line parameters in accordance with information supplied by cable manufacturers. Shunt capacitances are important in cable-based MV networks in order to provide appropriate reactive power compensation. Underground cables are mainly encountered in urban areas with high load densities.

6.3.4 Loads

Load values can be modified as necessary. If unbalanced loads are desired for the European MV distribution network benchmark, a load unbalance of ±10 % would be reasonable. Furthermore, LV subnetworks from Chapter 7 can replace the lumped loads used in this chapter.

6.3.5 Transformers for HV/MV Integration

If the MV distribution network benchmark is to be used to replace a load of the HV transmission network benchmark of Chapter 5, as was described in Section 5.3.4, an alternative to a subtransmission representation is to use a single transformer to step up the voltage to transmission levels. The data for such transformers are given for the North American and European MV distribution network benchmarks in Table 6.16 and Table 6.17, respectively. These transformers could thus substitute for those given above in Section 6.1.2 and Section 6.2.2.

Table 6.16: Suggested transformer parameters in lieu of subtransmission of North American HV-MV network benchmark integration

Node from	Node to	Connection	V_1	V_2	Z_{tr}†	S_{rated}
			[kV]	[kV]	[Ω]	[MVA]
0	1	3-ph Dyn1	230	12.47	0.12 + j1.24	15
0	12	3-ph Dyn1	230	12.47	0.16 + j1.55	12

† refers to V_2 side

Table 6.17: Suggested transformer parameters in lieu of subtransmission of European HV-MV network benchmark integration

Node from	Node to	Connection	V_1	V_2	Z_{tr}†	S_{rated}
			[kV]	[kV]	[Ω]	[MVA]
0	1	3-ph Dyn1	220	20	0.19+j1.91	25
0	12	3-ph Dyn1	220	20	0.19+j1.91	25

† refers to V_2 side

6.4 Case Study: DER in Medium Voltage Systems

The Gas Research Institute of the United States predicts that DER will capture about 30 % of the energy market by 2030. To support such a significant transition, it is important to develop an understanding of the behavior of DER in power electric networks. In the following study, it is shown how the medium voltage distribution network benchmark can be used to study the impact of DER on voltage profile and power flow patterns.

6.4.1 System Specification

The European version of the medium voltage distribution network benchmark described in Section 6.2 was used. The daily profiles of the loads listed in Table 6.15 are modeled as shown in Figure 6.4. The simulations were performed using the commercially available PSS^{TM} NETOMAC program. Generation and storage units were added at various nodes as listed in Table 6.18. The photovoltaic and wind turbine units are implemented as generation units with stochastic outputs and the residential fuel cells and combined heat and power (CHP) units are implemented as deterministic generation. The voltage at the primary transmission HV system is set at 220 kV. Topology of the network in which DER units are integrated is shown in Figure 6.7.

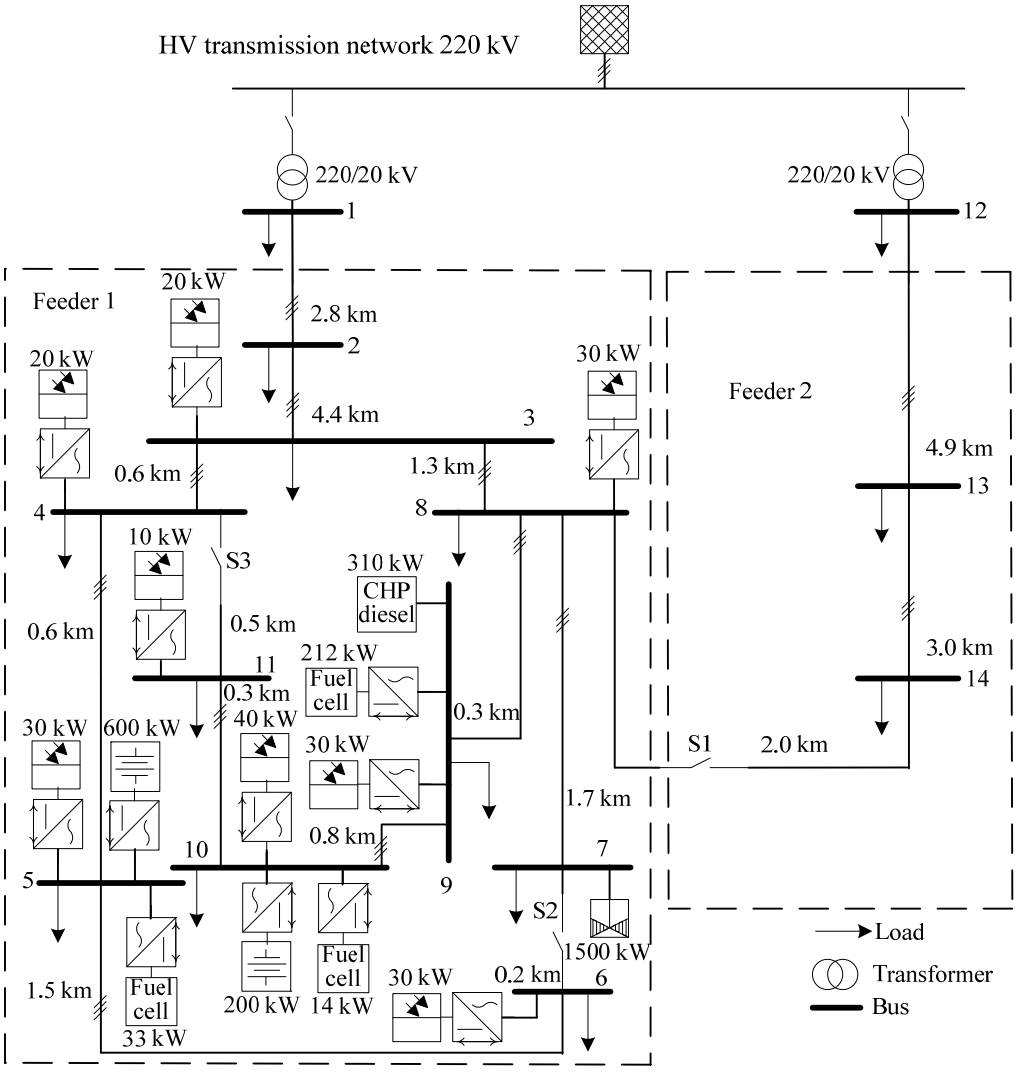

Figure 6.7: MV distribution network benchmark application example: model

Table 6.18: MV distribution network benchmark application example: parameters of DER units

Node	DER type	P_{max} [kW]
3	Photovoltaic	20
4	Photovoltaic	20
5	Photovoltaic	30
5	Battery	600
5	Residential fuel cell	33
6	Photovoltaic	30
7	Wind turbine	1500
8	Photovoltaic	30
9	Photovoltaic	30
9	CHP diesel	310
9	CHP fuel cell	212
10	Photovoltaic	40
10	Battery	200
10	Residential fuel cell	14
11	Photovoltaic	10

6.4.2 Simulation

Figure 6.8 shows the generation profiles of each DER type: wind turbine, photovoltaic array, battery, fuel cell, CHP fuel cell, and CHP diesel, respectively. During the test simulation only one wind turbine with the rated power of 1.5 MW was connected to the network. As the first subplot shows, the wind conditions through the whole simulation day were quite good. The second subplot gives the sum of the power production from photovoltaic arrays connected to the benchmark network. Characteristic for this generation group is its limited availability influenced by available sunlight.

The third subplot of Figure 6.8 gives the sum of the battery system outputs connected to the benchmark network. The state of the batteries was adjusted by a control system that either charges the batteries or injects power into the grid. The operation of the battery system can be controlled in many ways depending on the desired objective. For example, it can be used for peak shaving during peak loads or to avoid the need for DER output limitation in case of bottlenecks on the tie line. Those may occur during periods of low demand and high generation.

The fourth subplot of Figure 6.8 presents the sum of the outputs for the residential fuel cell units. The electrical power generated by each unit is actually higher than that plotted because some power is used to cover the demand of local loads and is therefore not injected into the grid. At the points where the power curve is negative, the electrical demand of the local load exceeds the local generation.

The simulation results for the fuel cell CHP and diesel CHP are presented in the last two subplots of Figure 6.8, respectively. Both units are used as local generation in industrial facilities. The operation of the diesel CHP is more flexible than the operation of the fuel cell CHP, as it can be switched on and off faster. Thus, diesel CHP can be quickly dispatched if there is peak load in the network.

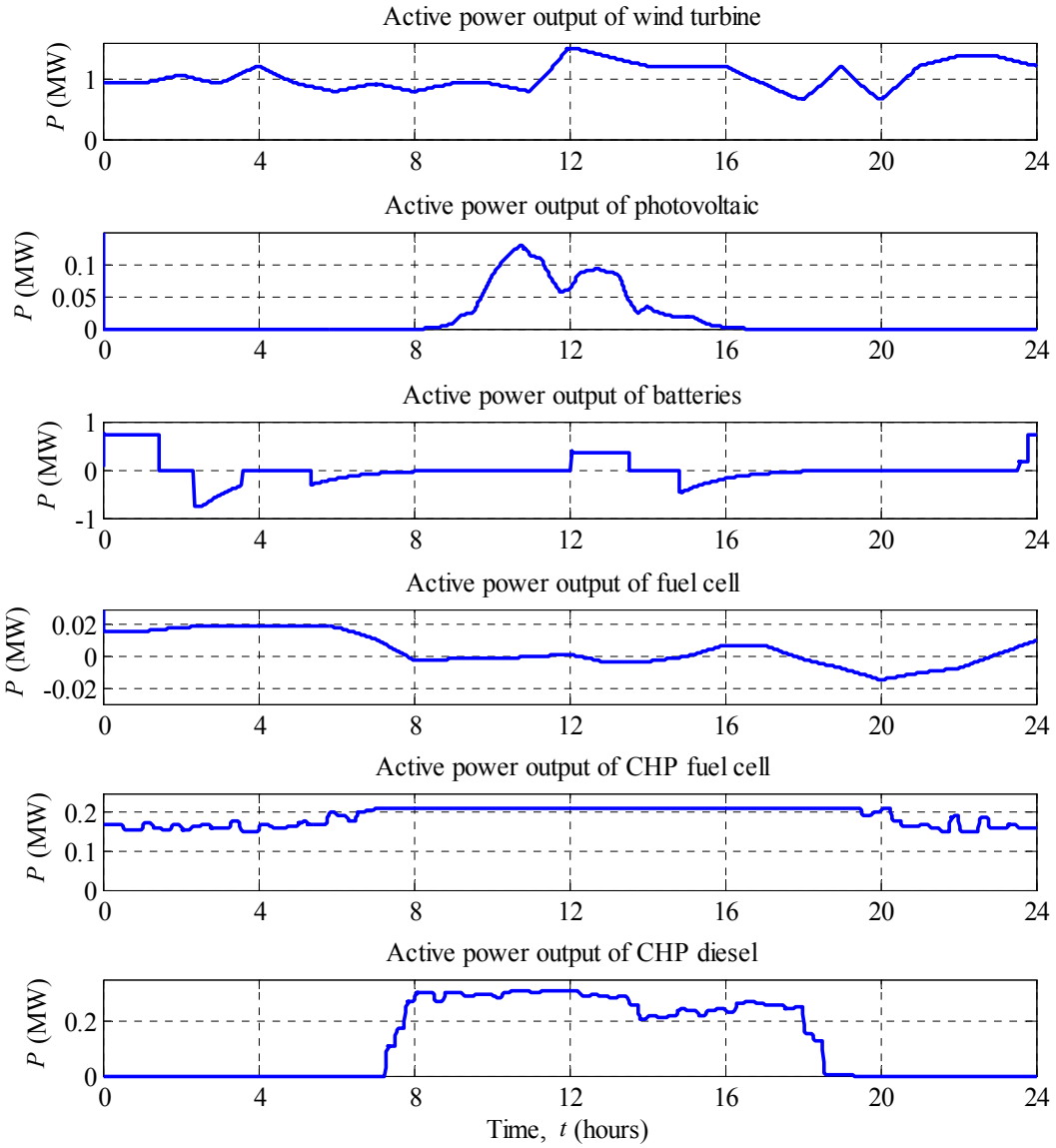

Figure 6.8: MV distribution network benchmark application example: power flow of diverse resources

The results in Figure 6.9 illustrate how the stressed system of the benchmark network can be improved by connecting DER units. The solid curve shows the result for the scenario without DER units connected to the network and the dashed curve shows the result for the scenario with DER as per Table 6.18. The top subplot of the figure shows power flow in the line connecting nodes 2 and 3; the second and third subplots show the voltage profile at nodes 3 and 11, respectively. Due to integration of DER units into the network, the voltage profile has been improved, but still at some points the voltage exceeds the acceptable limits. In the first part of the simulation time it can be seen that the power flow direction in the feeder is reversed and the voltage for this moment is too high. This situation occurs because the energy demand in the network is low at this moment and the generated energy from DER units is high. This situation is very interesting for investigations because the operation of the protection system can be well tested and new protection systems can be evaluated. Secondly, for such a situation with light loading and high DER generation, the application of a

decentralized energy management system (DEMS) and limitation of the DER output power may be needed.

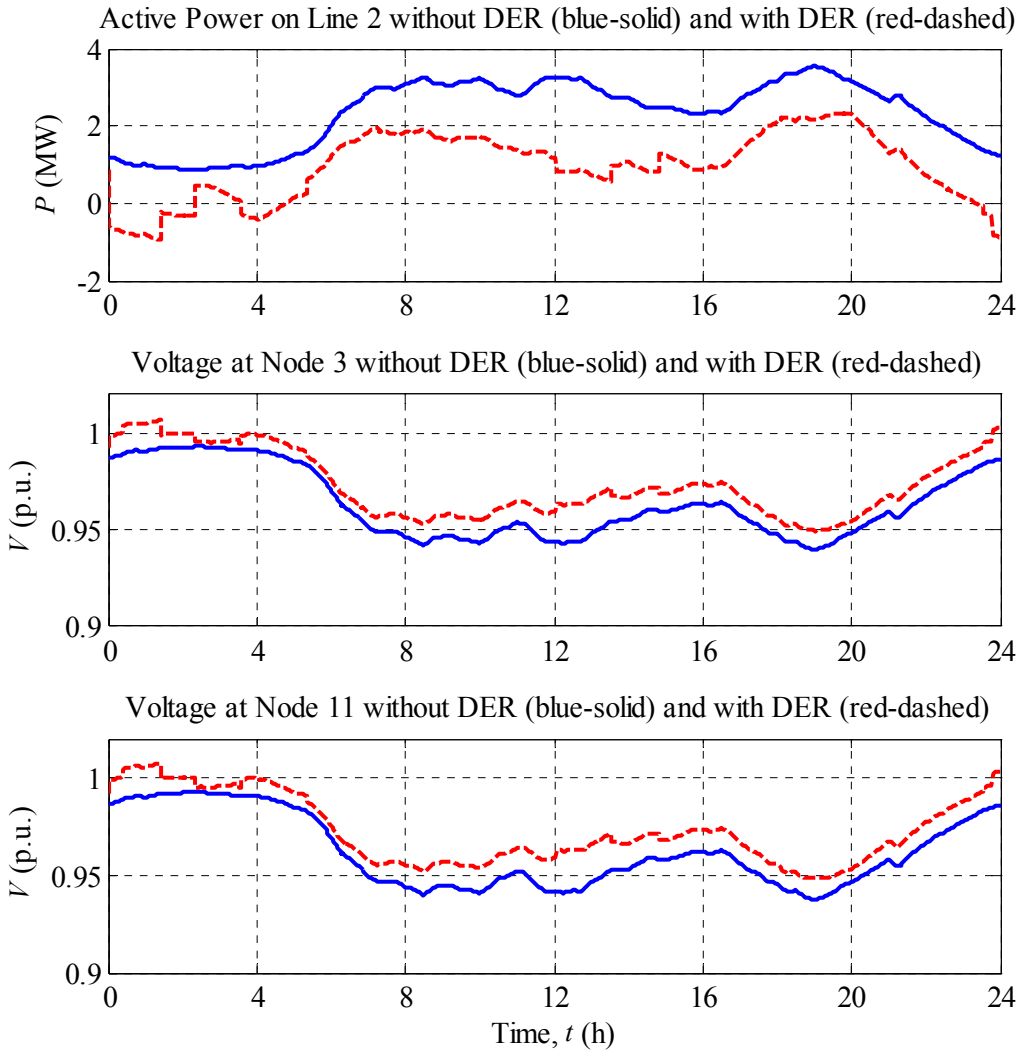

Figure 6.9: MV distribution network benchmark application example: modification of voltage profiles due to DER units

7. Low Voltage Distribution Network Benchmark

The low-voltage (LV) distribution benchmark network is representative of a real-world LV network while also supporting user friendliness and flexibility for studies of DER integration. The benchmark comprises three feeders of residential, industrial, and commercial character, respectively. Any combination of these lines may be used in studies. Note that the distribution installation common practices vary greatly between North America and Europe. A discussion of these differences is given in Appendix 9.1.

7.1 North American Configuration

Structure: Physical LV distribution networks typically originate from an MV/LV transformer and are of radial structure. The LV distribution network may include one or multiple lines. Consumers are connected anywhere along the lines. The system frequency is 60 Hz.

Symmetry: The connection of single-phase consumers makes LV distribution networks inherently unbalanced. While effort is made to reduce the unbalance, single-phase lines may exist.

Line types: LV network lines are either underground, mainly encountered in urban areas with a high load density, or overhead as mainly encountered in rural areas with a comparatively low load density. Variations do exist. Underground cables are usually enclosed in either metallic or galvanized conduit.

Grounding: The grounding of the LV network largely depends on regional preferences. In North American LV distribution networks grounding are often of the TN type. The first letter T implies that the neutral of the transformer is connected to ground. The second letter N implies that the frame of the application being supplied is connected to neutral.

7.1.1 Topology

The topology of the North American benchmark version is shown in Figure 7.1. It is composed of three subnetworks as typically laid out to supply loads of respectively residential, light industrial, and light commercial character.

7.1.2 Network Data

The physical geometry of distribution lines of a typical North American LV network is shown in Figure 7.2, and the specifications are given in Table 7.1 and Table 7.2. Overhead lines are shown in the top half of the figure. MV overhead lines are also included in the figure for reference because LV overhead lines are usually mounted on the same poles as used for MV lines.

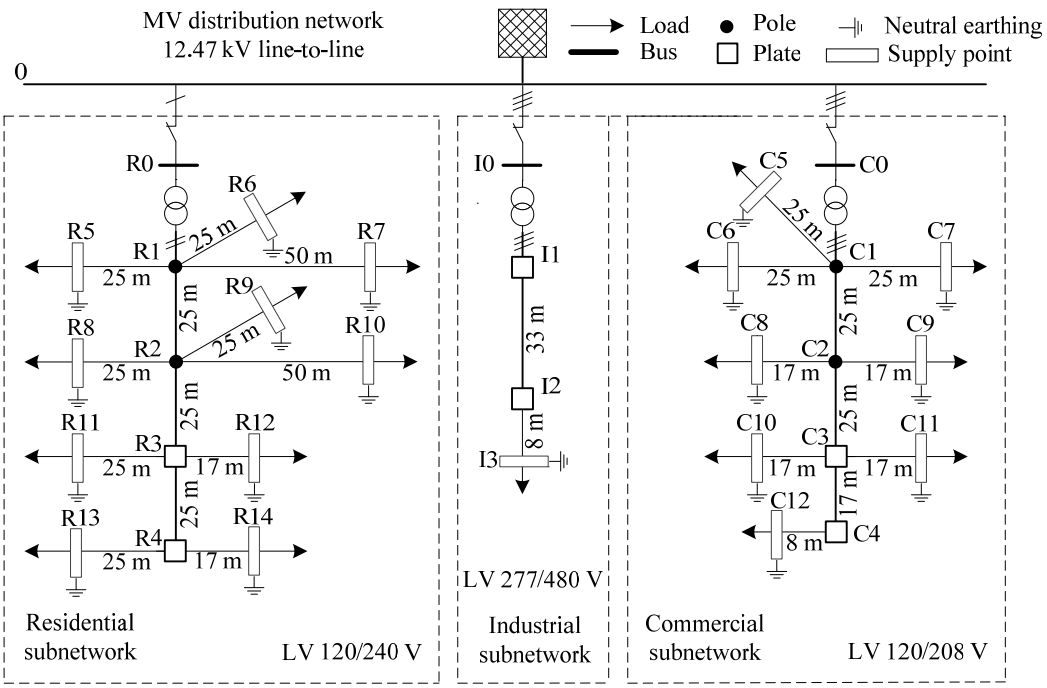

Figure 7.1: Topology of North American LV distribution network benchmark

In the case of single-phase overhead lines, the MV is stepped down with a single-phase MV/LV transformer mounted on the pole between the MV and LV lines, as depicted in Figure 7.2. The single-phase LV line is a set of three bundled conductors shown as the bottom group of conductors on the top left quadrant of Figure 7.2.

Three-phase overhead lines have a similar configuration, with the MV lines located at the top of the structure, and the LV lines as a set of bundled conductors below. In this case, three single-phase transformers step down voltage from the MV to the LV level. This is shown in the top right quadrant of Figure 7.2. For underground LV distribution, sets of bundled conductors are employed similarly to the overhead case, as shown in the bottom half of Figure 7.2.

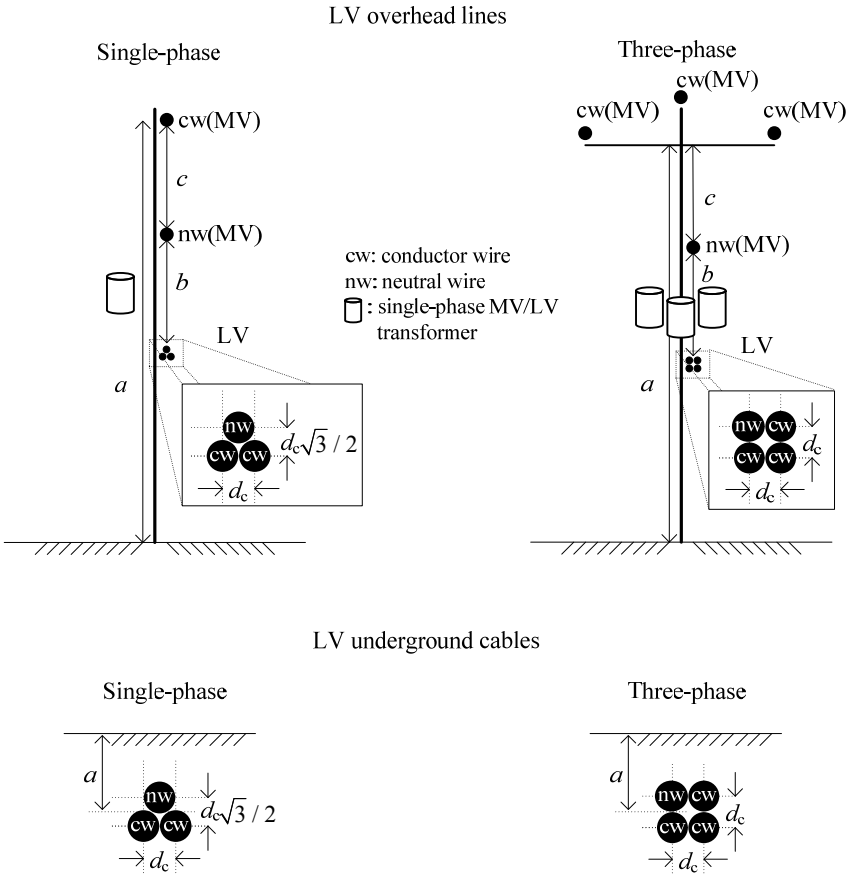

Figure 7.2: Geometry of overhead and underground lines of North American LV distribution network benchmark

Table 7.1: Geometry of overhead lines of North American LV distribution network benchmark

Conductor ID	Type	Size [kcmil or AWG]	Number of strands	d_c [cm]	R'_{ac} at 90 ºC [Ω/km]	*GMR* [cm]	*a* [m]	*b* [m]	*c* [m]
OH1	Al	750	61	2.53	0.102	0.957	13.72	2.13	2.13
OH2	Al	350	37	1.73	0.209	0.650	13.72	2.13	2.13
OH3	Al	2	7	0.74	1.092	0.267	13.72	2.13	2.13

Note: Values of stranding, R'_{ac}, and *GMR* are obtained from Table 3.10 [16] with d_c from Table 3.6 [16].

Table 7.2: Geometry of underground lines of North American LV distribution network benchmark

Conductor ID	Type	Size [kcmil or AWG]	Number of strands	d_c [cm]	R'_{ac} at 90 ºC [Ω/km]	*GMR* [cm]	*a* [m]
UG1	Al	750	61	2.53	0.102	0.957	0.90
UG2	Al	500	37	2.06	0.148	0.775	0.90
UG3	Al	4/0	19	1.34	0.343	0.500	0.90
UG4	Al	2	7	0.74	1.092	0.267	0.90

See notes at bottom of Table 7.1.

In what follows, benchmark network data are organized in a number of tables. Table 7.3, Table 7.4, and Table 7.5 give the line installation data of residential, industrial, and

commercial subnetworks, respectively. The Conductor ID given in the fourth columns refers to the conductor specifications given in Table 7.1 and Table 7.2.

Table 7.3: Connections and line parameters of residential feeder of North American LV distribution network benchmark

Line segment	Node from	Node to	Conductor ID	*L* [m]	Installation
1	R1	R2	OH2	25	OH 1-ph
2	R2	R3	UG3	25	UG 1-ph
3	R3	R4	UG3	25	UG 1-ph
4	R1	R5	OH3	25	OH 1-ph
5	R1	R6	OH3	25	OH 1-ph
6	R1	R7	OH3	50	OH 1-ph
7	R2	R8	OH3	25	OH 1-ph
8	R2	R9	OH3	25	OH 1-ph
9	R2	R10	OH3	50	OH 1-ph
10	R3	R11	UG4	17	UG 1-ph
11	R3	R12	UG4	25	UG 1-ph
12	R4	R13	UG4	17	UG 1-ph
13	R4	R14	UG4	25	UG 1-ph

Table 7.4 Connections and line parameters of industrial feeder of North American LV distribution network benchmark

Line segment	Node from	Node to	Conductor ID	*l* [m]	Installation
1	I1	I2	UG1	33	UG 3-ph
2	I2	I3	UG2	8	UG 3-ph

Table 7.5: Connections and line parameters of commercial feeder of North American LV distribution network benchmark

Line segment	Node from	Node to	Conductor ID	*l* [m]	Installation
1	C1	C2	OH1	25	OH 3-ph
2	C2	C3	UG3	25	UG 3-ph
3	C3	C4	UG3	17	UG 3-ph
4	C1	C5	OH3	25	OH 3-ph
5	C1	C6	OH3	25	OH 3-ph
6	C1	C7	OH3	25	OH 3-ph
7	C2	C8	OH3	17	OH 3-ph
8	C2	C9	OH3	17	OH 3-ph
9	C3	C10	UG4	17	UG 3-ph
10	C3	C11	UG4	17	UG 3-ph
11	C4	C12	UG4	8	UG 3-ph

Table 7.6 to Table 7.9 give phase impedance matrices after Kron reduction for overhead and underground lines, both for single-phase and three-phase networks. The effect of the neutral wire is included in the calculations based on the method presented in the Appendix. When using simulators where the neutral wires are not explicitly available in the line model library,

the phase impedance matrices after Kron reduction are particularly useful. That way, the effect of the neutral wire on phase conductors is included. Due to the short lengths of lines, capacitances per unit length are neglected.

Table 7.6: Phase impedance matrices of single-phase overhead lines of North American LV distribution network benchmark

Conductor ID/ Installation		Phase impedance matrix after Kron reduction [Ω/km]	
		A_1	A_2
OH2 / 1-ph	A_1	0.371 + j0.191	0.162 + j0.109
	A_2	0.162 + j0.109	0.371 + j0.191
OH3 / 1-ph	A_1	1.487 + j0.588	0.395 + j0.493
	A_2	0.395 + j0.493	1.487 + j0.588

Table 7.7: Phase impedance matrices of three-phase overhead lines of North American LV distribution network benchmark

Conductor ID/ Installation		Phase impedance matrix after Kron reduction [Ω/km]		
		A	B	C
OH1 / 3-ph	A	0.185 + j0.159	0.080 + j0.104	0.083 + j0.054
	B	0.080 + j0.104	0.180 + j0.205	0.080 + j0.104
	C	0.083 + j0.054	0.080 + j0.104	0.185 + j0.159
OH3 / 3-ph	A	1.487 + j0.588	0.384 + j0.504	0.395 + j0.467
	B	0.384 + j0.504	1.465 + j0.609	0.384 + j0.504
	C	0.395 + j0.467	0.384 + j0.504	1.487 + j0.588

Table 7.8: Phase impedance matrices of single-phase underground lines of North American LV distribution network benchmark

Conductor ID/ Installation		Phase impedance matrix after Kron reduction [Ω/km]	
		A_1	A_2
UG3 / 1-ph	A_1	0.587 + j0.248	0.244 + j0.163
	A_2	0.244 + j0.163	0.587 + j0.248
UG4 / 1-ph	A_1	1.486 + j0.589	0.394 + j0.493
	A_2	0.394 + j0.493	1.486 + j0.589

Table 7.9: Phase impedance matrices of three-phase underground lines of North American LV distribution network benchmark

Conductor ID/ Installation		Phase impedance matrix after Kron reduction [Ω/km]		
		A	B	C
UG1 / 3-ph	A	0.185 + j0.159	0.080 + j0.104	0.083 + j0.054
	B	0.080 + j0.104	0.180 + j0.205	0.080 + j0.104
	C	0.083 + j0.054	0.080 + j0.104	0.185 + j0.159
UG2 / 3-ph	A	0.266 + j0.172	0.115 + j0.114	0.118 + j0.065
	B	0.115 + j0.114	0.259 + j0.217	0.115 + j0.114
	C	0.118 + j0.0651	0.115 + j0.114	0.266 + j0.172
UG3 / 3-ph	A	0.587 + j0.248	0.237 + j0.183	0.244 + j0.137
	B	0.237 + j0.183	0.573 + j0.288	0.237 + j0.183
	C	0.244 + j0.137	0.237 + j0.183	0.587 + j0.248
UG4 / 3-ph	A	1.486 + j0.589	0.383 + j0.504	0.394 + j0.467
	B	0.383 + j0.504	1.465 + j0.609	0.383 + j0.504
	C	0.394 + j0.467	0.383 + j0.504	1.486 + j0.589

Table 7.10 to Table 7.13 provide primitive impedance matrices for overhead and underground lines, both for single-phase and three-phase networks. The primitive impedance matrices are calculated based on the presented method in the Appendix. As opposed to the phase impedance matrices, these primitive matrices can be used when the line models in the library of simulators have a neutral wire included.

Table 7.10: Primitive impedance matrices of single-phase overhead lines of North American LV distribution network benchmark

Conductor ID/ Installation		The primitive impedance matrix [Ω/km]		
		A_1	A_2	N
OH2 / 1-ph	A_1	0.268 + j0.888	0.059 + j0.806	0.059 + j0.806
	A_2	0.059 + j0.806	0.268 + j0.888	0.059 + j0.806
	N	0.059 + j0.806	0.059 + j0.806	0.268 + j0.888
OH3 / 1-ph	A_1	1.151 + j0.955	0.059 + j0.860	0.059 + j0.860
	A_2	0.059 + j0.860	1.151 + j0.955	0.059 + j0.860
	N	0.059 + j0.860	0.059 + j0.860	1.151 + j0.955

Table 7.11: Primitive impedance matrices of three-phase overhead lines of North American LV distribution network benchmark

Conductor ID/ Installation		The primitive impedance matrix [Ω/km]			
		A	B	C	N
OH1 / 3-ph	A	0.161 + j0.859	0.059 + j0.780	0.059 + j0.754	0.059 + j0.780
	B	0.059 + j0.780	0.161 + j0.859	0.059 + j0.780	0.059 + j0.754
	C	0.059 + j0.754	0.059 + j0.780	0.161 + j0.859	0.059 + j0.780
	N	0.059 + j0.780	0.059 + j0.754	0.059 + j0.780	0.161 + j0.859
OH3 / 3-ph	A	1.151 + j0.955	0.059 + j0.860	0.059 + j0.834	0.059 + j0.860
	B	0.059 + j0.860	1.151 + j0.955	0.059 + j0.860	0.059 + j0.834
	C	0.059 + j0.834	0.059 + j0.860	1.151 + j0.955	0.059 + j0.860
	N	0.059 + j0.860	0.059 + j0.834	0.059 + j0.860	1.151 + j0.955

Table 7.12: Primitive impedance matrices of single-phase underground lines of North American LV distribution network benchmark

Conductor ID/ Installation		The primitive impedance matrix [Ω/km]		
		A_1	A_2	N
UG3 / 1-ph	A_1	0.402 + j0.908	0.059 + j0.823	0.059 + j0.823
	A_2	0.059 + j0.823	0.402 + j0.908	0.059 + j0.823
	N	0.059 + j0.823	0.059 + j0.823	0.402 + j0.908
UG4 / 1-ph	A_1	1.151 + j0.955	0.059 + j0.860	0.059 + j0.860
	A_2	0.059 + j0.860	1.151 + j0.955	0.059 + j0.860
	N	0.059 + j0.860	0.059 + j0.860	1.151 + j0.955

Table 7.13: Primitive impedance matrices of three-phase underground lines of North American LV distribution network benchmark

Conductor ID/ Installation		The primitive impedance matrix [Ω/km]			
		A	B	C	N
UG1 / 3-ph	A	0.161 + j0.859	0.059 + j0.780	0.059 + j0.754	0.059 + j0.780
	B	0.059 + j0.780	0.161 + j0.859	0.059 + j0.780	0.059 + j0.754
	C	0.059 + j0.754	0.059 + j0.780	0.161 + j0.859	0.059 + j0.780
	N	0.059 + j0.780	0.059 + j0.754	0.059 + j0.780	0.161 + j0.859
UG2 / 3-ph	A	0.207 + j0.875	0.059 + j0.794	0.059 + j0.768	0.059 + j0.794
	B	0.059 + j0.794	0.207 + j0.875	0.059 + j0.794	0.059 + j0.768
	C	0.059 + j0.768	0.059 + j0.794	0.207 + j0.875	0.059 + j0.794
	N	0.059 + j0.794	0.059 + j0.768	0.059 + j0.794	0.207 + j0.875
UG3 / 3-ph	A	0.402 + j0.908	0.059 + j0.823	0.059 + j0.797	0.059 + j0.823
	B	0.059 + j0.823	0.402 + j0.908	0.059 + j0.823	0.059 + j0.797
	C	0.059 + j0.797	0.059 + j0.823	0.402 + j0.908	0.059 + j0.823
	N	0.059 + j0.823	0.059 + j0.797	0.059 + j0.823	0.402 + j0.908
UG4 / 3-ph	A	1.151 + j0.955	0.059 + j0.860	0.059 + j0.834	0.059 + j0.860
	B	0.059 + j0.860	1.151 + j0.955	0.059 + j0.860	0.059 + j0.834
	C	0.059 + j0.834	0.059 + j0.860	1.151 + j0.955	0.059 + j0.860
	N	0.059 + j0.860	0.059 + j0.834	0.059 + j0.860	1.151 + j0.955

A detailed schematic of the electrical connections of this center-tapped single-phase transformer is depicted for the residential system in Figure 7.3. A detailed schematic of the electrical connections of a transformer for the industrial system is presented in Figure 7.4. Figure 7.5 shows the electrical connections of a three-phase transformer for the commercial system underground lines.

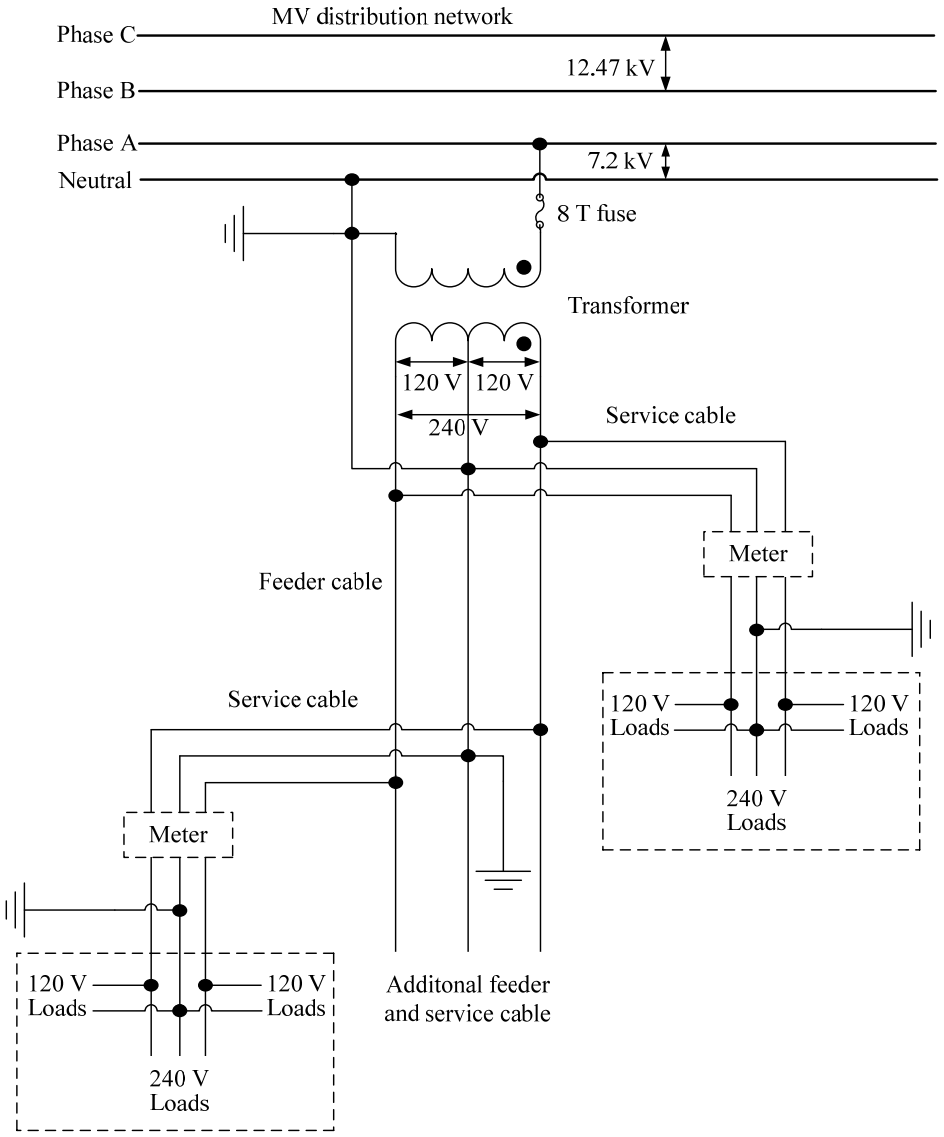

Figure 7.3: Residential transformer, load, and grounding connections of North American LV distribution network benchmark

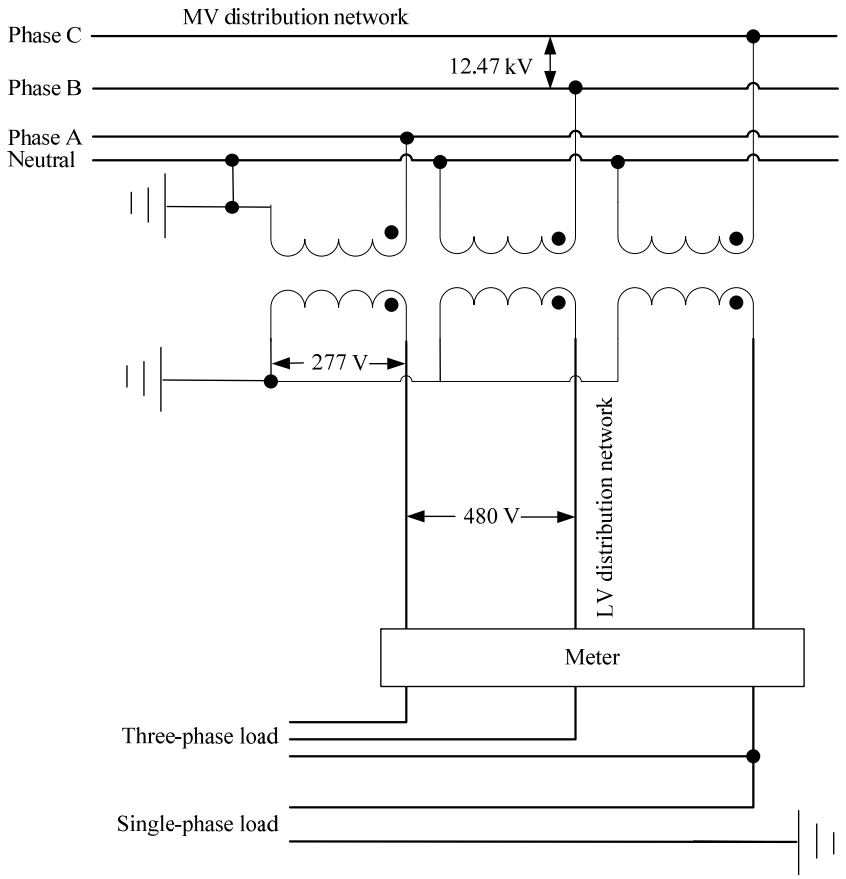

Figure 7.4: Industrial transformer, load, and grounding connections of North American LV distribution network benchmark

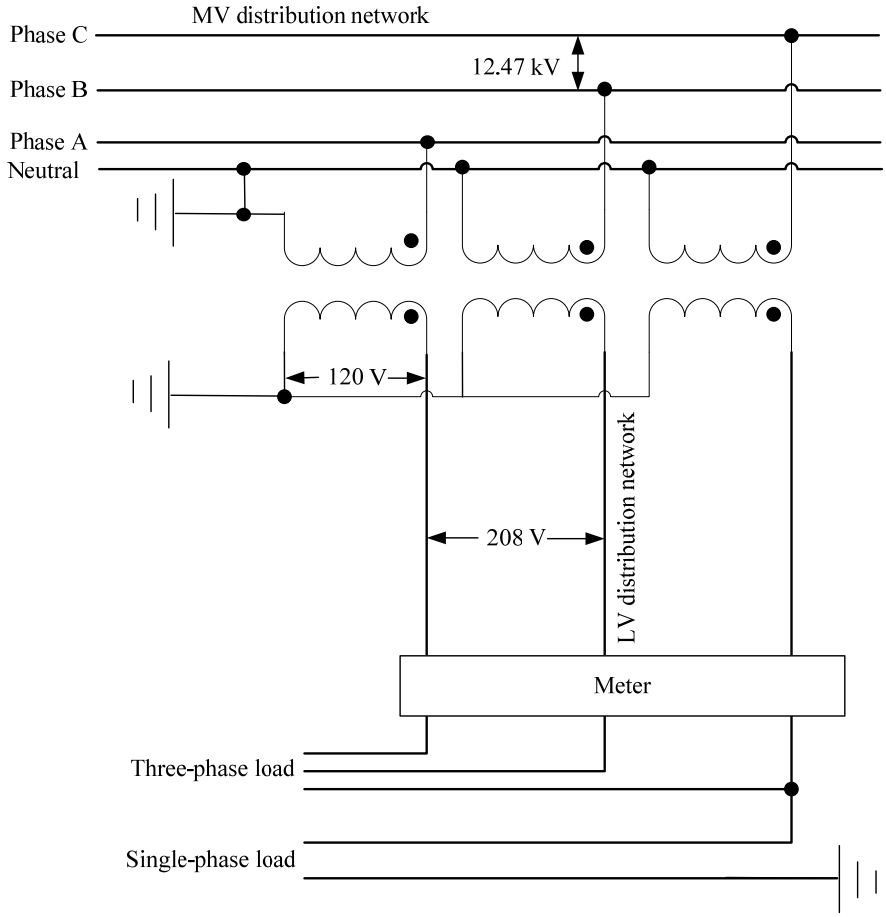

Figure 7.5: Commercial transformer, load, and grounding connections of North American LV distribution network benchmark

Table 7.14 gives the grounding impedances for both poles and transformers. The data of the subnetwork MV/LV distribution transformers are given in Table 7.15. The data for the MV network voltage and short circuit power are given in Table 7.16.

Table 7.14: Grounding impedances of North American LV distribution network benchmark

Pole grounding impedance, Z_{pole}	Transformer grounding impedance, Z_{tx}
[Ω]	[Ω]
3	3

Table 7.15: Transformer parameters of North American LV distribution network benchmark

Node from	Node to	Connection	V_1	V_2	Z_{tr}†	S_{rated}
			[kV]	[kV]	[Ω]	[kVA]
R0	R1	1-phase both sides grounded	7.2 LN	0.240 LL center tapped	0.0144 + j0.0249	50
I0	I1	3-ph YNyn0	12.47 LL	0.480 LL	0.0154 + j0.0266	300
C0	C1	3-ph YNyn0	12.47 LL	0.208 LL	0.0048 + j0.0083	3 x 37.5

† refers to V_2 side

Table 7.16: MV distribution network parameters of North American LV distribution network benchmark

Nominal system voltage	Short circuit power, S_{SC}	R/X ratio
[kV]	[MVA]	
12.47 LL	100	1

7.1.3 Load Data

Table 7.17 gives the values of the coincident peak loads for each node of the benchmark. The single-phase values assume 120 V loads balanced across the center tapped transformer as was shown in Figure 7.3. Each load represents a group of users. Note that the appropriate coincidence factor was applied in Table 7.17. The coincidence factor is a function of the number of customers served. The use of coincidence factors is described in Appendix 9.3.4.

Table 7.17: Load parameters of North American LV distribution network benchmark

Node	Apparent Power, *S* [kVA]			Power Factor, *pf*
	Phase A	Phase B	Phase C	
R5	6.6	N/A	N/A	0.90
R6	4.6	N/A	N/A	0.90
R7	6.6	N/A	N/A	0.90
R8	4	N/A	N/A	0.95
R9	2.6	N/A	N/A	0.95
R10	4.6	N/A	N/A	0.95
R11	3.3	N/A	N/A	0.95
R12	4.6	N/A	N/A	0.90
R13	6.6	N/A	N/A	0.90
R14	5.3	N/A	N/A	0.90
I3	200			0.85
C5	10.1			0.90
C6	13.5			0.90
C7	16.9			0.85
C8	13.5			0.90
C9	16.9			0.95
C10	10.1			0.95
C11	16.9			0.95
C12	10.1			0.90

Daily load profiles for residential, industrial, and commercial loads are given in Figure 7.6.

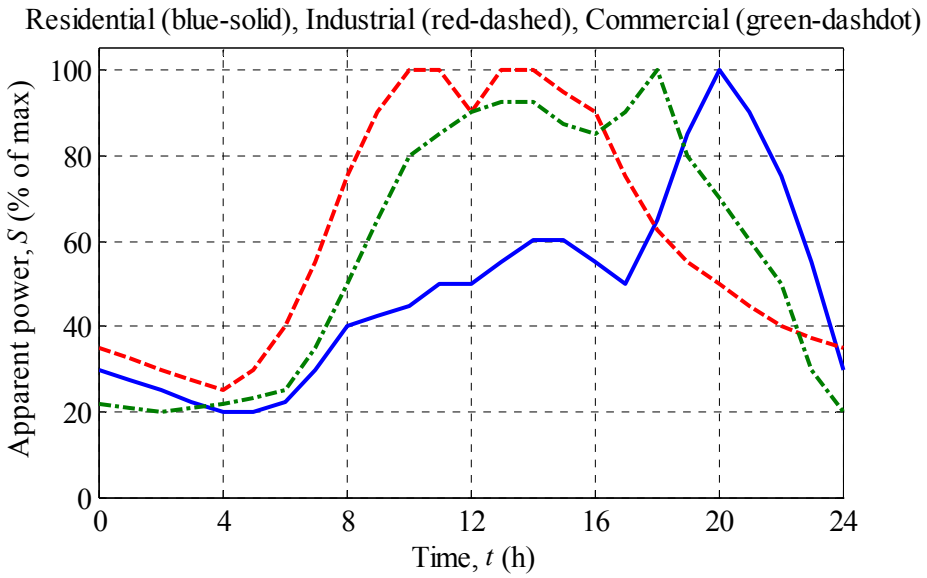

Figure 7.6: Daily load profiles of LV distribution network benchmark

7.2 European Configuration

Structure: Physical LV distribution networks typically originate from an MV/LV transformer and are of radial structure. The LV distribution network may include one or multiple lines. Consumers are connected anywhere along the lines. The system frequency is 50 Hz.

Symmetry: The connection of single-phase consumers makes LV distribution networks inherently unbalanced. Effort is made to reduce the unbalance.

Line types: LV network lines are either underground, mainly encountered in urban areas with a high load density, or overhead as mainly encountered in rural areas with a comparatively low load density. Overhead lines are mainly constructed with bare conductors made of Al. Variations do exist. Cables are usually enclosed in either metallic or galvanized conduit.

Grounding: The grounding of the LV network largely depends on regional preferences. Using the classification of IEC 60364 [14], public LV networks are often of the TN type or the TT type. The first letter T implies that the neutral of the transformer is connected to ground. The second letter N implies that the frame of the application being supplied is connected to neutral. The second letter T implies that the frame of the application being supplied is connected to ground locally. Variations of the TN type exist, and more information on the topic is provided in [15].

7.2.1 Topology

The topology of the European benchmark version is shown in Figure 7.7. Framed by dashed lines are residential, industrial, and commercial sector subnetworks. Studies may comprise any combination of the three subnetworks depending on the status of the configuration switches S1, S2, and S3. In residential and industrial subnetworks, underground cables are used, while in the commercial subnetwork, connections are made through overhead lines. In the commercial subnetwork, the locations of the poles are indicated as circles. All paths shown are realized through three phases.

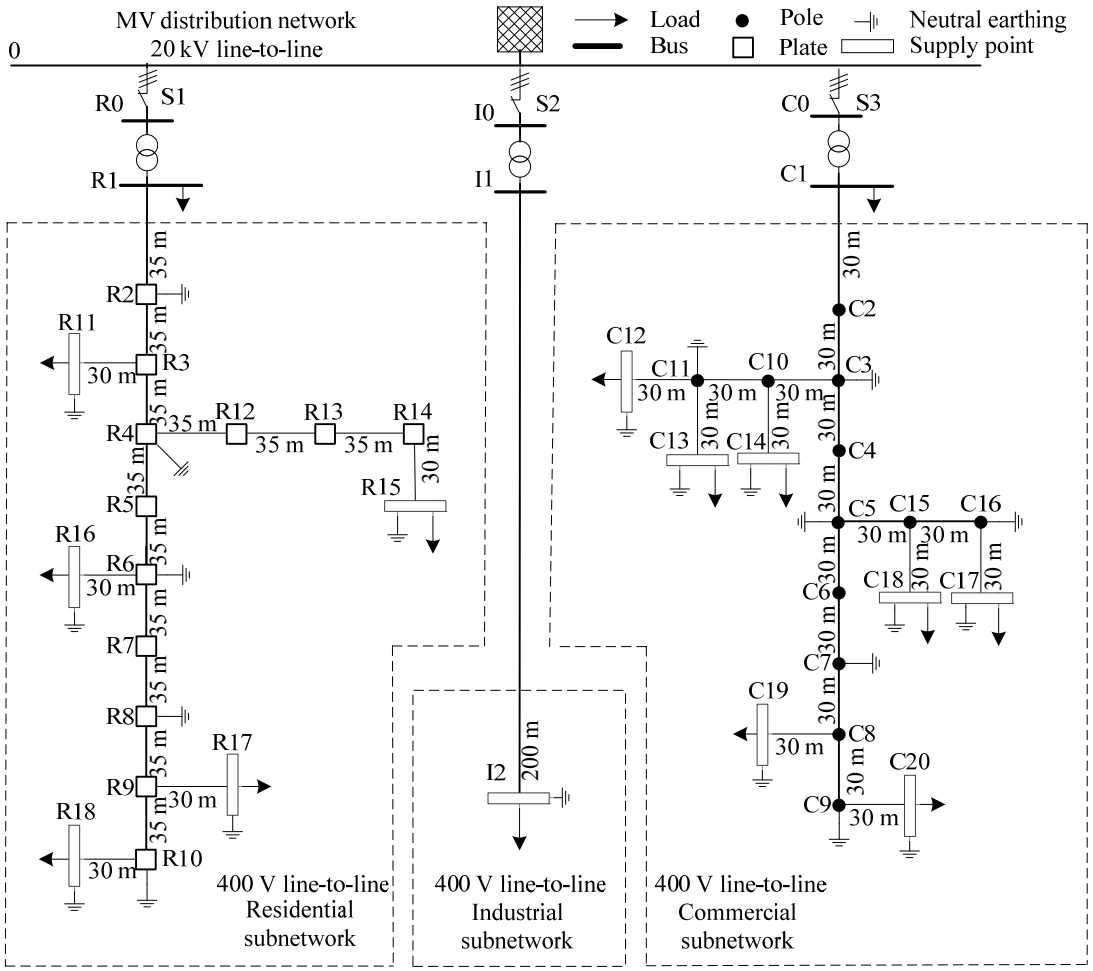

Figure 7.7: Topology of European LV distribution network benchmark

7.2.2 Network Data

The physical geometry of both overhead and underground lines for a typical European LV network is shown in Figure 7.8, and specifications are given in Table 7.18 and Table 7.19. It is worth noting that a separate pole structure may not always be used for European LV lines. Streetlight poles and building walls may also be used [16].

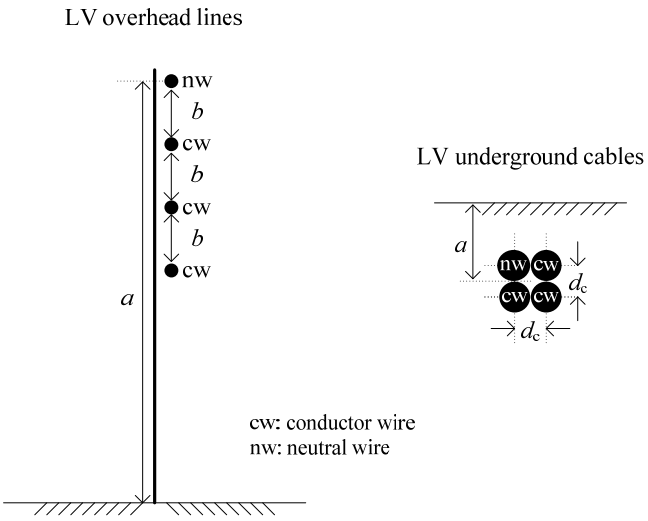

Figure 7.8: Geometry of overhead and underground lines of European LV distribution network benchmark

Table 7.18: Geometry of overhead lines of European LV distribution network benchmark

Conductor ID	Type	Size	Number of strands	d_c	R'_{ac} at 50 ºC	*GMR*	*a*	*b*
		[mm^2]		[cm]	[Ω/km]	[cm]	[m]	[m]
OH1	Al	70	19	1.05	0.491	0.398	8	0.3
OH2	Al	25	7	0.63	1.320	0.228	8	0.3
OH3	Al	16	7	0.51	2.016	0.185	8	0.3

Note: Conductor type is designated using the German DIN notation for overhead bare conductors. Stranding and d_c are obtained from data sheet of overhead line conductors of Südkabel. R'_{ac} is calculated based on the equation given in the Appendix. *GMR* is obtained from Table 2.6 of [16].

Table 7.19: Geometry of underground lines of European LV distribution network benchmark

Conductor ID	Type	Size	Number of strands	d_c	R'_{ac} at 90 ºC / 70 ºC†	*GMR*	*a*
		[mm^2]		[cm]	[Ω/km]	[cm]	[m]
UG1	NA2XY	240	1	1.75	0.162	0.634	0.90
UG2	NA2XY	150	1	1.38	0.265	0.501	0.90
UG3	NA2XY	50	1	0.80	0.822	0.289	0.90

Note: Conductor type is designated using the German DIN VDE notation for underground cables. Values of R'_{ac}, and d_c are obtained from Table 5.6.2 and Table 5.1.13 of [12] with stranding and *GMR* from Table 2.6 of [16].

In what follows, benchmark network data are organized in a number of tables. Table 7.20, Table 7.21, and Table 7.22 give line installation data of residential, industrial, and commercial subnetworks, respectively. Table 7.23 and Table 7.24 give phase impedance matrices after Kron reduction for overhead lines and underground cables, respectively. The effect of a neutral wire is included in the calculations based on the presented method in the Appendix. When neutral wires are not available in the line model library of a simulator, the phase impedance matrices after Kron reduction are particularly useful. The effect of the neutral wire on phase conductors is so included. Due to the short lengths of lines, capacitances per unit length are neglected.

Table 7.20: Connections and line parameters of residential feeder of European LV distribution network benchmark

Line segment	Node from	Node to	Conductor ID	l [m]	Installation
1	R1	R2	UG1	35	UG 3-ph
2	R2	R3	UG1	35	UG 3-ph
3	R3	R4	UG1	35	UG 3-ph
4	R4	R5	UG1	35	UG 3-ph
5	R5	R6	UG1	35	UG 3-ph
6	R6	R7	UG1	35	UG 3-ph
7	R7	R8	UG1	35	UG 3-ph
8	R8	R9	UG1	35	UG 3-ph
9	R9	R10	UG1	35	UG 3-ph
10	R3	R11	UG3	30	UG 3-ph
11	R4	R12	UG3	35	UG 3-ph
12	R12	R13	UG3	35	UG 3-ph
13	R13	R14	UG3	35	UG 3-ph
14	R14	R15	UG3	30	UG 3-ph
15	R6	R16	UG3	30	UG 3-ph
16	R9	R17	UG3	30	UG 3-ph
17	R10	R18	UG3	30	UG 3-ph

Table 7.21: Connections and line parameters of industrial feeder of European LV distribution network benchmark

Line segment	Node from	Node to	Conductor ID	l [m]	Installation
1	I1	I2	UG2	200	UG 3-ph

Table 7.22: Connections and line parameters of commercial feeder of European LV distribution network benchmark

Line segment	Node from	Node to	Conductor ID	l [m]	Installation
1	C1	C2	OH1	30	OH 3-ph
2	C2	C3	OH1	30	OH 3-ph
3	C3	C4	OH1	30	OH 3-ph
4	C4	C5	OH1	30	OH 3-ph
5	C5	C6	OH1	30	OH 3-ph
6	C6	C7	OH1	30	OH 3-ph
7	C7	C8	OH1	30	OH 3-ph
8	C8	C9	OH1	30	OH 3-ph
9	C3	C10	OH2	30	OH 3-ph
10	C10	C11	OH2	30	OH 3-ph
11	C11	C12	OH3	30	OH 3-ph
12	C11	C13	OH3	30	OH 3-ph
13	C10	C14	OH3	30	OH 3-ph
14	C5	C15	OH2	30	OH 3-ph
15	C15	C16	OH2	30	OH 3-ph
16	C15	C17	OH3	30	OH 3-ph

Line segment	Node from	Node to	Conductor ID	l [m]	Installation
17	C16	C18	OH3	30	OH 3-ph
18	C8	C19	OH3	30	OH 3-ph
19	C9	C20	OH3	30	OH 3-ph

Table 7.23: Phase impedance matrices of overhead lines of European LV distribution network benchmark

Conductor ID/ Installation		Phase impedance matrix after Kron reduction [Ω/km]		
		A	B	C
OH1 / 3-ph	A	0.616 + j0.588	0.131 + j0.306	0.141 + j0.245
	B	0.131 + j0.306	0.628 + j0.566	0.147 + j0.276
	C	0.141 + j0.245	0.147 + j0.276	0.650 + j0.527
OH2 / 3-ph	A	1.457 + j0.728	0.143 + j0.417	0.152 + j0.367
	B	0.143 + j0.417	1.469 + j0.720	0.159 + j0.405
	C	0.152 + j0.367	0.159 + j0.405	1.490 + j0.704
OH3 / 3-ph	A	2.137 + j0.776	0.125 + j0.453	0.133 + j0.406
	B	0.125 + j0.453	2.146 + j0.771	0.138 + j0.447
	C	0.133 + j0.406	0.138 + j0.447	2.163 + j0.762

Table 7.24: Phase impedance matrices of underground lines of European LV distribution network benchmark

Conductor ID/ Installation		Phase impedance matrix after Kron reduction [Ω/km]		
		A	B	C
UG1 / 3-ph	A	0.287 + j0.167	0.121 + j0.110	0.125 + j0.070
	B	0.121 + j0.110	0.279 + j0.203	0.121 + j0.110
	C	0.125 + j0.070	0.121 + j0.110	0.287 + j0.167
UG2 / 3-ph	A	0.455 + j0.204	0.185 + j0.146	0.190 + j0.107
	B	0.185 + j0.146	0.444 + j0.238	0.185 + j0.146
	C	0.190 + j0.107	0.185 + j0.146	0.455 + j0.204
UG3 / 3-ph	A	1.152 + j0.458	0.321 + j0.390	0.330 + j0.359
	B	0.321 + j0.390	1.134 + j0.477	0.321 + j0.390
	C	0.330 + j0.359	0.321 + j0.390	1.152 + j0.458

Table 7.25 and Table 7.26 provide primitive matrices for overhead lines and underground cables, respectively. The primitive impedance matrices are calculated based on the method in the Appendix. As opposed to the phase impedance matrices, these primitive matrices can be used when the line models in the library of simulators have a neutral wire included.

Table 7.25: Primitive impedance matrices of overhead lines of European LV distribution network benchmark

Conductor ID/ Installation		The primitive impedance matrix [Ω/km]			
		A	B	C	N
OH1 / 3-ph	A	0.540 + j0.777	0.049 + j0.505	0.049 + j0.462	0.049 + j0.436
	B	0.049 + j0.505	0.540 + j0.777	0.049 + j0.505	0.049 + j0.462
	C	0.049 + j0.462	0.049 + j0.505	0.540 + j0.777	0.049 + j0.505
	N	0.049 + j0.436	0.049 + j0.462	0.049 + j0.505	0.540 + j0.777
OH2 / 3-ph	A	1.369 + j0.812	0.049 + j0.505	0.049 + j0.462	0.049 + j0.436
	B	0.049 + j0.505	1.369 + j0.812	0.049 + j0.505	0.049 + j0.462
	C	0.049 + j0.462	0.049 + j0.505	1.369 + j0.812	0.049 + j0.505
	N	0.049 + j0.436	0.049 + j0.462	0.049 + j0.505	1.369 + j0.812
OH3 / 3-ph	A	2.065 + j0.825	0.049 + j0.505	0.049 + j0.462	0.049 + j0.436
	B	0.049 + j0.505	2.065 + j0.825	0.049 + j0.505	0.049 + j0.462
	C	0.049 + j0.462	0.049 + j0.505	2.065 + j0.825	0.049 + j0.505
	N	0.049 + j0.436	0.049 + j0.462	0.049 + j0.505	2.065 + j0.825

Table 7.26: Primitive impedance matrices of underground lines of European LV distribution network benchmark

Conductor ID/ Installation		The primitive impedance matrix [Ω/km]			
		A	B	C	N
UG1 / 3-ph	A	0.211 + j0.747	0.049 + j0.673	0.049 + j0.651	0.049 + j0.673
	B	0.049 + j0.673	0.211 + j0.747	0.049 + j0.673	0.049 + j0.651
	C	0.049 + j0.651	0.049 + j0.673	0.211 + j0.747	0.049 + j0.673
	N	0.049 + j0.673	0.049 + j0.651	0.049 + j0.673	0.211 + j0.747
UG2 / 3-ph	A	0.314 + j0.762	0.049 + j0.687	0.049 + j0.665	0.049 + j0.687
	B	0.049 + j0.687	0.314 + j0.762	0.049 + j0.687	0.049 + j0.665
	C	0.049 + j0.665	0.049 + j0.687	0.314 + j0.762	0.049 + j0.687
	N	0.049 + j0.687	0.049 + j0.665	0.049 + j0.687	0.314 + j0.762
UG3 / 3-ph	A	0.871 + j0.797	0.049 + j0.719	0.049 + j0.697	0.049 + j0.719
	B	0.049 + j0.719	0.871 + j0.797	0.049 + j0.719	0.049 + j0.697
	C	0.049 + j0.697	0.049 + j0.719	0.871 + j0.797	0.049 + j0.719
	N	0.049 + j0.719	0.049 + j0.697	0.049 + j0.719	0.871 + j0.797

A detailed schematic of the earthing connections is presented in Figure 7.9.

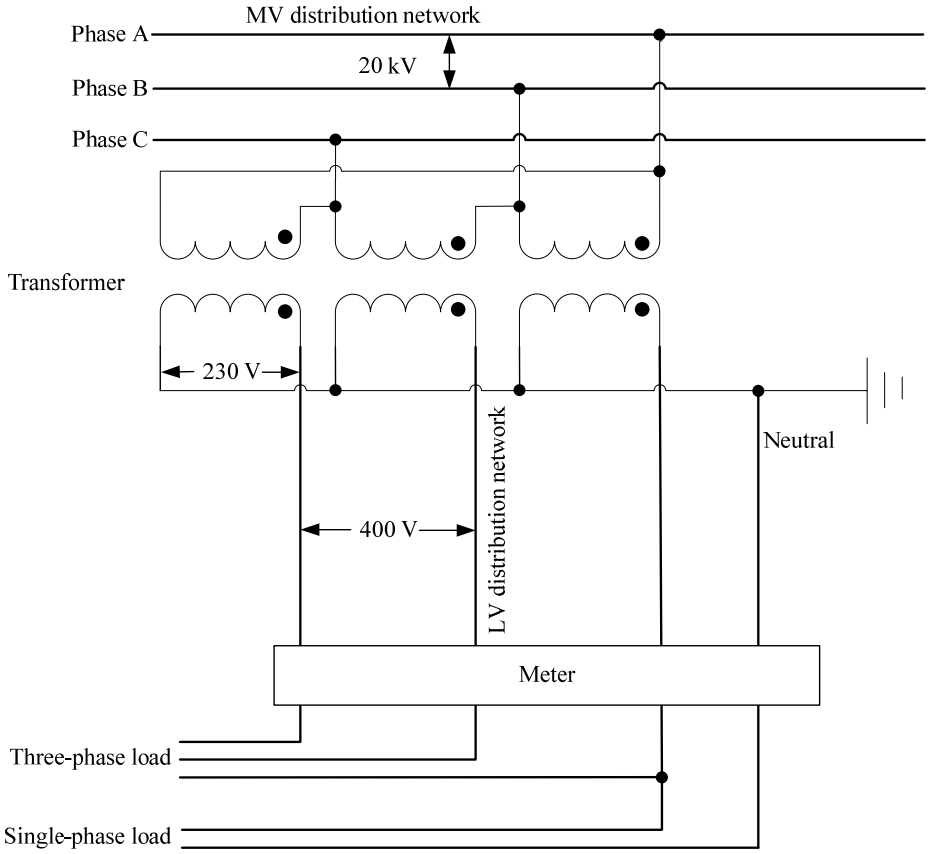

Figure 7.9: Grounding connections for European LV distribution network benchmark

Table 7.27 gives the grounding impedances for both poles and transformers. The data of the subnetwork MV/LV distribution transformer are given in Table 7.28. The data for the MV network voltage and short circuit power are given in Table 7.29.

Table 7.27: Grounding resistances of European LV distribution network benchmark

Pole grounding Z_{pole}	Transformer grounding Z_{tx}
[Ω]	[Ω]
40	3

Table 7.28: Transformer parameters of European LV distribution network benchmark

Node from	Node to	Connection	V_1	V_2	Z_{tr}†	S_{rated}
			[kV]	[kV]	[Ω]	[kVA]
R0	R1	3-ph Dyn1	20	0.4	0.0032+j0.0128	500
I0	I1	3-ph Dyn1	20	0.4	0.0107+j0.0427	150
C0	C1	3-ph Dyn1	20	0.4	0.0053+j0.0213	300

† refers to V_2 side

Table 7.29: MV equivalent network parameters of European LV distribution network benchmark

Nominal system voltage	Short circuit power, S_{SC}	R/X ratio
[kV]	[MVA]	
20 LL	100	1

7.2.3 Load Data

Table 7.30 gives the values of the coincident peak loads for each node of the three-phase sections. Each load represents a group of users. Note that the appropriate coincidence factor was applied in Table 7.30. The coincidence factor is a function of the number of customers served. The use of coincidence factors is described in Appendix 9.3.4.

The load values given for nodes R1 and C1 are much larger than those given for the other nodes. These loads represent additional feeders served by transformers and are not actually part of feeders that are modeled in detail. Daily load profiles for residential, industrial, and commercial loads are given in Figure 7.6.

Table 7.30: Load parameters of European LV distribution network benchmark

Node	Apparent Power, S [kVA]	Power Factor, pf
	[kVA]	
R1	200	0.95
R11	15	0.95
R15	52	0.95
R16	55	0.95
R17	35	0.95
R18	47	0.95
I2	100	0.85
C1	120	0.90
C12	20	0.90
C13	20	0.90
C14	25	0.90
C17	25	0.90
C18	8	0.90
C19	16	0.90
C20	8	0.90

7.3 Flexibility

For certain studies, it may be of interest to evaluate the impact of DER under different network conditions. In what follows, suggestions are made on how such changes may be accommodated.

7.3.1 Voltages

The base voltages of the per-unit system may be modified to study different voltage levels as long as the chosen values are realistic.

7.3.2 Line Lengths

The line lengths may be modified as long as the typical distribution network character is retained.

7.3.3 Line Types and Parameters

The residential and commercial subnetworks were represented with both overhead lines and underground cables, while the industrial subnetwork uses underground cables. It is also possible to change these arrangements and use overhead instead underground lines and vice versa. It would then be necessary to modify the line parameters in accordance with information supplied by manufacturers.

7.3.4 Loads

Loads may be modified as necessary.

7.4 Case Study: Microgrid Islanding

Through the connection of DER to LV distribution networks, the networks can be operated as Microgrids [17]. The low voltage distribution network benchmark serves as a platform suitable for studying microgrid performance.

7.4.1 System Specification

In Figure 7.10, an example of the European LV distribution network benchmark described in Section 7.2 is shown. In this example, the pole grounding resistances are 80 Ω. Two battery units are respectively connected at the nodes designated A and B in Figure 7.10 to provide frequency regulation during the isolated operation. These units with their DC-AC inverters are rated to 35 kVA and 25 kVA respectively at 0.85 power factor lagging. Their inverters are controlled with P-f and Q-V droops in order to share the network load. They produce zero active and reactive power when the microgrid is connected with the upstream MV network. Two PV units with 3 kW and 4 kW respectively are connected at nodes designated C and D, and a 5.5 kW fixed speed wind turbine is directly connected at node E. The network loading for both of the two cases is considered and also shown in Figure 7.10.

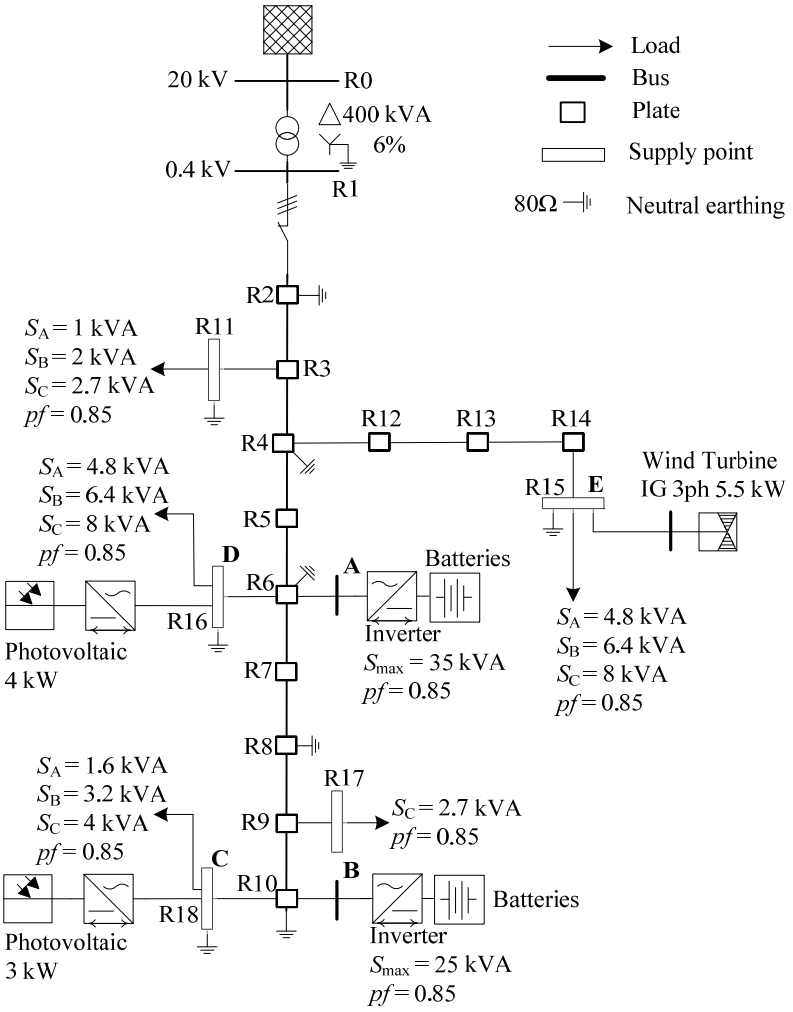

Figure 7.10: LV distribution network benchmark application example: model

7.4.2 Simulation

The first case simulates the isolation of the microgrid when opening the breaker of the feeder at instant 1 second. This is followed by a 25 % load increase at 2.5 seconds at nodes C, D, and E. Only the battery units are considered connected in this case. The results are shown in Figure 7.11, Figure 7.12, and Figure 7.13. Real power and reactive power are plotted in the same graph with continuous and dotted lines, respectively.

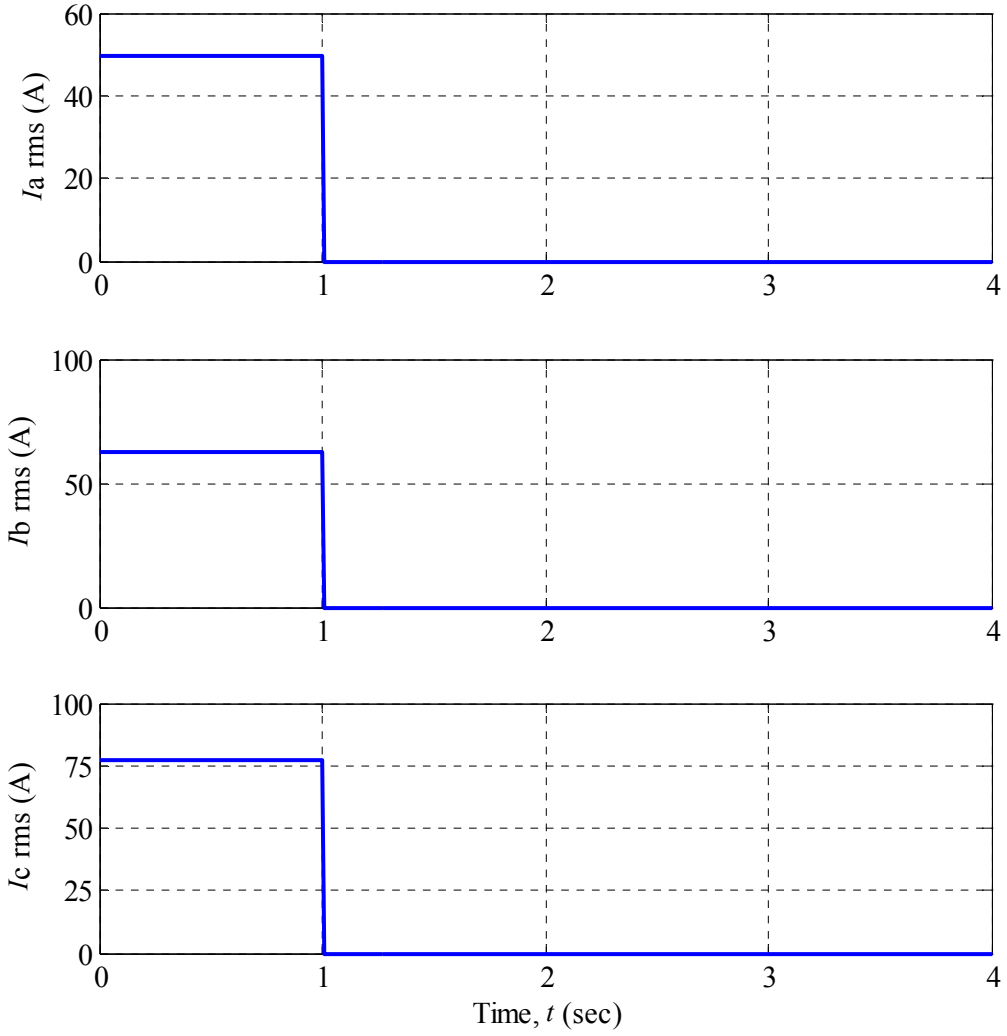

Figure 7.11: LV distribution network benchmark application example: currents at departure of the microgrid feeder

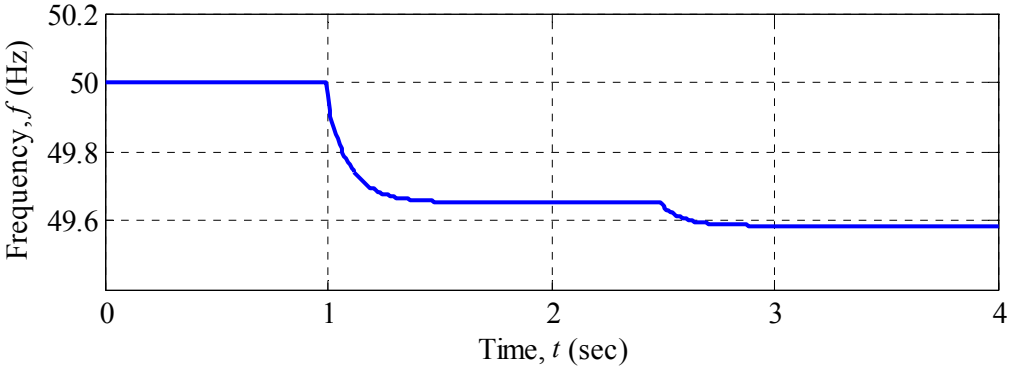

Figure 7.12: LV distribution network benchmark application example: microgrid frequency

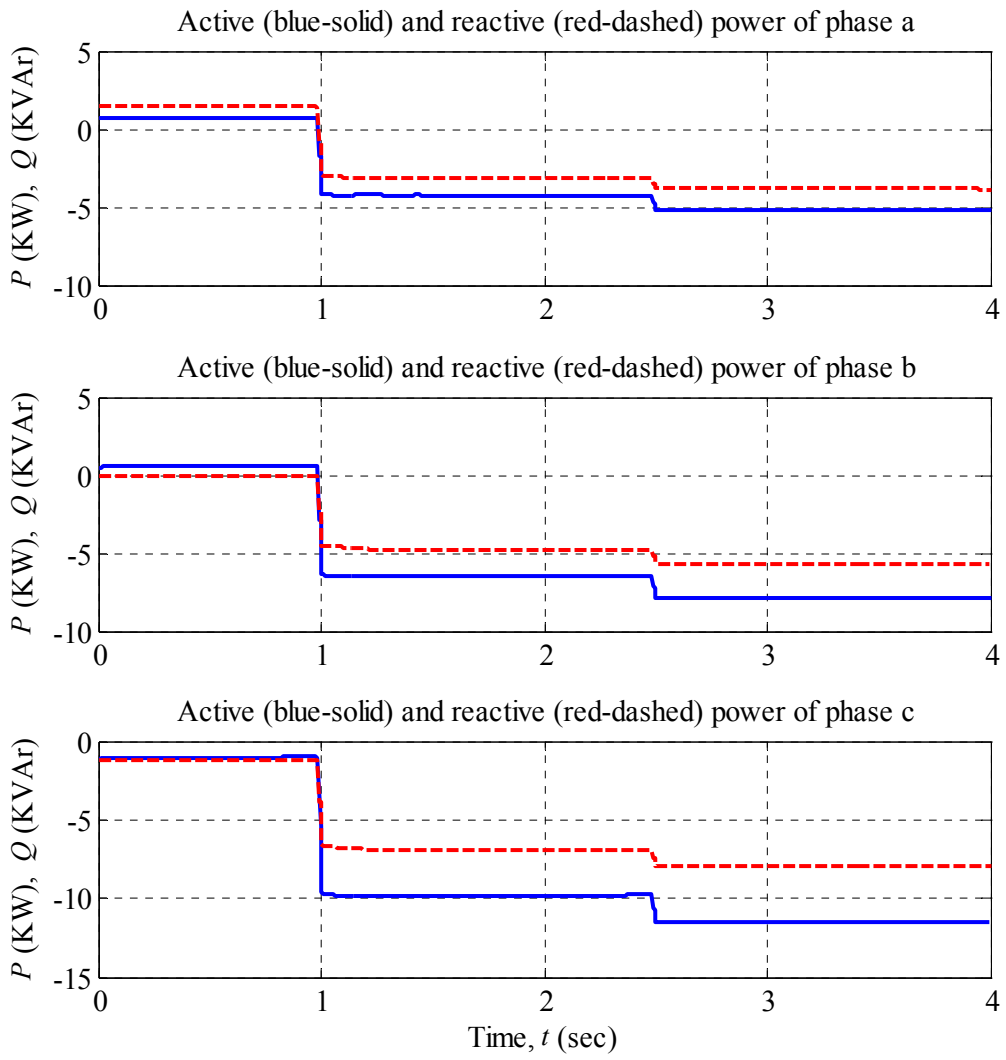

Figure 7.13: LV distribution network benchmark application example: power flows per phase of the inverter at node A with load convention

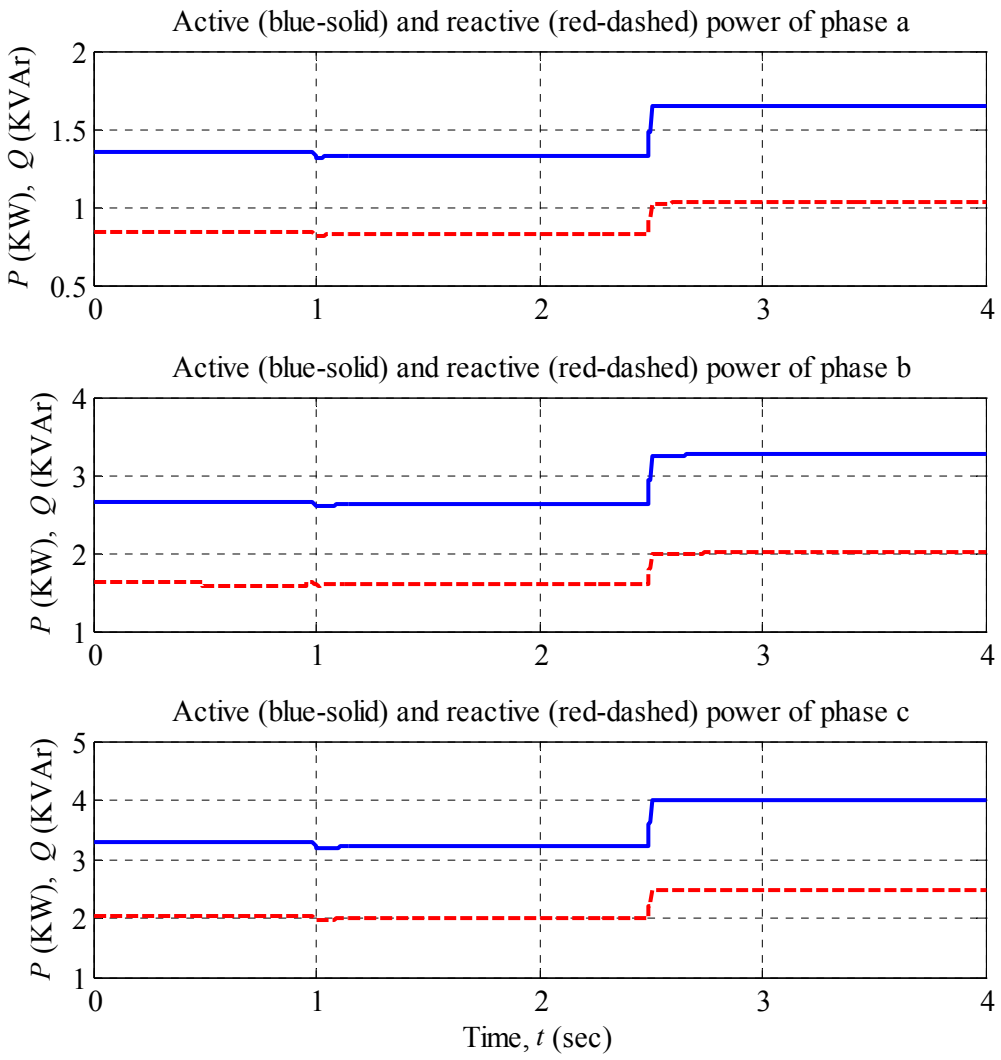

Figure 7.14: LV distribution network benchmark application example: power flows per phase through the supply cable to node C

8. Application Examples

In Chapter 3, an overview of the scope of application of the benchmarks was given. In Chapters 4, 5, 6, and 7, the benchmark systems themselves were detailed. The present Chapter is devoted to two application examples. In Section 8.1, the resource-side benchmark is used for testing inverter controls. In Section 8.2, the MV distribution network benchmark is used to analyze the islanding of an MV network that is dominated by renewable generation.

8.1 Testing of DER Inverter Controls

The exploitation of distributed sources of generation relies to a good extent on the power electronic circuits and controls for interfacing the prime source with the AC grid.

8.1.1 Context

Photovoltaic arrays, fuel cells, and storage batteries provide DC power. Microturbines and some kinds of wind energy conversion systems produce AC power at a frequency different from 50 Hz or 60 Hz. In both cases, the prime source cannot be directly connected to the grid, and power electronic conversion is necessary. A general representation of such a configuration is given in Figure 8.1. The shown prime source block contains a DC-DC converter for a DC source. It contains a rectifier or a rectifier plus a chopper for an AC source. The inverter scheme usually adopted is a VSI.

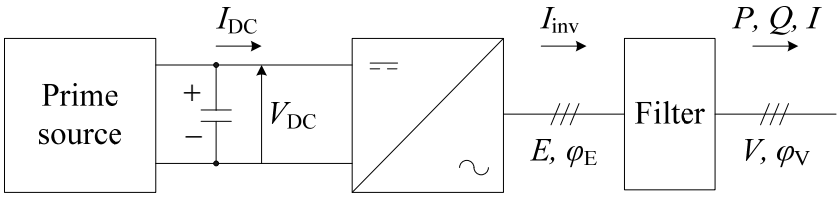

Figure 8.1: Reference scheme of inverter interfaced sources.

Various options for controlling the inverters are of interest for study:

- The first case is to make the DERs act as negative loads; they then only operate when the grid is energized and are shut down when the grid is no longer active.
- The second case is to create a standalone network supplied by the DERs.
- The third case is to enable the DERs to supply a local network whenever the connection to the main grid becomes unavailable.
- The fourth case is to enable the DERs to also supply power to the main grid if that is needed.

In the first case, DER units may simply feed through the inverter in current-mode control [18] in which the current amplitude and phase with respect to the grid voltage define the real and reactive power. In the case of serious longer network faults, the inverter voltage protection shuts down the device. It will resume operation when the network voltage is restored.

In the second case of DERs supplying a standalone network, at least one of the inverters must be voltage-controlled [18] to regulate the voltage and frequency on the grid. The other DERs can either have current-controlled inverters or voltage-controlled inverters with a so-called

PQ control loop [19], [20]. An alternative solution is to adopt a droop control for the units [21], [22], [23].

Regarding the third case when DERs supply local loads in parallel with the main grid, the inverters can be current-controlled with a proper choice of current amplitude and phase to obtain the desired power generation. Alternatively, they can also be voltage-controlled with an additional PQ control. When a disturbance occurs on the grid, these DERs should continue to supply the local load within a separate island. Therefore, at least one of the DERs within the island needs to switch its control to a fixed-frequency voltage-mode control. A coordinating control would determine the power sharing among the DERs.

The fourth case considers the situation where DERs cannot only supply local loads, but also the grid. This allows them to contribute to grid security.

As an example, DER controls with the following features are considered:

- operating only on the basis of locally available measurements;
- being suitable for operating in parallel to the grid, or within a standalone system;
- neither influencing the action of the grid protections, nor be forced to shut down by automatic actions of other grid equipment;
- needing not to recognize whether it operates in parallel to the grid or within a standalone system.

The control scheme can be used when it is possible to keep the DC bus voltage of the DERs within a given range. For this purpose, the prime source may need to comprise storage depending on the characteristics of the generating unit.

8.1.1.1 Structure of Control Scheme

The control scheme considered is structured into the three hierarchical loops depicted in Figure 8.2. The outer loop is a voltage control that is split into voltage frequency control and voltage amplitude control. It is suitable for working both in parallel to the grid and within a standalone system. An inner loop for current peak control acts each time the instantaneous inverter current exceeds a maximum threshold value and cuts its peak at the specified threshold. The second inner loop acts when a resynchronization with the grid is to appear as it is the case following a fault. It is aimed at keeping the current in a band close to zero to allow a smooth synchronization procedure.

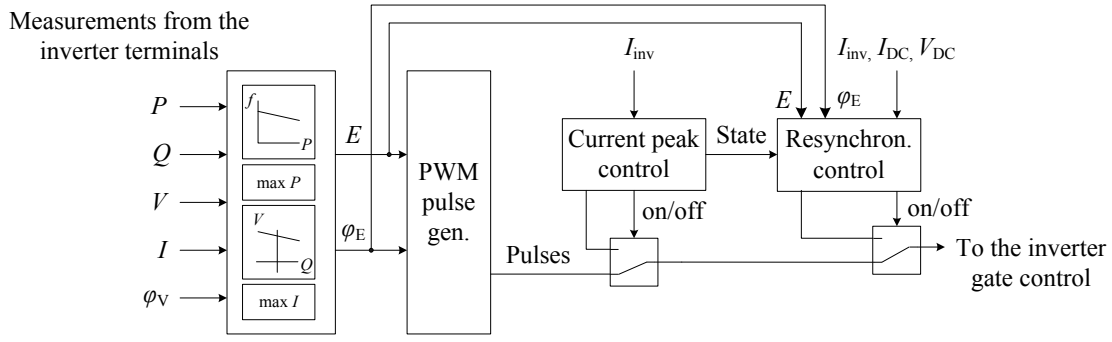

Figure 8.2: Block diagram of inverter control

Both the inner loops are hysteresis controls as those can offer fast transient responses.

8.1.1.2 Voltage Frequency Control

Based on the usual droop characteristic of synchronous generators to increase power output at falling frequencies, a control system linking the fundamental frequency of the inverter to its power output ensures the correct operation both in parallel to other sources and on a standalone load [20], [21], [22], [23]. When the inverter is connected to the grid, the grid determines the frequency. Therefore, if the inverter frequency is higher, the phase shift φ_E - φ_V of the inverter with respect to the terminal voltage increases together with the power output. Thus, the inverter frequency will be reduced according to the droop, and the inverter will synchronize to the grid. If several inverters are connected in parallel to supply an isolated network, they will share the load power according to their droop characteristics in the same way as large power plants subject to primary frequency regulation do. Frequency droop for inverter control is depicted in Figure 8.3.

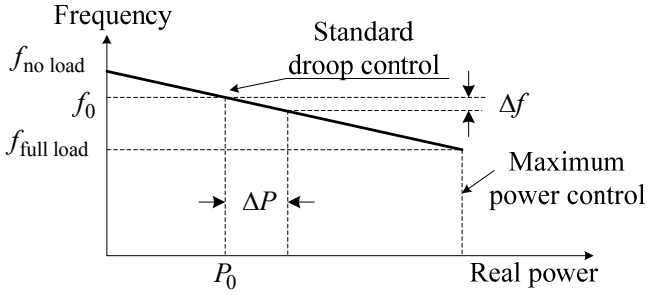

Figure 8.3: Frequency droop for inverter control

When reaching the maximum allowable power output, i.e. the maximum power that the prime source can supply, the control system automatically switches to a fixed power control, acting on the phase shift φ_E - φ_V. The system returns to normal control when the frequency exceeds the maximum frequency by a given margin [9]. Similarly a minimum power control loop, which is not shown in Figure 8.3, prevents working below the minimum source power.

8.1.1.3 Voltage Amplitude Control

As for active power, reactive power is also shared among the sources via a droop characteristic. The latter relates the voltage reference of the inverter to its reactive power output as shown in Figure 8.4. If the measured voltage drops, more reactive power will be supplied by the DERs, and vice versa. When the rms current I of the inverter reaches its maximum value I_{max}, then the scheme switches to a current control whose purpose is to maintain a constant current rms value.

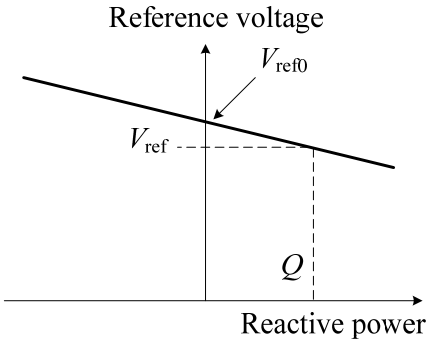

Figure 8.4: Voltage droop for inverter control

8.1.1.4 Current Peak Control

Under certain conditions, the speed of certain control loops may not be high enough to ensure that the maximum current limit of the switches is not exceeded. For example, when a fault very close to the inverter terminals or a reconnection to the network without proper synchronization occurs, then the rate of rise of the current can be very high. The hysteresis control here provides a fast-acting protective function: when the instantaneous current on a phase reaches a threshold I_{th}, then the lower part of the corresponding bridge arm is activated to bypass the PWM pulse sequence. This action is released as soon as the current falls below the proper threshold. An analogous control acts on the negative half waves. When this current peak control is active, the current adopts a squared form. If I_{th} is properly chosen to be higher than I_{max} as mentioned above in the previous paragraph, then the voltage amplitude is reduced within some tenths of milliseconds so that the instantaneous current peak control is no more needed and the normal operation can be resumed.

8.1.1.5 Resynchronization Control

This control uses a hysteresis control on the instantaneous value of the inverter current to keep the latter within a band around zero and so allow reconnection of the DERs and the grid. The resynchronization loop releases the control to the normal loop when the phase shift between the grid voltage and the inverter voltage is below a given threshold.

8.1.2 Simulation

Figure 8.5 shows the test setup using the resource-side benchmark. A constant voltage on the DC bus is assumed. Only the inverter control is therefore studied.

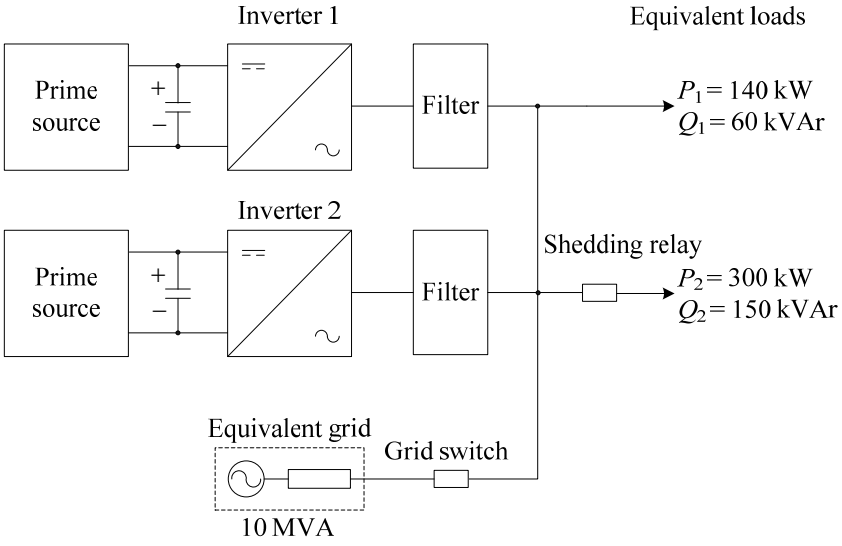

Figure 8.5: Resource-side benchmark applied to testing of DER inverter controls

Table 8.1: Inverter parameters

Inverter No.	I_{max} [p.u.]	I_{th} [p.u.]	Voltage droop	V_{ref0} [p.u.]	f_0 [p.u.]
1	1.5	2.2	5 %	1.000	1.015
2	1.5	2.2	2 %	1.000	1.020

The scenario begins with a three-phase grid fault which is cleared in 100 ms by disconnecting the grid. One second after the fault, the breaker automatically recloses. It is worthwhile noticing that no communication exists between the DER units and between the protection system and the DER units. A load shedding relay is installed to keep the local load within the capability of DER when the grid is disconnected. The scenario unfolds as follows:

- Initially two inverters operate in parallel to the grid supplying the local load by sharing the real and reactive power shown in Figure 8.6 in accordance with the droop characteristics. As can be seen from Figure 8.7, none of the inverters operates under the limiting action of the maximum current rms control. The grid voltage is near 1 p.u. as shown in Figure 8.8.
- At t = 0.2 s a three-phase fault happens. During the fault the current peak control cuts the maximum instantaneous value of each inverter current at I_{th} = 2.2 p.u. as seen in Figure 8.9. As a consequence of the square shape of the current, its rms value reaches 2.5 p.u. The power supplied by the inverters and the grid voltage suddenly falls down near zero as evidenced by Figure 8.6 and Figure 8.8. During the first cycles of the fault current, the maximum current rms control starts reducing the value of the inverter voltage. At t = 0.28 s, it succeeds in bringing the current peak below 2.2 p.u. in Figure 8.9; the current peak control stops its action and the current waveform becomes sinusoidal again.
- At t = 0.3 s, the fault is cleared and an isolated network is created and supplied by the two DERs. The local load is larger than what the DERs can deliver. As shown in Figure 8.8, the voltage is reduced due to the action of the maximum current rms controls. The latter has the two inverters supply their maximum current as shown in Figure 8.7. The share of active power supplied by each inverter depends on the setting of the droop characteristics. Different load type and size might require the maximum power control loop to be activated. In this case frequency would be reduced.
- At t = 0.6 s, load is shed, and Figure 8.8 shows the voltage on the main busbar to be restored at its rated value. No limiting loop is now active, and the two inverters supply the isolated load sharing real and reactive power according to the droop characteristics. One of the inverters supplies 25 % active power more than the other.
- Finally, at t = 1.2 s the automatic reclose of the grid switch happens when the phase shift between the two voltages is around 90 degrees as shown in Figure 8.10. Prior to the reclosing, the resynchronization control forces the current to go to zero and allows the normal inverter controls to resynchronize within 40 ms as shown in Figure 8.11. Figure 8.12 shows the behavior of the resynchronization control at the automatic reclose.

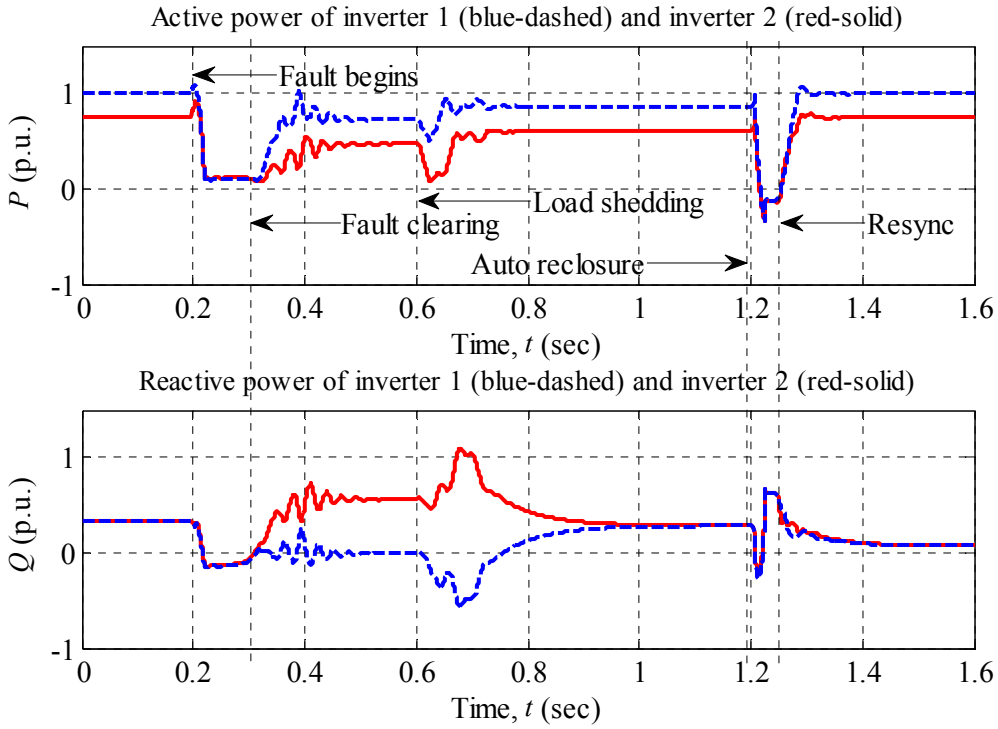

Figure 8.6: Active and reactive power injected by the two inverters

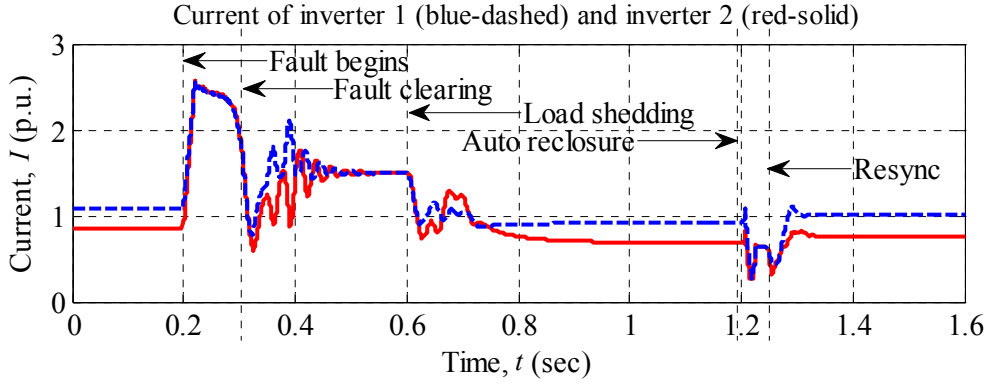

Figure 8.7: Rms currents supplied by the two inverters

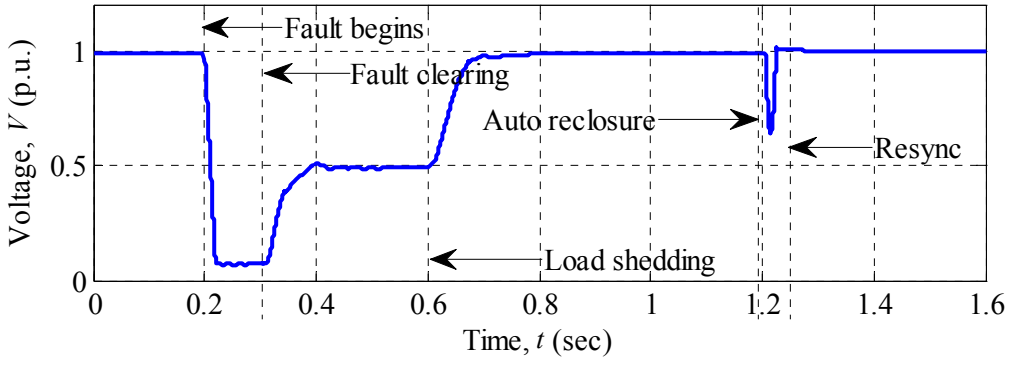

Figure 8.8: Rms voltage at the local grid main busbar

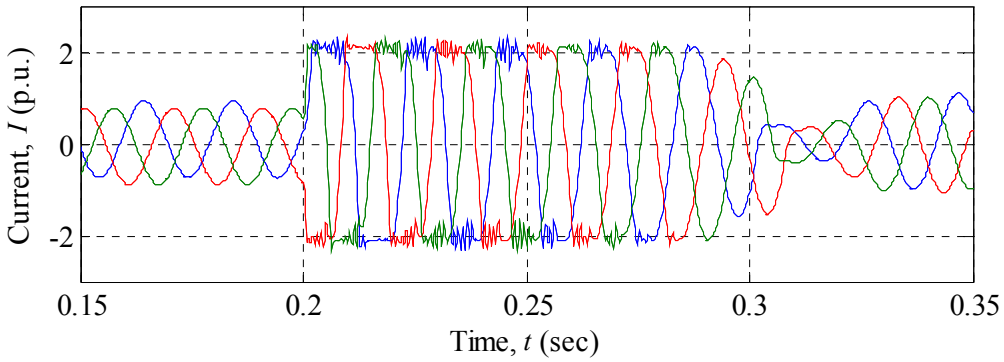

Figure 8.9: Inverter three-phase currents during short circuit

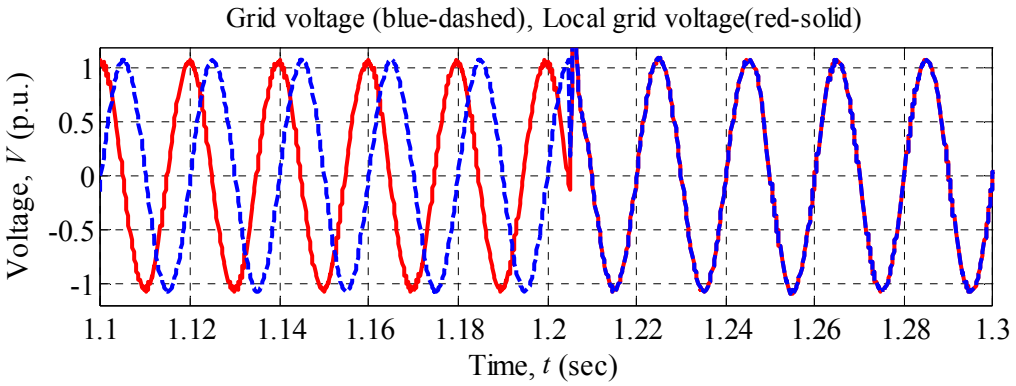

Figure 8.10: Grid and local grid voltages at reclosing time

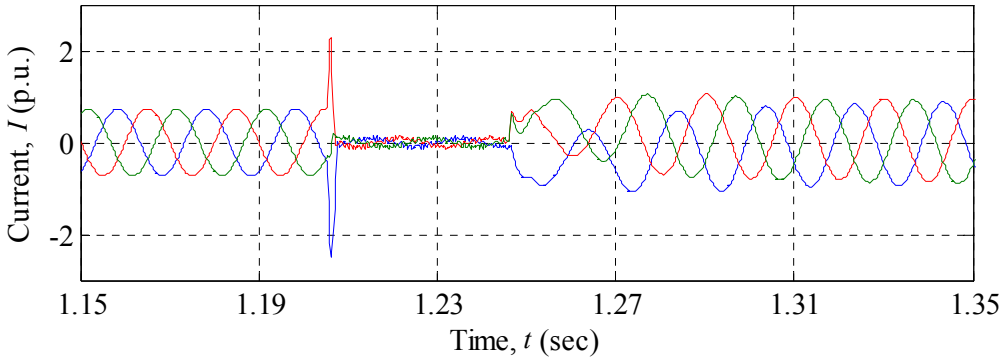

Figure 8.11: Inverter three-phase currents at reclosing time

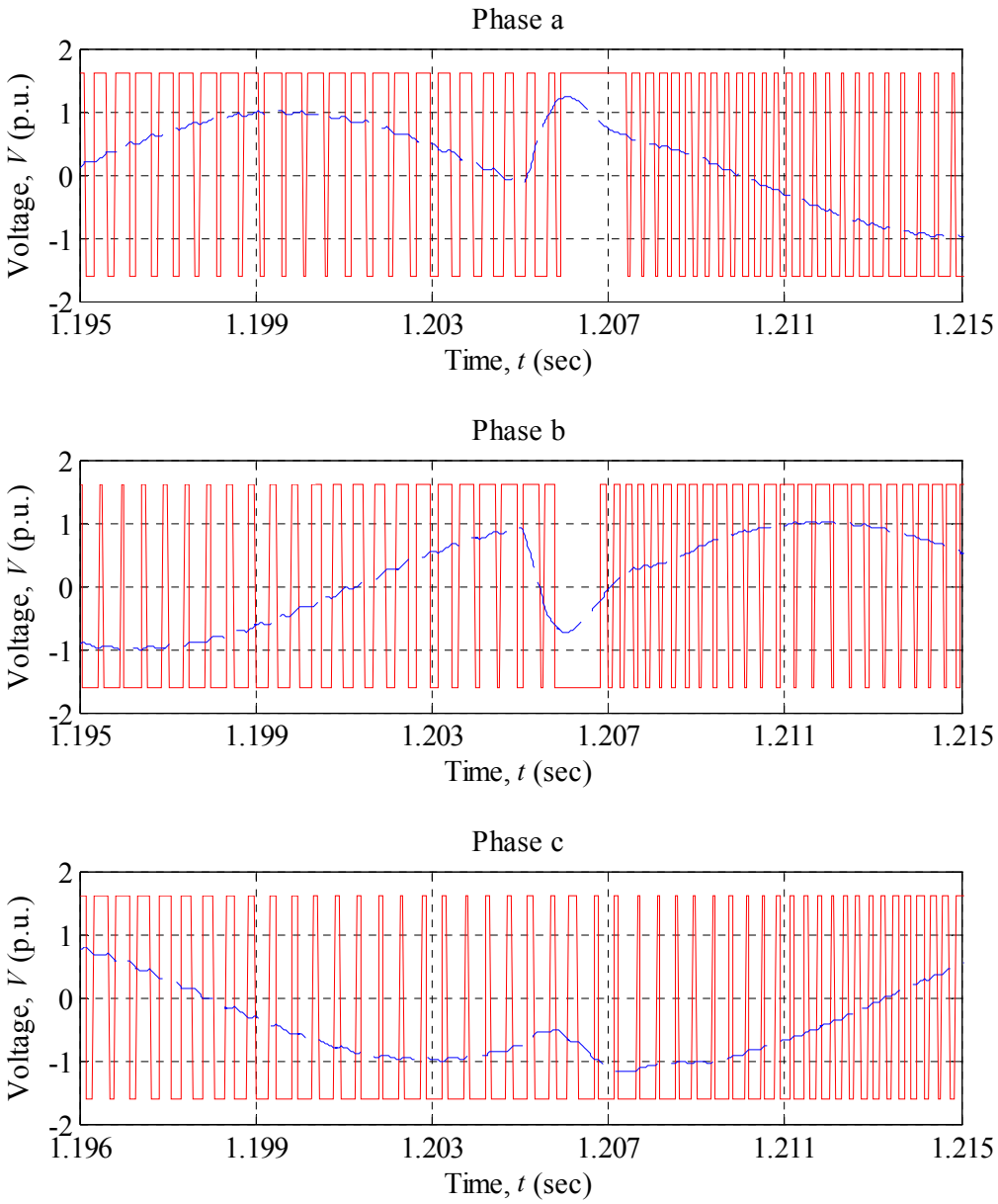

Figure 8.12: Inverter bridge voltages and terminal voltages at reclosing time

8.2 Planned Islanded Operation of an MV Distribution Network

Distribution networks capable of planned islanding are also referred to as microgrids. Preparing for the islanding capability necessitates more involved planning studies than those required of other distribution networks or even of distributed generation interconnection. Here, the MV distribution network benchmark is used to investigate the operation of an MV microgrid that comprises wind energy conversion and storage.

8.2.1 Context

Planned islanding implies a greater degree of sophistication in terms of operation of DG since local generation must control frequency and voltage within acceptable bounds. This section demonstrates how the MV distribution network benchmark can be used to test a specific DG

planned islanding configuration and associated control strategy. There are different possibilities to control a microgrid in islanding operation as presented in [24], [25], [26]. Simulation will, at least in most cases, be the first step to analyze the operation of the system. Field trials are not economically feasible in all cases, and furthermore they subject local customers to risk in the event when the controllers are not compatible or require tuning. Real-time simulation is another tool that can be used and was implemented as a validation tool [27].

Energy storage is a technology that will likely be used frequently in microgrids, particularly in systems that are supplied primarily from non-dispatchable renewable power sources. Various storage topologies have also been proposed to offer firm power control on various time scales [2], [3], [28], [29], [30].

8.2.2 Simulation

Coordinated operation of electric energy storage and wind energy systems can mitigate the impact of the stochastic nature of wind energy, and make the combined plant dispatchable. In addition, this operation offers the possibility of planned islanding, which is not possible with wind energy conversion alone. Here, the MV distribution network benchmark is used in order to investigate planned islanded operation. The models of the system were developed in MATLAB-SimPowerSystems and are simulated for operation in parallel with the main grid and for transfer to the islanded condition.

Because the main motivation for the present study is the interaction of wind energy conversion and storage, wind is the sole distributed generation source connected to the network. A number of wind generators with a combined installed capacity of 75 % of the network peak load are connected to bus 7 as shown in Figure 8.13. The selection of this bus was based on the view that distributed wind is typically located towards the end of the feeder. Switches S1 and S2 were left open to simulate a radial feeder.

The wind energy converter was modeled as a current source, where the magnitude of the current source was determined from a wind speed profile [31] and a wind turbine power characteristic [31]. It was assumed that the current source be in phase with the voltage, operating in unity power factor mode.

The power electronic interface of the energy storage system controls frequency and voltage when in islanded mode. In one control strategy, the power electronic converter can be controlled in much of the same manner as a synchronous generator. The difference is that the frequency of the system, measured using a phase-locked loop (PLL), is used as the virtual speed of the converter. In this approach, the active power of the converter is defined by the combination of an energy storage power set point and a governor control signal as indicated in Figure 8.14. The energy storage set-point serves to control the power delivered from the substation to a desired amount. This is either to be enacted during a peak-shaving event or in preparation for a planned island. The smallest transient during transition to islanding will generally occur when there is no demand from the main grid prior to breaker activity. Therefore, the power reference is set to force zero power flow at the substation. Signal ΔP_{ES} is used to manage the energy state of the storage device itself. The general strategy is to curtail or increase the power reference when the state of charge of the storage system is close to its lower or upper limit. The speed droop loop, defined by K_{SD}, represented as the dotted line permits power sharing without further communication. It should be used when in grid parallel mode or when there is more than one inverter operating in island mode. In isochronous mode, the dotted line in Figure 8.14 is omitted, it will be required when operating independent from the grid to ensure that there is no steady-state frequency error. In

the multiple-inverter scenario this functionality can be either shared between the different units by communicating an AGC signal, or can be delegated to a single unit that would be operated in isochronous mode, with all other units operated under speed-droop control.

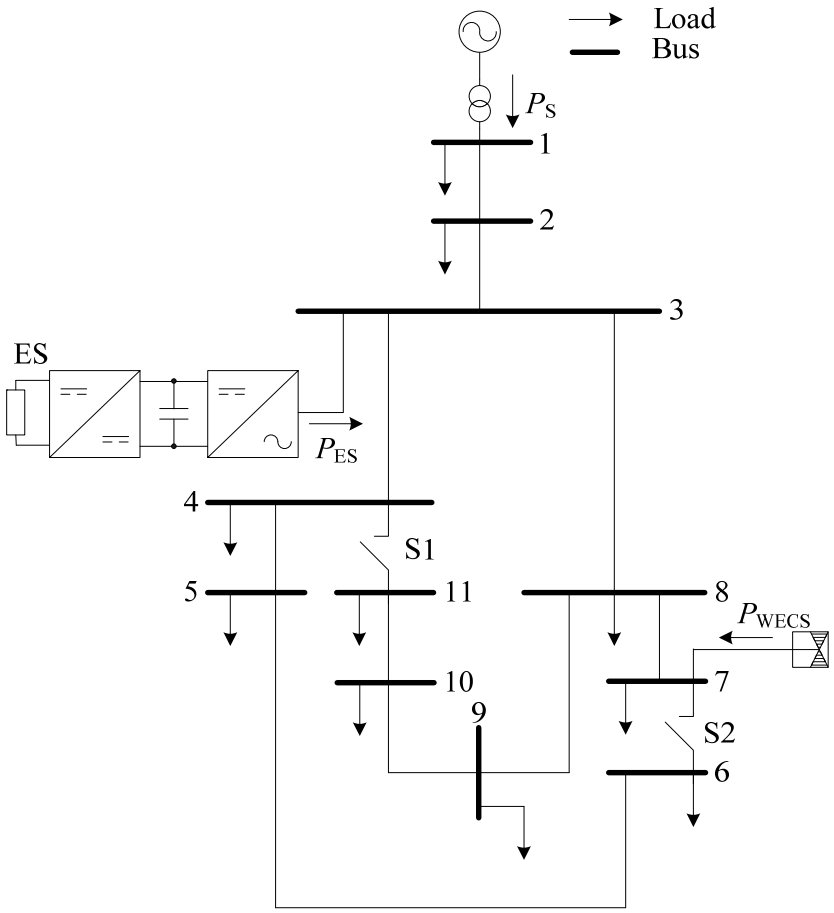

Figure 8.13: MV distribution network benchmark applied to testing of islanding

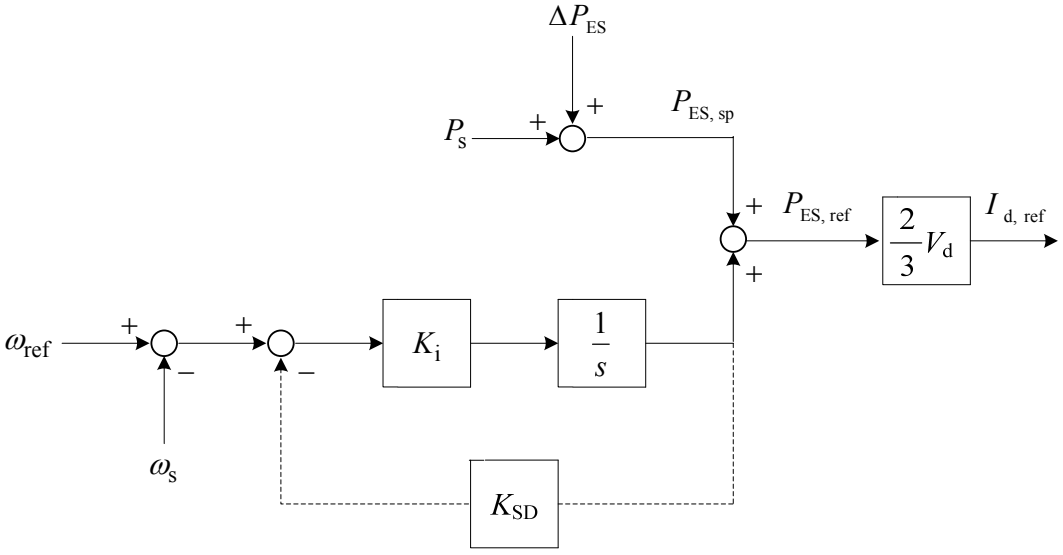

Figure 8.14: Block diagram of isochronous control for energy storage system converter

For governor control mentioned above, the converter still behaves like a current source because the governor control defines, together with the voltage regulation block, the current reference, which is forwarded to the inner current control loop. Alternatively, during islanding one could control the interface as a voltage source, particularly if there is only a single controllable source. In this mode of operation, the rotating frame becomes set by an internal clock rather than the signal from the PLL and the outputs of the current control are simply replaced by set values for V_d and V_q as shown in Figure 8.15. In the event that there are multiple inverters, this control is assigned to a single unit denoted the master and all other units are synchronized with respect to the master unit.

The mode of control involving the master is very simple in construction and works very well in islanded mode, especially when a single inverter is used. This does impose a number of requirements on the master inverter: information regarding breaker status is known; there exists sufficient power capacity to serve the load; and sufficient storage capacity on the dc bus is available to ride through the transient from grid-tied to isolated operation. Furthermore an additional protection loop is required to ensure that the current limit of the device is not exceeded. The latter consideration has been omitted from the present study.

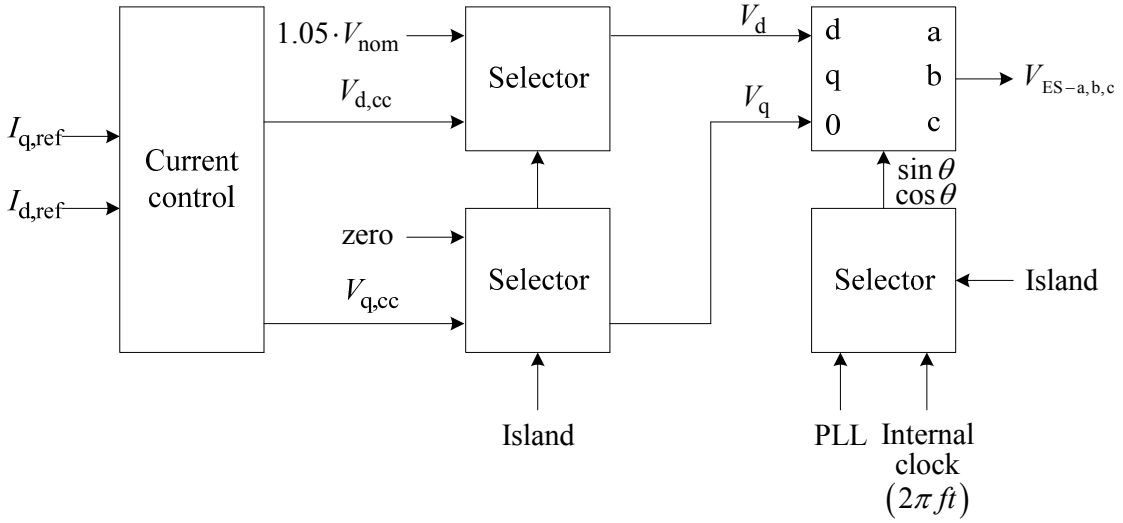

Figure 8.15: Block diagram of constant frequency control for energy storage system converter

The system was simulated for an islanding event at 2.5 seconds. At this point the control mode of the inverter is actually changed from power set point with speed droop to constant frequency mode. Considered differently, the converter is operated in a current-controlled mode and then switched to a voltage-controlled mode when the islanding condition is detected. Here it is assumed that the breaker status is communicated to the inverter, and the control mode is dictated by that signal.

The simulation results are given in Figure 8.16. Prior to islanding, the control strategy of energy storage device is to adjust its output to force zero power flow at the substation. At the moment of islanding, the substation power goes to zero instantaneously and stays there for the remainder of the simulation period. Immediately following the initiation of the island, there is a small transient associated with the storage power. This is caused by the switching of operation modes and the adjustment to the new operating point, which takes a very short amount of time. This transient depends on many factors: the level of load; the type of load; the relative phase angles between the clocked voltage and the voltage prior to islanding; and

of course the power imbalance. There are likely ways of minimizing the transient. For this case in question, the transient is very small and of little concern.

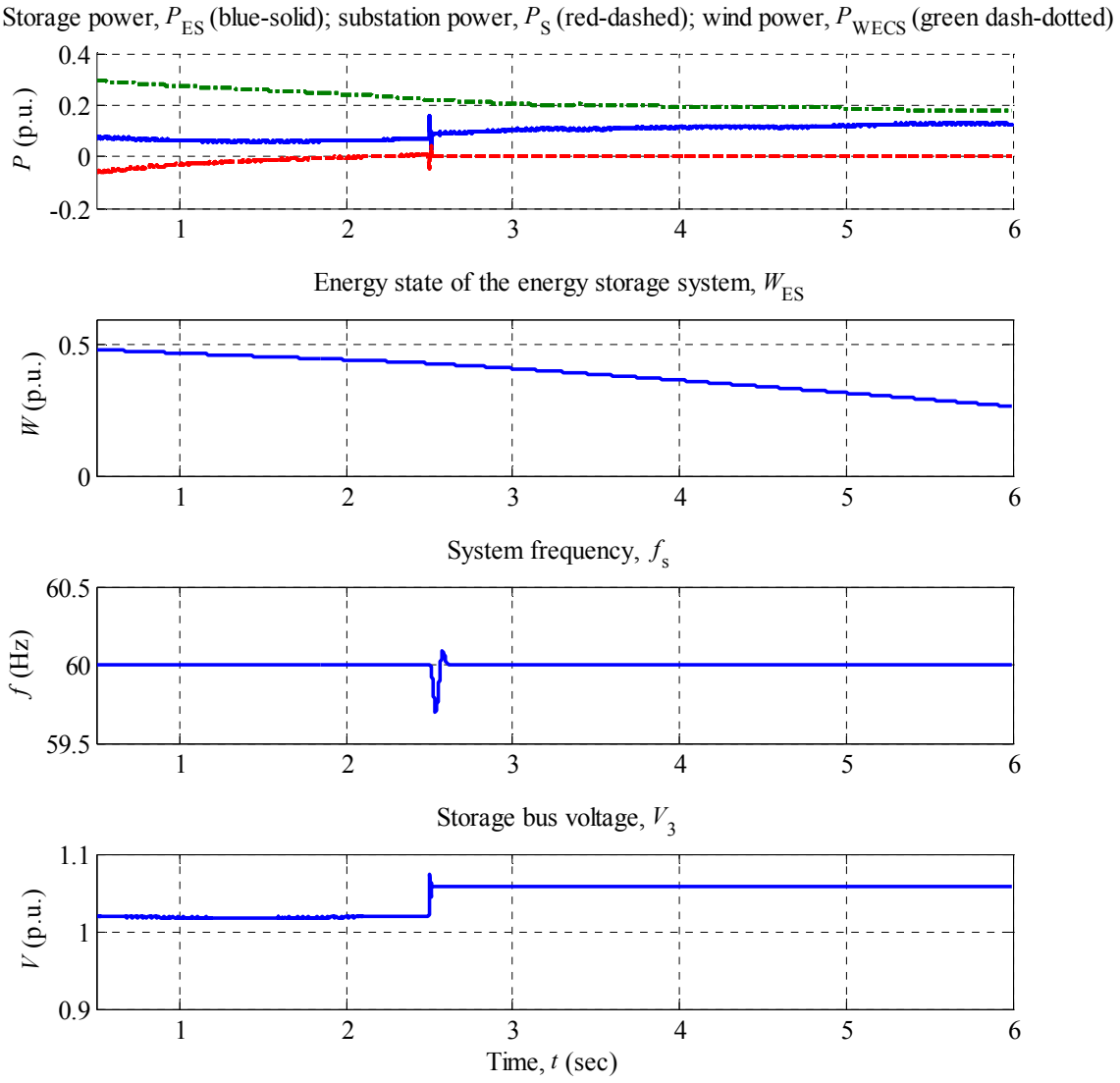

Figure 8.16: Variation of parameters for transfer to islanding operation under constant frequency control

Similar observations as for the storage power are made when looking at the frequency signal. There is a short transient at islanding; however, it is not visible whether this is due to actual changes in the frequency or simply the dynamics of the PLL that was used to measure the frequency. Following initiation of the island, the system frequency remains fixed at 60 Hz.

Turning to the voltage, a sharp jump in its magnitude is noticed. This is due to the fact that the direct component of the voltage V_d is set to 1.05 p.u. for constant frequency control. This was done to account for any drop in voltage along the line so that all of the load would see at least this voltage. Obviously this is in large part the cause of the transient seen in the power

and could be limited by ramping up the voltage magnitude instead of applying a direct change at the moment of islanding.

The results demonstrate the types of data that can be obtained and how the MV distribution network benchmark may be used to study planned islanding and microgrid operation. Furthermore, because the benchmark is representative, it can be used to compare different control algorithms, generation mixes, and load conditions, thereby providing a comprehensive view of this technology and the possible variations.

9. Appendices

9.1 Design of European Versus North American Distribution Network Benchmarks

The distribution network design approaches and installation common practices vary greatly between North America and Europe [32], [33]. These differences are discussed in this section.

The European distribution design typically consists of three-phase delta MV distribution systems of typically 11 kV or 20 kV and was first developed to service dense urban loads in the cities of Europe. The electrification first occurred in the cities, where high load densities justified the use of large 300 kVA to 500 kVA three-phase transformers. Primary MV networks were looped to provide added system reliability. The MV/LV transformers are commonly three-phase connected delta-wye grounded. Six to ten three-phase four-wire multi-grounded LV feeders of 300 m or more are served from each MV/LV distribution substation with consumers connected along the LV feeders and LV branches. Some LV branches are single-phase secondary laterals. This European distribution design approach was adopted for service to rural applications as the distribution system spread outside the urban centers. Somewhat smaller MV/LV 50 kVA to 200 kVA transformers are used for rural areas. The majority of service connections are three-phase at 0.4 kV. Both residential and commercial loads are commonly served by a common MV/LV transformer. The LV secondary system is grounded. Secondary length depends on voltage drop limitations.

In contrast, North America typically utilizes a three-phase four-wire distribution MV system of typically 12.47 kV or 24.0 kV and was first designed primarily to serve widely spaced rural farms throughout North America. Lateral MV circuits are predominantly single-phase two-wire circuits. The secondary LV systems are mostly single-phase, except for larger commercial and industrial consumers, who are supplied from three-phase systems. This four-wire multi-grounded North American system was developed by the Rural Electrification Administration (REA) during the 1930s as a method of economically electrifying U.S. farms. Earlier, urban electrification had largely followed the European model, utilizing an MV ungrounded delta connection system. Utilities throughout the U.S. adopted the four-wire multi-grounded MV system after witnessing its successful implementation by the REA. The three-phase four-wire system provided flexibility to serve incremental future load growth. As load is increased, the incremental line additions could be charged to the new growth consumers. Most North American MV feeders are radial with little backup capability. The MV/LV distribution transformers are small single-phase 15 to 75 kVA and provide service to only a few, less than eight, homogeneous consumers. Typically, residential and commercial customers are not connected to the same transformer. The LV secondary lines rarely extend 200 feet from the transformers and are not looped. Rural areas often have one transformer per consumer where urban area transformers have more consumers per transformer. Where customer loads are greater than 75 kVA as in commercial buildings, light industrial settings or in apartment complexes, each is served by a dedicated distribution transformer. The LV secondary system is grounded at the transformer and at the consumer's service entrance.

9.2 Power Flow Results for Network Benchmarks

9.2.1 Power Flow Results of North American HV Transmission Network Benchmark

Table 9.1 gives the power flow results for the base case of the North American HV transmission system. The length of Line Segment 9, which connects Busses 6a and 6b, is equal to zero (i.e. Bus 6a merges with Bus 6b). All other data are as specified in the appropriate tables in Section 5.1.

Table 9.1: Power flow results of North American HV transmission network benchmark

Bus	Voltage		Generation		Load		Shunt capacitance	To bus	Transferred power	
	Magnitude	Angle	*P*	*Q*	*P*	*Q*			*P*	*Q*
	[p.u.]	[degree]	[MW]	[MVAR]	[MW]	[MVAR]	[MVAR]		[MW]	[MVAR]
1	1.032	-2.9	0	0	0	0	0	2	-17.0	16.7
								6	219.3	18.4
								7	334.8	-64.9
								9	-537.0	29.8
2	1.011	-1.9	0	0	285	200	0	1	17.2	-34.8
								5	197.8	17.3
								10	-500.0	-182.5
3	1.003	-42.8	0	0	325	244	0	4	93.5	25.4
								4	93.5	25.4
								8	-312.1	-21.9
								11	-200.0	-273.0
4	0.963	-47.5	0	0	326	244	-160	3	-92.3	-34.0
								3	-92.3	-34.0
								5	-76.9	-5.2
								6	-64.6	-22.4
5	0.964	-34.1	0	0	103	62	-80	2	-182.5	39.0
								4	79.5	-26.7
6a = 6b	0.997	-37.0	0	0	435	296	-180	1	-201.3	53.9
								4	66.3	-17.6
								12	-300.0	-153.2
7	1.038	-4.7	0	0	0	0	0	1	-334.8	75.8
								8	334.8	-75.8
8	1.005	-41.0	0	0	0	0	0	3	312.1	31.7
								7	-312.1	-31.7
9	1.030	0.0	537	-2.6	0	0	0	1	537.0	-2.6
10	1.030	0.9	500	210.2	0	0	0	2	500.0	210.2
11	1.030	-41.7	200	284.4	0	0	0	3	200.0	284.4
12	1.030	-33.6	300	176.0	0	0	0	6	300.0	176.0

9.2.2 Power Flow Results of European HV Transmission Network Benchmark

Table 9.2 gives the power flow results for the base case of the European HV transmission system. The length of Line Segment 9, which connects Buses 6a and 6b, is equal to zero (i.e., Bus 6a = Bus 6b). All other data are as specified in the appropriate tables in Section 5.2.

Table 9.2: Power flow results of European HV transmission network benchmark

Bus	Voltage		Generation		Load		Shunt capacitance	To bus	Transferred power	
	Magnitude	Angle	*P*	*Q*	*P*	*Q*			*P*	*Q*
	[p.u.]	[degree]	[MW]	[MVAR]	[MW]	[MVAR]	[MVAR]		[MW]	[MVAR]
1	1.032	-3.7	0	0	0	0	0	2	-31.7	31.3
								6	201.5	13.1
								7	357.7	-81.1
								9	-527.5	36.7
2	1.006	-2.0	0	0	285	200	0	1	32.0	-43.7
								5	183.0	11.5
								10	-500.0	-167.8
3	0.996	-34.3	0	0	325	244	0	4	107.9	34.6
								4	107.9	34.6
								8	-340.9	-56.9
								11	-200.0	-256.3
4	0.951	-39.4	0	0	326	244	-160	3	-106.1	-36.6
								3	-106.1	-36.6
								5	-64.2	-4.7
								6	-49.5	-21.3
5	0.958	-29.0	0	0	103	62	-80	2	-169.2	32.6
								4	66.2	-21.2
6a = 6b	0.987	-32.0	0	0	435	296	-180	1	-185.6	41.5
								4	50.6	-10.9
								12	-300.0	-151.2
7	1.044	-6.2	0	0	0	0	0	1	-357.7	97.5
								8	357.7	-97.5
8	1.005	-31.8	0	0	0	0	0	3	340.9	72.6
								7	-340.9	-72.6
9	1.030	0.0	527.5	-2.6	0	0	0	1	527.5	-2.6
10	1.030	1.6	500	203.5	0	0	0	2	500.0	203.5
11	1.030	-32.9	200	270.1	0	0	0	3	200.0	270.1
12	1.030	-27.6	300	181.3	0	0	0	6	300.0	181.3

9.2.3 Power Flow Results of North American MV Distribution Network Benchmark

Table 9.3 and Table 9.4 give the power flow results for the base case of the North American MV distribution system. The base case is a radial system, thus the positions of configuration switches S1, S2, and S3 are all open. All other data are as specified in the appropriate tables in Section 6.1. In order to maintain reasonable voltage levels at the ends of the feeders, tap changing transformers were used as specified in Section 6.1.2 with tap settings specified in Table 9.5.

Table 9.3: Power flow results of three-phase sections of North American MV distribution network benchmark

Bus	Voltage			From bus to bus	Current		
	Phase	LL rms	angle		Phase	rms	angle
		[kV]	[degree]			[A]	[degree]
0	AB	115	0	HV bus - 0	A	206.22	-34.14
0	BC	115	-120	HV bus - 0	B	208.75	-155.25
0	CA	115	120	HV bus - 0	C	204.00	84.69
1	AB	12.49	19.36	0-1	A	1360.01	-5.72
1	BC	12.52	-100.28	0-1	B	1317.23	-125.58
1	CA	12.57	139.41	0-1	C	1275.83	114.08
2	AB	12.19	18.04	1-2	A	238.80	-6.89
2	BC	12.20	-101.48	1-2	B	275.76	-128.47

Bus	Voltage			From bus to bus	Current		
	Phase	LL rms	angle		Phase	rms	angle
		[kV]	[degree]			[A]	[degree]
2	CA	12.29	138.25	1-2	C	246.26	112.27
3	AB	12.02	17.13	2-3	A	162.94	-7.38
3	BC	11.99	-102.26	2-3	B	228.49	-127.80
3	CA	12.11	137.56	2-3	C	178.37	112.25
4	AB	11.98	16.90	3-4	A	66.61	-5.38
4	BC	11.95	-102.42	3-4	B	86.91	-127.42
4	CA	12.09	137.38	3-4	C	54.99	114.70
5	AB	11.96	16.73	4-5	A	39.91	-3.24
5	BC	11.91	-102.54	4-5	B	73.66	-127.15
5	CA	12.06	137.26	4-5	C	41.54	115.59
6	AB	11.95	16.65	5-6	A	6.68	-1.06
6	BC	11.89	-102.76	5-6	B	13.18	-121.55
6	CA	12.02	137.18	5-6	C	34.94	117.40
7	AB	11.89	16.37	8-7	A	13.29	-1.32
7	BC	11.83	-103.00	8-7	B	26.24	-121.89
7	CA	11.97	136.95	8-7	C	13.34	118.97
8	AB	11.94	16.56	3-8	A	85.89	-7.45
8	BC	11.86	-102.86	3-8	B	104.57	-126.71
8	CA	11.99	137.06	3-8	C	106.11	82.11
9	AB	11.89	16.47	8-9	A	59.39	-8.53
9	BC	11.84	-102.95	8-9	B	58.71	-128.02
9	CA	11.97	136.98	8-9	C	66.19	110.97
10	AB	11.86	16.35	9-10	A	46.23	-10.61
10	BC	11.81	-103.11	9-10	B	39.18	-131.21
10	CA	11.93	136.83	9-10	C	53.04	108.94
11	AB	11.85	16.31	10-11	A	26.36	-11.73
11	BC	11.80	-103.14	10-11	B	26.08	-132.08
11	CA	11.93	136.80	10-11	C	19.91	105.21
12	AB	12.55	25.83	0-12	A	401.77	-1.84
12	BC	12.55	-94.16	0-12	B	401.74	-121.84
12	CA	12.55	145.84	0-12	C	401.23	118.09
13	AB	12.18	24.29	12-13	A	77.72	-1.18
13	BC	12.18	-95.69	12-13	B	77.70	-121.15
13	CA	12.18	144.31	12-13	C	77.19	118.40
14	AB	12.14	24.14	13-14	A	12.20	-1.73
14	BC	12.12	-96.21	13-14	B	12.16	-121.55
14	CA	12.07	144.04	13-14	C	46.96	122.13

Table 9.4: Power flow results of single-phase sections of North American MV distribution network benchmark

Bus	Subnetwork Bus	Phase	Voltage		From bus to bus	Current	
			LN rms	angle		rms	angle
			[kV]	[degree]		[A]	[degree]
2	1	A	7.05	-12.01	MV bus 2 - 1	35.49	-31.93
2	2	A	7.04	-12.06	1-2	33.46	-31.58
2	3	A	7.03	-12.09	2-3	19.38	-31.01

Bus	Subnetwork Bus	Phase	Voltage		From bus to bus	Current	
			LN rms	angle		rms	angle
			[kV]	[degree]		[A]	[degree]
2	4	A	7.03	-12.09	3-4	1.36	-30.29
2	5	A	7.04	-12.06	2-5	4.07	-37.83
2	6	A	7.04	-12.07	5-6	2.04	-37.91
2	7	A	7.04	-12.07	2-7	8.01	-30.24
2	8	A	7.04	-12.08	7-8	6.65	-30.28
2	9	A	7.03	-12.09	3-9	3.38	-34.79
2	10	A	7.03	-12.10	9-10	1.36	-30.29
2	11	A	7.03	-12.10	3-11	8.00	-30.27
2	12	A	7.03	-12.11	11-12	6.65	-30.31
5	1	B	6.85	-133.32	MV bus 5 - 1	34.46	-153.25
5	2	B	6.84	-133.38	1-2	32.46	-153.90
5	3	B	6.83	-133.41	2-3	18.82	-152.33
5	4	B	6.83	-133.41	3-4	1.32	-151.60
5	5	B	6.84	-133.38	2-5	3.95	-159.15
5	6	B	6.84	-133.38	5-6	1.98	-159.23
5	7	B	6.84	-133.39	2-7	7.78	-151.55
5	8	B	6.83	-133.40	7-8	6.46	-151.59
5	9	B	6.83	-133.41	3-9	3.29	-156.11
5	10	B	6.83	-133.41	9-10	1.32	-151.61
5	11	B	6.83	-133.42	3-11	7.77	-151.55
5	12	B	6.83	-133.43	11-12	6.45	-151.63
6	1	C	6.94	107.32	MV bus 6 - 1	34.94	87.40
6	2	C	6.93	107.27	1-2	32.94	87.75
6	3	C	6.93	107.24	2-3	19.08	88.31
6	4	C	6.93	107.24	3-4	1.34	89.04
6	5	C	6.93	107.27	2-5	4.01	87.50
6	6	C	6.93	107.26	5-6	2.01	87.75
6	7	C	6.93	107.26	2-7	7.88	89.09
6	8	C	6.93	107.25	7-8	6.55	89.05
6	9	C	6.93	107.24	3-9	3.33	84.54
6	10	C	6.93	107.23	9-10	1.34	89.04
6	11	C	6.92	107.23	3-11	7.88	89.06
6	12	C	6.92	107.22	11-12	6.54	89.02
13	1	A	7.03	-5.71	MV bus 13 -1	35.38	-25.64
13	2	A	7.02	-5.76	1-2	33.36	-25.29
13	3	A	7.02	-5.80	2-3	19.32	-24.72
13	4	A	7.01	-5.80	3-4	1.35	-23.99
13	5	A	7.02	-5.77	2-5	4.06	-31.54
13	6	A	7.02	-5.77	5-6	2.03	-31.61
13	7	A	7.02	-5.78	2-7	7.98	-23.94
13	8	A	7.01	-5.79	7-8	6.63	-23.98
13	9	A	7.01	-5.80	3-9	3.37	-28.50
13	10	A	7.01	-5.80	9-10	1.35	-24.00
13	11	A	7.02	-5.81	3-11	7.98	-23.97
13	12	A	7.01	-5.82	11-12	6.63	-23.98
13	1	B	7.03	-125.71	MV bus 13 - 1	35.39	-145.64
13	2	B	7.02	-125.76	1-2	33.37	-145.29
13	3	B	7.02	-125.80	2-3	19.32	-144.72

Bus	Subnetwork Bus	Phase	Voltage		From bus to bus	Current	
			LN rms	angle		rms	angle
			[kV]	[degree]		[A]	[degree]
13	4	B	7.02	-125.80	3-4	1.35	-143.99
13	5	B	7.02	-125.77	2-5	4.06	-151.54
13	6	B	7.02	-125.77	5-6	2.03	-151.61
13	7	B	7.02	-125.78	2-7	7.99	-143.94
13	8	B	7.02	-125.79	7-8	6.63	-143.94
13	9	B	7.02	-125.80	3-9	3.37	-148.50
13	10	B	7.02	-125.80	9-10	1.35	-144.00
13	11	B	7.01	-125.81	3-11	7.98	-143.97
13	12	B	7.01	-125.82	11-12	6.63	-144.01
14	1	C	6.94	113.57	MV bus 14 - 1	34.95	93.65
14	2	C	6.93	113.52	1-2	32.96	93.65
14	3	C	6.93	113.49	2-3	19.09	94.56
14	4	C	6.93	113.49	3-4	1.34	95.29
14	5	C	6.93	113.52	2-5	4.01	87.74
14	6	C	6.93	113.51	5-6	2.01	87.67
14	7	C	6.93	113.51	2-7	7.89	95.34
14	8	C	6.93	113.50	7-8	6.55	95.30
14	9	C	6.93	113.49	3-9	3.33	90.79
14	10	C	6.93	113.48	9-10	1.34	95.29
14	11	C	6.93	113.48	3-11	7.88	95.31
14	12	C	6.93	113.47	11-12	6.55	95.27

Table 9.5: Transformer tap parameters of North American MV distribution network benchmark

Node from	Node to	Feeder	Primary tap setting, $V_{1,tap}$	Secondary tap setting, $V_{2,tap}$
			[% of winding voltage]	[% of winding voltage]
0	1	1	2.5	9.375
0	12	2	0	5.0

9.2.4 Power Flow Results of European MV Distribution Network Benchmark

Table 9.6 gives the power flow results for the base case of the European MV distribution system. The base case is a radial system, thus the positions of configuration switches S1, S2, and S3 are all open. All other data are as specified in the appropriate tables in Section 6.2. In order to maintain reasonable voltage levels at the ends of the feeders, tap changing transformers were used as specified in Section 6.2.2 with tap settings specified in Table 9.7.

Table 9.6: Power flow results of European MV distribution network benchmark

Bus	Voltage			From bus to Bus	Current		
	Phase	LL rms	angle		Phase	rms	angle
		[kV]	[degree]			[A]	[degree]
0	AB	110	0	HV bus - 0	A	256.06	-19.78
0	BC	110	120	HV bus - 0	B	256.06	-139.78
0	CA	110	-120	HV bus - 0	C	256.06	100.22
1	AB	20.52	23.66	0-1	A	727.89	9.75

1	BC	20.52	-96.34	0-1	B	727.89	-110.75
1	CA	20.52	143.66	0-1	C	727.89	129.75
2	AB	20.09	22.75	1-2	A	125.27	5.41
2	BC	20.09	-97.25	1-2	B	125.27	-114.59
2	CA	20.09	142.75	1-2	C	125.27	125.41
3	AB	19.43	21.25	2-3	A	125.98	4.37
3	BC	19.43	-98.75	2-3	B	125.98	-115.63
3	CA	19.43	141.25	2-3	C	125.98	124.37
4	AB	19.40	21.16	3-4	A	48.98	8.30
4	BC	19.40	-98.84	3-4	B	48.98	-111.70
4	CA	19.40	141.16	3-4	C	48.98	128.30
5	AB	19.38	21.10	4-5	A	36.57	8.25
5	BC	19.38	-98.90	4-5	B	36.57	-111.75
5	CA	19.38	141.10	4-5	C	36.57	128.25
6	AB	19.35	21.03	5-6	A	15.79	6.97
6	BC	19.35	-98.97	5-6	B	15.79	-113.03
6	CA	19.35	141.03	5-6	C	15.79	126.97
7	AB	19.33	21.03	8-7	A	2.52	-10.59
7	BC	19.33	-98.97	8-7	B	2.52	-130.59
7	CA	19.33	141.03	8-7	C	2.52	79.41
8	AB	19.33	21.04	3-8	A	62.31	1.79
8	BC	19.33	-98.96	3-8	B	62.31	-118.21
8	CA	19.33	141.04	3-8	C	62.31	121.79
9	AB	19.31	21.00	8-9	A	43.43	-0.83
9	BC	19.31	-99.00	8-9	B	43.43	-120.83
9	CA	19.31	141.00	8-9	C	43.43	119.17
10	AB	19.29	20.95	9-10	A	25.21	5.73
10	BC	19.29	-99.05	9-10	B	25.21	-114.27
10	CA	19.29	140.95	9-10	C	25.21	125.73
11	AB	19.29	20.94	10-11	A	9.48	6.89
11	BC	19.29	-99.06	10-11	B	9.48	-113.11
11	CA	19.29	140.94	10-11	C	9.48	126.89
12	AB	20.04	24.50	0-12	A	612.21	10.95
12	BC	20.04	-95.50	0-12	B	612.21	-119.05
12	CA	20.04	144.50	0-12	C	612.21	130.95
13	AB	19.94	24.45	12-13	A	18.27	-1.17
13	BC	19.94	-95.55	12-13	B	18.27	-121.17
13	CA	19.94	144.45	12-13	C	18.27	118.83
14	AB	19.88	24.43	13-14	A	17.18	-1.08
14	BC	19.88	-95.57	13-14	B	17.18	-121.08
14	CA	19.88	144.43	13-14	C	17.18	118.92

Table 9.7: Transformer tap parameters of European MV distribution network benchmark

Node from	Node to	Feeder	Primary tap setting, $V_{1,tap}$	Secondary tap setting, $V_{2,tap}$
			[% of winding voltage]	[% of winding voltage]
0	1	1	0	6.250
0	12	2	0	3.125

9.2.5 Power Flow Results of North American LV Distribution Network Benchmark

Table 9.8 gives the power flow results for the base case of the North American LV distribution system. All data are as specified in the appropriate tables in Section 7.1.

Table 9.8: Power flow results of North American LV distribution network benchmark

Bus	Voltage			From Bus to Bus	Current		
	Phase	LN/LL† rms [V]	angle [degree]		Phase	rms [A]	angle [degree]
0	AB	12470	0	MV bus - 0	A	21.92	-19.83
0	BC	12470	-120	MV bus - 0	B	13.71	-149.68
0	CA	12470	120	MV bus - 0	C	13.76	90.32
R1	A_1	118.80	-30.44	R0-R1	A_1	99.39	-24.01
R2	A_1	118.15	-30.47	R1-R2	A_1	62.94	-22.71
R3	A_1	117.51	-30.46	R2-R3	A_1	40.14	-25.01
R4	A_1	117.13	-30.45	R3-R4	A_1	24.12	-26.28
R5	A_1	118.26	-30.42	R1-R5	A_1	13.55	-26.26
R6	A_1	118.43	-30.43	R1_R6	A_1	9.46	-26.27
R7	A_1	117.73	-30.40	R1_R7	A_1	13.49	-26.25
R8	A_1	117.82	-30.48	R2-R8	A_1	8.18	-18.67
R9	A_1	117.94	-30.48	R2-R9	A_1	5.32	-18.67
R10	A_1	117.40	-30.49	R2-R10	A_1	9.38	-18.69
R11	A_1	117.14	-30.45	R3-R11	A_1	9.35	-26.29
R12	A_1	117.33	-30.47	R3-R12	A_1	6.72	-18.66
R13	A_1	116.70	-30.44	R4_R13	A_1	10.74	-26.28
R14	A_1	116.76	-30.44	R4-R14	A_1	13.38	-26.28
I1	AB	469.11	-0.69	I0-I1	A	230.69	-32.36
I1	BC	469.08	-120.69	I0-I1	B	231.34	-152.57
I1	CA	469.10	119.31	I0-I1	C	232.28	87.42
I2	AB	467.25	-0.70	I1-I2	A	230.69	-32.36
I2	BC	467.55	-120.73	I1-I2	B	231.34	-152.57
I2	CA	467.22	119.25	I1-I2	C	232.28	87.42
I3	AB	461.44	-0.63	I2-I3	A	230.69	-32.36
I3	BC	462.57	-120.72	I2-I3	B	231.34	-152.57
I3	CA	461.39	119.20	I2-I3	C	232.28	87.42
C1	AB	204.11	-0.79	C0-C1	A	289.06	-24.35
C1	BC	204.11	-120.79	C0-C1	B	289.48	-144.40
C1	CA	204.11	119.22	C0-C1	C	289.89	95.61
C2	AB	203.03	-0.86	C1-C2	A	180.36	-21.59
C2	BC	203.25	-120.88	C1-C2	B	180.74	-141.68
C2	CA	203.07	119.08	C1-C2	C	181.13	98.34
C3	AB	201.47	-0.80	C2-C3	A	98.80	-20.98
C3	BC	201.81	-120.84	C2-C3	B	99.05	-141.08
C3	CA	201.53	119.10	C2-C3	C	99.30	98.94
C4	AB	201.18	-0.78	C3-C4	A	26.95	-26.52
C4	BC	201.54	-120.82	C3-C4	B	27.02	-146.63
C4	CA	201.24	119.11	C3-C4	C	27.09	93.39
C5	AB	202.47	-0.61	C1-C5	A	34.47	-26.45
C5	BC	202.51	-120.62	C1-C5	B	34.48	-146.46

C5	CA	202.47	119.38	C1-C5	C	34.49	93.54
C6	AB	202.15	-0.51	C1-C6	A	45.58	-32.30
C6	BC	202.20	-120.52	C1-C6	B	45.60	-152.31
C6	CA	202.15	119.48	C1-C6	C	45.60	87.69
C7	AB	202.88	-0.65	C1-C7	A	27.34	-26.50
C7	BC	202.91	-120.66	C1-C7	B	27.35	-146.50
C7	CA	202.88	119.34	C1-C7	C	27.35	93.50
C8	AB	201.59	-0.76	C2-C8	A	45.41	-18.94
C8	BC	201.84	-120.79	C2-C8	B	45.48	-139.02
C8	CA	201.63	119.16	C2-C8	C	45.56	101.00
C9	AB	201.92	-0.74	C2-C9	A	36.33	-26.57
C9	BC	202.17	-120.76	C2-C9	B	36.39	-146.64
C9	CA	201.96	119.19	C2-C9	C	36.46	93.37
C10	AB	200.03	-0.71	C3-C10	A	45.03	-18.89
C10	BC	200.40	-120.75	C3-C10	B	45.15	-138.99
C10	CA	200.10	119.18	C3-C10	C	45.26	101.03
C11	AB	200.61	-0.74	C3-C11	A	26.99	-18.93
C11	BC	200.97	-120.78	C3-C11	B	27.06	-139.03
C11	CA	200.67	119.15	C3-C11	C	27.12	100.99
C12	AB	200.35	-0.69	C4-C12	A	26.95	-26.52
C12	BC	200.74	-120.74	C4-C12	B	27.02	-146.63
C12	CA	200.42	119.19	C4-C12	C	27.09	93.39

†LN for residential network and LL for industrial and commercial

9.2.6 Power Flow Results of European LV Distribution Network Benchmark

Table 9.9 gives the power flow results for the base case of the European LV distribution system. All data are as specified in the appropriate tables in Section 7.2.

Table 9.9: Power flow results of European LV distribution network benchmark

Bus	Voltage			From bus to Bus	Current		
	Phase	LL rms [V]	angle [degree]		Phase	rms [A]	angle [degree]
0	AB	20000	0	MV bus - 0	A	20.52	-23.90
0	BC	20000	-120	MV bus - 0	B	20.52	-143.78
0	CA	20000	120	MV bus - 0	C	20.56	96.17
R1	AB	393.04	28.45	R0-R1	A	557.69	10.27
R1	BC	393.02	-91.55	R0-R1	B	559.38	-109.84
R1	CA	393.01	148.45	R0-R1	C	561.07	130.18
R2	AB	389.88	28.41	R1-R2	A	274.02	10.28
R2	BC	390.24	-91.61	R1-R2	B	275.74	-109.95
R2	CA	389.94	148.35	R1-R2	C	277.45	130.10
R3	AB	386.71	28.37	R2-R3	A	274.02	-10.28
R3	BC	387.47	-91.67	R2-R3	B	275.74	-109.95
R3	CA	386.86	148.25	R2-R3	C	277.45	130.10
R4	AB	383.79	28.33	R3-R4	A	253.18	-10.29
R4	BC	384.91	-91.73	R3-R4	B	254.84	-109.95
R4	CA	384.02	148.16	R3-R4	C	256.50	130.10

R5	AB	381.67	28.30	R4-R5	A	183.99	-10.17
R5	BC	383.05	-91.77	R4-R5	B	185.29	-110.10
R5	CA	381.95	148.09	R4-R5	C	186.62	129.96
R6	AB	379.54	28.28	R5-R6	A	183.99	-10.17
R6	BC	381.18	-91.81	R5-R6	B	185.29	-110.10
R6	CA	379.89	148.02	R5-R6	C	186.62	129.96
R7	AB	378.27	28.26	R6-R7	A	109.71	-10.17
R7	BC	380.07	-91.83	R6-R7	B	110.56	-110.10
R7	CA	378.65	147.98	R6-R7	C	111.44	129.91
R8	AB	377.00	28.24	R7-R8	A	109.71	-10.17
R8	BC	378.96	-91.86	R7-R8	B	110.56	-110.10
R8	CA	377.42	147.94	R7-R8	C	111.44	129.91
R9	AB	375.73	28.23	R8-R9	A	109.71	-10.17
R9	BC	377.84	-91.88	R8-R9	B	110.56	-110.10
R9	CA	376.19	147.89	R8-R9	C	111.44	129.91
R10	AB	375.01	28.22	R9-R10	A	62.80	-10.14
R10	BC	377.21	-91.89	R9-R10	B	63.30	-110.17
R10	CA	375.48	147.87	R9-R10	C	63.81	129.90
R11	AB	385.83	28.40	R3-R11	A	20.84	-10.22
R11	BC	386.61	-91.64	R3-R11	B	20.90	-109.89
R11	CA	385.98	148.28	R3-R11	C	20.96	130.13
R12	AB	380.34	28.45	R4-R12	A	69.19	-10.60
R12	BC	381.55	-91.62	R4-R12	B	69.55	-109.56
R12	CA	380.59	148.26	R4-R12	C	69.88	130.47
R13	AB	376.90	28.56	R12-R13	A	69.19	-10.60
R13	BC	378.20	-91.50	R12-R13	B	69.55	-109.56
R13	CA	377.17	148.36	R12-R13	C	69.88	130.47
R14	AB	373.46	28.68	R13-R14	A	69.19	-10.60
R14	BC	374.84	-91.39	R13-R14	B	69.55	-109.56
R14	CA	373.75	148.46	R13-R14	C	69.88	130.47
R15	AB	370.02	28.80	R14-R15	A	69.19	-10.60
R15	BC	371.49	-91.27	R14-R15	B	69.55	-109.56
R15	CA	370.33	148.57	R14-R15	C	69.88	130.47
R16	AB	375.84	28.40	R6-R16	A	74.28	-10.23
R16	BC	377.58	-91.68	R6-R16	B	74.73	-110.01
R16	CA	376.21	148.13	R6-R16	C	75.18	130.05
R17	AB	373.40	28.31	R9-R17	A	46.91	-10.14
R17	BC	375.56	-91.80	R9-R17	B	47.27	-110.16
R17	CA	373.86	147.97	R9-R17	C	47.63	129.91
R18	AB	372.32	28.31	R10-R18	A	62.80	-10.14
R18	BC	374.59	-91.80	R10-R18	B	63.30	-110.17
R18	CA	372.81	147.95	R10-R18	C	63.81	129.90
I1	AB	392.52	28.95	I0-I1	A	136.54	-2.23
I1	BC	392.48	-91.05	I0-I1	B	137.02	-122.42
I1	CA	392.49	148.95	I0-I1	C	137.51	117.57
I2	AB	379.41	29.52	I1-I2	A	136.54	-2.23
I2	BC	380.39	-90.57	I1-I2	B	137.02	-122.42
I2	CA	379.38	149.35	I1-I2	C	137.51	117.57
C1	AB	391.79	28.60	C0-C1	A	332.61	2.82
C1	BC	391.77	-91.40	C0-C1	B	333.52	-117.15
C1	CA	391.78	148.61	C0-C1	C	333.37	122.84

C2	AB	386.85	28.58	C1-C2	A	162.96	-2.87
C2	BC	387.18	-91.42	C1-C2	B	163.88	-117.05
C2	CA	386.86	148.52	C1-C2	C	163.73	122.91
C3	AB	381.91	28.55	C2-C3	A	162.96	-2.87
C3	BC	382.60	-91.50	C2-C3	B	163.88	-117.05
C3	CA	381.94	148.43	C2-C3	C	163.73	122.91
C4	AB	379.60	28.54	C3-C4	A	76.24	-2.71
C4	BC	380.45	-91.53	C3-C4	B	76.73	-117.21
C4	CA	379.64	148.39	C3-C4	C	76.64	122.76
C5	AB	377.28	28.52	C4-C5	A	76.24	-2.71
C5	BC	378.30	-91.55	C4-C5	B	76.73	-117.21
C5	CA	377.34	148.35	C4-C5	C	76.64	122.76
C6	AB	376.31	28.52	C5-C6	A	32.16	-2.59
C6	BC	377.39	-91.57	C5-C6	B	32.38	-117.31
C6	CA	376.37	148.33	C5-C6	C	32.34	122.66
C7	AB	375.33	28.51	C6-C7	A	32.16	-2.59
C7	BC	376.49	-91.58	C6-C7	B	32.38	-117.31
C7	CA	375.40	148.32	C6-C7	C	32.34	122.66
C8	AB	374.36	28.51	C7-C8	A	32.16	-2.59
C8	BC	375.58	-91.59	C7-C8	B	32.38	-117.31
C8	CA	374.42	148.30	C7-C8	C	32.34	122.66
C9	AB	374.03	28.51	C8-C9	A	10.73	-2.56
C9	BC	375.28	-91.59	C8-C9	B	10.81	-117.35
C9	CA	374.10	148.29	C8-C9	C	10.79	122.63
C10	AB	375.83	28.76	C3-C10	A	86.73	-3.02
C10	BC	376.70	-91.31	C3-C10	B	87.15	-116.91
C10	CA	375.88	148.61	C3-C10	C	87.09	123.04
C11	AB	372.11	28.89	C10-C11	A	53.20	-3.05
C11	BC	373.09	-91.19	C10-C11	B	53.47	-116.87
C11	CA	372.16	148.72	C10-C11	C	53.43	123.08
C12	AB	369.37	29.02	C11-C12	A	26.60	-3.05
C12	BC	370.40	-91.07	C11-C12	B	26.73	-116.87
C12	CA	369.42	148.83	C11-C12	C	26.71	123.08
C13	AB	369.37	29.02	C11-C13	A	26.60	-3.05
C13	BC	370.40	-91.07	C11-C13	B	26.73	-116.87
C13	CA	369.42	148.83	C11-C13	C	26.71	123.08
C14	AB	372.38	28.92	C10-C14	A	33.53	-2.96
C14	BC	373.32	-91.16	C10-C14	B	33.68	-116.97
C14	CA	372.43	148.75	C10-C14	C	33.66	122.99
C15	AB	374.20	28.63	C5-C15	A	44.08	-2.79
C15	BC	375.30	-91.46	C5-C15	B	44.35	-117.13
C15	CA	374.26	148.44	C5-C15	C	44.30	122.84
C16	AB	373.45	28.66	C15-C16	A	10.72	-2.73
C16	BC	374.57	-91.43	C15-C16	B	10.79	-117.19
C16	CA	373.51	148.46	C15-C16	C	10.77	122.78
C17	AB	372.34	28.71	C16-C17	A	10.72	-2.73
C17	BC	373.49	-91.38	C16-C17	B	10.79	-117.19
C17	CA	372.40	148.51	C16-C17	C	10.77	122.78
C18	AB	370.76	28.79	C15-C18	A	33.36	-2.81
C18	BC	371.93	-91.30	C15-C18	B	33.56	-117.11
C18	CA	370.82	148.59	C15-C18	C	33.53	122.86

C19	AB	372.05	28.61	C8-C19	A	21.42	-2.61
C19	BC	373.41	-91.49	C8-C19	B	21.57	-117.30
C19	CA	372.22	148.39	C8-C19	C	21.54	122.68
C20	AB	372.93	28.56	C9-C20	A	10.73	-2.56
C20	BC	374.19	-91.54	C9-C20	B	10.81	-117.35
C20	CA	373.00	148.34	C9-C20	C	10.79	122.63

9.3 Component Parameter Calculation

9.3.1 Overhead Lines

Tabulated values of conductor diameter d_c, geometric mean radius *GMR*, and AC resistance per phase unit length R'_{ac} are given in the tables for each network benchmark. From these basic data, calculation of phase resistance R'_{ph}, reactance X'_{ph} and susceptance B'_{ph}, and zero sequence resistance R'_0, reactance X'_0 and susceptance B'_0 is then possible. A methodology, based on the modified Carson's equations and Kron reduction method, as described in [34] unless otherwise noted, is given below. Note that the calculation of zero sequence parameters is not applicable to single-phase lines.

9.3.1.1 Series Impedance

The self and mutual impedances of overhead and underground lines including the earth return can be calculated from the modified Carson's equations:

$$Z'_{ii} = R'_i + R'_{\text{earth}} + \mathrm{j}\cdot 2\pi f \cdot k_1 \ln\left(\frac{D_e}{GMR_i}\right), \quad (1)$$

$$Z'_{ij} = R'_{\text{earth}} + \mathrm{j}\cdot 2\pi f \cdot k_1 \ln\left(\frac{D_e}{D_{ij}}\right). \quad (2)$$

where the constant $k_1=2\times10^{-4}$ H/km, $R'_{\text{earth}} = 9.869\times10^{-4}$ Ωs/km · *f*, and *i* and *j* are conductor indices. The frequency *f* is 60 Hz for North American systems and 50 Hz for European systems, D_{ij} is the center-to-center distance between conductors *i* and *j*, and D_e is the equivalent distance between overhead conductors and their fictitious earth return conductors:

$$D_e = k_2\sqrt{\frac{\rho_g}{f}}, \quad (3)$$

with $k_2 = 658.4$ (m/H)$^{1/2}$ and the earth resistivity ρ_g whose typical value is 100 Ωm.

The geometric mean radius (GMR) of individual conductors, GMR_i, is provided in the tables describing each benchmark. For bundled conductors, which frequently appear in HV transmission systems, each bundle needs to be treated as one conductor, therefore an effective GMR, GMR_{bundle}, is calculated. In this report, two-conductor bundles are used. The bundle GMR in this case becomes:

$$GMR_{\text{bundle}} = \sqrt{GMR\cdot d}, \quad (4)$$

where d is the distance between two conductors of one bundle as shown in Figure 5.2 and Figure 5.4. The unit of *d*, GMR_i, and D_{ij} is meter for use in the Carson's equations, and the unit of Z'_{ii} and Z'_{ij} is Ω/km.

The resistance per phase per unit length R'ac can be obtained directly from the appropriate table such as Table 5.3 for North American HV lines. If resistances for conductor

temperatures other than 20 oC as for R'dc and 50 oC as for R'ac are desired, the following equation can be used to calculate new values:

$$R'_2 = R'_1\left(1 + \alpha_1(\vartheta_2 - \vartheta_1)\right), \tag{5}$$

where R'_1 is the resistance per km at ϑ_1, R'_2 is the resistance per km at ϑ_2, and α_1 is the temperature coefficient of resistance at ϑ_1. For AAC 1350-H19 conductor with 61.2 % IACS, α_1 = 0.00404 per ^{o}C at 20 ^{o}C and α_1 = 0.00361 per ^{o}C at 50 ^{o}C [5].

Normally, it is best to use R'_{ac} values for overhead conductors because they take into account the increased resistance due to skin effect. Proximity effect is usually negligible for overhead lines due to tower configurations and is thus neglected [5]. For ACSR conductors and steel ground wires, both effective AC resistance and inductance increase with current density due to core magnetization, thus it is important to use the appropriate resistance and GMR values as determined from manufacturer tables consistent with the expected current flowing through these wires.

The primitive impedance matrix [34] for an overhead line can be built from (1) and (2). For a three-phase line with m neutrals, the primitive impedance matrix is (3+m)×(3+m) as:

$$\boldsymbol{Z}_{\text{primitive}} = \begin{pmatrix} \boldsymbol{Z}_{\text{pp}} & \boldsymbol{Z}_{\text{pn}} \\ \boldsymbol{Z}_{\text{np}} & \boldsymbol{Z}_{\text{nn}} \end{pmatrix}, \tag{6}$$

where subscript p indicates phase conductor, n indicates neutral conductor,

$$\boldsymbol{Z}_{\text{pp}} = \begin{pmatrix} \boldsymbol{Z}'_{\text{p\_AA}} & \boldsymbol{Z}'_{\text{pp\_AB}} & \boldsymbol{Z}'_{\text{pp\_AC}} \\ \boldsymbol{Z}'_{\text{pp\_BA}} & \boldsymbol{Z}'_{\text{p\_BB}} & \boldsymbol{Z}'_{\text{pp\_BC}} \\ \boldsymbol{Z}'_{\text{pp\_CA}} & \boldsymbol{Z}'_{\text{pp\_CB}} & \boldsymbol{Z}'_{\text{p\_CC}} \end{pmatrix}, \tag{7}$$

$$\boldsymbol{Z}_{\text{pn}} = \begin{pmatrix} \boldsymbol{Z}'_{\text{pn\_A N1}} & \cdots & \boldsymbol{Z}'_{\text{pn\_AN}\boldsymbol{m}} \\ \boldsymbol{Z}'_{\text{pn\_BN1}} & \cdots & \boldsymbol{Z}'_{\text{pn\_BN}\boldsymbol{m}} \\ \boldsymbol{Z}'_{\text{pn\_CN1}} & \cdots & \boldsymbol{Z}'_{\text{pn\_CN}\boldsymbol{m}} \end{pmatrix}, \tag{8}$$

$\boldsymbol{Z}_{\text{np}} = \boldsymbol{Z}_{\text{pn}}{}^{\text{T}}$ and

$$\boldsymbol{Z}_{\text{nn}} = \begin{pmatrix} \boldsymbol{Z}'_{\text{n\_N1N1}} & \cdots & \boldsymbol{Z}'_{\text{n\_N1N}\boldsymbol{m}} \\ \vdots & \cdots & \vdots \\ \boldsymbol{Z}'_{\text{n\_N}\boldsymbol{m}\text{ N1}} & \cdots & \boldsymbol{Z}'_{\text{n\_N}\boldsymbol{m}\text{ N}\boldsymbol{m}} \end{pmatrix}. \tag{9}$$

From the primitive impedance matrix, the phase impedance matrix can be obtained from Kron reduction:

$$\boldsymbol{Z}_{\text{ABC}} = \boldsymbol{Z}_{\text{pp}} - \boldsymbol{Z}_{\text{pn}}\boldsymbol{Z}_{\text{nn}}^{-1}\boldsymbol{Z}_{\text{np}}, \tag{10}$$

For three-phase lines, the phase impedance matrix $\boldsymbol{Z}_{\text{ABC}}$ has the form of

$$\boldsymbol{Z}_{\text{ABC}} = \begin{pmatrix} \boldsymbol{Z}'_{\text{AA}} & \boldsymbol{Z}'_{\text{AB}} & \boldsymbol{Z}'_{\text{AC}} \\ \boldsymbol{Z}'_{\text{BA}} & \boldsymbol{Z}'_{\text{BB}} & \boldsymbol{Z}'_{\text{BC}} \\ \boldsymbol{Z}'_{\text{CA}} & \boldsymbol{Z}'_{\text{CB}} & \boldsymbol{Z}'_{\text{CC}} \end{pmatrix}. \tag{11}$$

For two-phase lines, that share a common neutral, $\boldsymbol{Z}_{\text{ABC}}$ is 2×2, and for single-phase lines $\boldsymbol{Z}_{\text{ABC}}$ is a scalar. The line parameters specified in this report are given in terms of positive-, negative-, and zero-sequence values. To obtain these values, the $\boldsymbol{Z}_{\text{ABC}}$ matrix must be calculated from

$$\boldsymbol{Z}_{012} = \mathbf{A}_{\text{S}}^{-1}\boldsymbol{Z}_{\text{ABC}}\mathbf{A}_{\text{S}}, \tag{12}$$

with

$$\mathbf{A}_s = \begin{pmatrix} 1 & 1 & 1 \\ 1 & e^{-j\frac{2\pi}{3}} & e^{j\frac{2\pi}{3}} \\ 1 & e^{j\frac{2\pi}{3}} & e^{-j\frac{2\pi}{3}} \end{pmatrix}, \tag{13}$$

The sequence impedance matrix $\mathbf{Z}_{012}$ has the form of

$$\mathbf{Z}_{012} = \begin{pmatrix} Z'_{00} & Z'_{01} & Z'_{02} \\ Z'_{10} & Z'_{11} & Z'_{12} \\ Z'_{20} & Z'_{21} & Z'_{22} \end{pmatrix}. \tag{14}$$

where $Z'_{00}=R'_0+jX'_0$, and $Z'_{11}=R'_1+jX'_1$ are respectively the zero and positive sequence impedances.

For non-transposed lines, as typically for MV and LV overhead distribution lines, the off-diagonal terms of $\mathbf{Z}_{ABC}$ are not equal, so that $\mathbf{Z}_{012}$ is not a diagonal matrix. However, in most cases, the off-diagonal terms of $\mathbf{Z}_{012}$ are small so that they can be ignored. For balanced transposed HV transmission lines, $\mathbf{Z}_{ABC}$ can be simplified as follows:

$$\mathbf{Z}_{ABC} = \begin{pmatrix} Z'_s & Z'_m & Z'_m \\ Z'_m & Z'_s & Z'_m \\ Z'_m & Z'_m & Z'_s \end{pmatrix}, \tag{15}$$

where

$$Z'_s = \frac{1}{3}\left(Z'_{AA} + Z'_{BB} + Z'_{CC}\right), \tag{16}$$

and

$$Z'_m = \frac{1}{3}\left(Z'_{AB} + Z'_{BC} + Z'_{CA}\right), \tag{17}$$

Z_s and Z_m are the self and mutual impedances of the lines, respectively. From the modified $\mathbf{Z}_{ABC}$, $\mathbf{Z}_{012}$ is diagonal and

$$Z'_{00} = Z'_s + 2Z'_m, \tag{18}$$

$$Z'_{11} = Z'_s - Z'_m. \tag{19}$$

In this report, for HV and MV network benchmarks, $Z'_{ph}=R'_{ph}+jX'_{ph}$ and Z'_{00} are provided where Z'_{ph} is equal to Z'_s. Having Z'_{ph} and Z'_{00}, both mutual and positive sequence impedances can be obtained from (18) and (19). In LV networks, both primitive and phase impedance matrices after the Kron reduction are provided.

Another method that simplifies the above procedure for transposed line parameter calculation is to make use of the geometric mean distance (GMD). For three-phase lines, the GMD between phase conductors is

$$GMD_{pp} = \sqrt[3]{D_{AB} \times D_{BC} \times D_{CA}}, \tag{20}$$

where the subscript p indicates phase conductor, and the GMD between phase conductor and neutral is

$$GMD_{pn} = \sqrt[3]{D_{AN} \times D_{BN} \times D_{CN}}, \tag{21}$$

where the subscript n indicates neutral conductor.

Employing (1) and (2), results in the following equivalent impedances which are elements of the primitive impedance matrix in (6):

$$Z'_{\mathrm{p}} = R'_{\mathrm{ac}} + 9.869\times10^{-4}\,\Omega\mathrm{s/km}\cdot f + \mathrm{j}\cdot 2\pi f\cdot k_1 \ln\left(\frac{D_{\mathrm{e}}}{GMR_{\mathrm{p}}}\right), \tag{22}$$

$$Z'_{\mathrm{n}} = R'_{\mathrm{n}} + 9.869\times10^{-4}\,\Omega\mathrm{s/km}\cdot f + \mathrm{j}\cdot 2\pi f\cdot k_1 \ln\left(\frac{D_{\mathrm{e}}}{GMR_{\mathrm{n}}}\right), \tag{23}$$

$$Z'_{\mathrm{pp}} = 9.869\times10^{-4}\,\Omega\mathrm{s/km}\cdot f + \mathrm{j}\cdot 2\pi f\cdot k_1 \ln\left(\frac{D_{\mathrm{e}}}{GMD_{\mathrm{pp}}}\right), \tag{24}$$

$$Z'_{\mathrm{pn}} = 9.869\times10^{-4}\,\Omega\mathrm{s/km}\cdot f + \mathrm{j}\cdot 2\pi f\cdot k_1 \ln\left(\frac{D_{\mathrm{e}}}{GMD_{\mathrm{pn}}}\right). \tag{25}$$

Application of the phase impedance matrix (10) and the sequence impedance transformation (18) and (19) leads to the following equations for zero and positive sequence impedances:

$$Z'_{00} = Z'_{\mathrm{p}} + 2Z'_{\mathrm{pp}} - 3\left(\frac{Z'^{2}_{\mathrm{pn}}}{Z'_{\mathrm{n}}}\right), \tag{26}$$

$$Z'_{11} = Z'_{\mathrm{p}} - Z'_{\mathrm{pp}}. \tag{27}$$

9.3.1.2 Shunt Admittance

The potential coefficient matrix [34] ***P*** is used to calculate the shunt admittance of overhead lines. The elements in ***P*** are given by

$$P_{ii} = 17.975\times10^{6}\,\mathrm{km/F}\cdot\ln\frac{D_{ii'}\cdot 200\,\mathrm{cm}}{d_{\mathrm{c}}\cdot 1\,\mathrm{m}}, \tag{28}$$

$$P_{ij} = 17.975\times10^{6}\,\mathrm{km/F}\cdot\ln\frac{D_{ij'}}{D_{ij}}. \tag{29}$$

where $D_{ij'}$ is the distance between one phase conductor and the image of another phase conductor as illustrated in Figure 9.1.

If one of the conductors is a grounded neutral, the potential coefficient matrix must be reduced using the Kron reduction method. The inverse of the potential coefficient matrix will give the capacitance matrix.

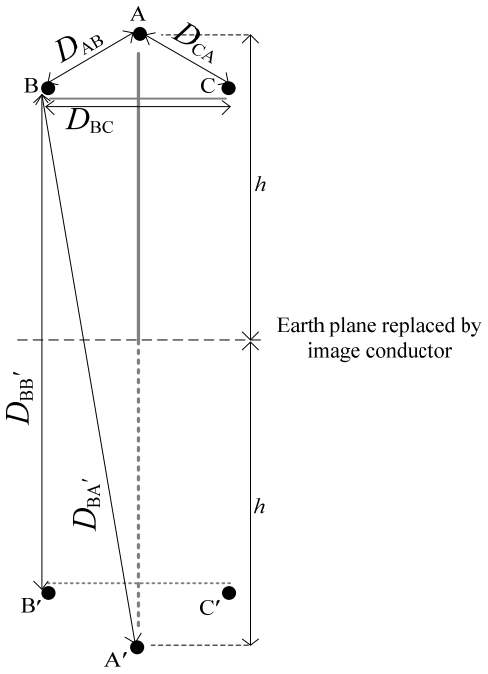

Figure 9.1: Transmission line images

9.3.2 Underground Cables

The phase and zero sequence resistance and reactance, R'_{ph}, X'_{ph}, R'_0, and X'_0 are used for the concentric-neutral and tape-shielded cables in the report. To obtain the sequence impedances by the procedures introduced in Section 9.3.1 using the modified Carson's equations, the equivalent neutral conductor must be considered. In the following, details of calculating the needed parameters to be used in the modified Carson's equations for both types of cables are introduced.

9.3.2.1 Tape-shielded Cable

The tape shield provides a neutral path for the tape-shielded cable. The resistance of the tape shield is

$$R'_n = \frac{46.961\,\Omega/\text{km}\cdot\text{mm}^2}{(d_c + 2t_i)t_{ts}}, \tag{30}$$

where the geometry of the tape-shielded cable can be found in Figure 6.6 and Table 6.11. The GMR of the tape shield can be calculated by

$$GMR_n = \frac{(d_c + 2t_i) - t_{ts}}{2000\text{ mm}} 1\text{ m}, \tag{31}$$

The distance between the phase conductor and its own tape shield is

$$D_{pini} = GMR_{ni}. \tag{32}$$

9.3.2.2 Concentric-neutral Cable

In this type of cable, the concentric neutrals provide the neutral path. The equivalent resistance of concentric neutrals is

$$R'_{\mathrm{n}} = \frac{R'_{\mathrm{s}}}{k}, \tag{33}$$

where R'_{s} is the resistance of a single neutral strand with the unit of Ω/km and k is the number of neutral strands. The GMR of concentric neutrals can be obtained by

$$GMR_{\mathrm{n}} = \sqrt[k]{GMR_{\mathrm{ns}}\, k \left(\frac{d_{\mathrm{ns}} + d_{\mathrm{c}} + 2t_{\mathrm{i}}}{2000\ \mathrm{mm}} 1\,\mathrm{m} \right)^{k-1}}, \tag{34}$$

where GMR_{ns} is the geometric mean radius of a neutral strand; d_{ns} is the diameter of the natural strands. Other cable parameters are shown in Figure 6.6. The distance between the phase conductor and its own concentric neutrals is

$$D_{\mathrm{p}i\mathrm{n}i} = \frac{d_{\mathrm{ns}} + d_{\mathrm{c}} + 2t_{\mathrm{i}}}{2000\mathrm{mm}} 1\mathrm{m}, \tag{35}$$

The distance between the concentric neutrals of one conductor to an adjacent phase conductor can be calculated by:

$$D_{\mathrm{n}i\mathrm{p}j} = \sqrt[k]{D_{ij}^{k} - D_{\mathrm{p}i\mathrm{n}i}^{k}}\ . \tag{36}$$

9.3.3 Transformer Calculations

Transformer impedances were calculated using the following equations:

$$Z_{\mathrm{tr}} = R_{\mathrm{tr}} + \mathrm{j}X_{\mathrm{tr}}$$

$$X_{\mathrm{tr}} = Z_{\mathrm{base}} X_{\mathrm{pu}} = \frac{V_{\mathrm{base}}^2}{S_{\mathrm{base}}} \sqrt{Z_{\mathrm{pu}}^2 - R_{\mathrm{pu}}^2}$$

$$R_{\mathrm{tr}} = Z_{\mathrm{base}} R_{\mathrm{pu}} = \frac{V_{\mathrm{base}}^2}{S_{\mathrm{base}}} R_{\mathrm{pu}}$$

with calculations based on the low voltage side of the transformer. In what follows, example calculations are given for the North American network benchmark configurations. The European calculations follow the same approach.

The parameters of the North American HV-MV subtransmission auto-transformer can be calculated from the given data in Table 9.10.

Table 9.10: Nameplate data of North American HV-MV subtransmission auto-transformer

Voltage	Rating	Z_{tr} on lowest MVA base	R_{tr}
230/115 kV	150MVA	4 %	0.4 %

Therefore: $Z_{\mathrm{pu}} = 0.04$, $R_{\mathrm{pu}} = 0.004$, $S_{\mathrm{base}} = 150$ MVA and $V_{\mathrm{base}} = 115$ kV.

$$R_{\mathrm{tr}} = \frac{(115\mathrm{kV})^2}{150\mathrm{MVA}} 0.004 = 0.353\Omega$$

$$X_{\mathrm{tr}} = \frac{(115\mathrm{kV})^2}{150\mathrm{MVA}} \sqrt{0.04^2 - 0.004^2} = 3.509\Omega$$

The transformer parameters in the North American MV distribution network benchmark can be calculated from the given data in Table 9.11.

Table 9.11: Nameplate data of North American MV transformer

Voltage	Rating	Z_{tr} on lowest MVA base	R_{tr}
115/12.47 kV	15MVA	12 %	1 %

Therefore: $Z_{pu} = 0.12$, $R_{pu} = 0.01$, $S_{base} = 15$ MVA, and $V_{base} = 12.47$ kV.

$$R_{tr} = \frac{(12.47\text{kV})^2}{15\text{MVA}} 0.01 = 0.104\,\Omega$$

$$X_{tr} = \frac{(12.47\text{kV})^2}{15\text{MVA}} \sqrt{0.12^2 - 0.01^2} = 1.240\Omega$$

The parameters of the North American LV residential distribution transformer can be calculated from the given data in Table 9.12.

Table 9.12: Nameplate data of North American LV residential distribution transformer

Voltage	Rating	Z_{tr} on lowest MVA base	R_{tr}
7.2/0.24 kV	50 kVA	2.5 %	1.25 %

Therefore: $Z_{pu} = 0.025$, $R_{pu} = 0.0125$, $S_{base} = 50$ kVA, and $V_{base} = 0.24$ kV.

$$R_{tr} = \frac{(0.24\text{kV})^2}{0.050\text{MVA}} 0.0125 = 0.014\,\Omega$$

$$X_{tr} = \frac{(0.24\text{kV})^2}{0.050\text{MVA}} \sqrt{0.025^2 - 0.0125^2} = 0.025\Omega$$

The parameters of the North American LV industrial distribution transformer can be calculated from the given data in Table 9.13.

Table 9.13: Nameplate data of North American LV industrial distribution transformer

Voltage	Rating	Z_{tr} on lowest MVA base	R_{tr}
12.47/0.480 kV	300 kVA	4 %	2 %

Therefore: $Z_{pu} = 0.04$, $R_{pu} = 0.02$, $S_{base} = 300$ kVA, and $V_{base} = 0.48$ kV.

$$R_{tr} = \frac{(0.48\text{kV})^2}{0.300\text{MVA}} 0.02 = 0.015\,\Omega$$

$$X_{tr} = \frac{(0.48\text{kV})^2}{0.300\text{MVA}} \sqrt{0.04^2 - 0.02^2} = 0.027\,\Omega$$

The parameters of the North American LV commercial distribution transformer can be calculated from the given data in Table 9.14.

Table 9.14: Nameplate data of North American LV commercial distribution transformer

Voltage	Rating	Z_{tr} on lowest MVA base	R_{tr}
12.47/0.208 kV	3 x 37.5 kVA	2.5 %	1.25 %

Therefore: $Z_{pu} = 0.025$, $R_{pu} = 0.0125$, $S_{base} = 112.5$ kVA, $V_{base} = 0.208$ kV.

$$R_{tr} = \frac{(0.208\text{kV})^2}{0.1125\text{MVA}} 0.0125 = 0.005\,\Omega$$

$$X_{tr} = \frac{(0.208\text{kV})^2}{0.1125\text{MVA}} \sqrt{0.025^2 - 0.0125^2} = 0.008\,\Omega$$

9.3.4 Load Coincidence Calculations

When determining the voltage drop and loading on a line section, it is necessary to apply the appropriate coincidence factor to the loads served by the line section or transformer [35]. Coincidence factors should also be used when the single-phase subnetworks of Section 6.1 are not modeled in detail but are instead reduced to a single equivalent load. The coincidence factor is a function of the number of consumers served, N_{ld}. Calculation of an equivalent load, S_{CF}, can be performed by summing the individual loads, S_k, and multiplying by the coincidence factor, CF, as shown in the following equation:

$$S_{CF} = CF \sum_{k=1}^{N_{ld}} S_k \,, \tag{37}$$

where $CF = 0.6\ (1 + 1/N_{ld})$.

Additionally, the equivalent weighted power factor, pf_{eq}, for a subnetwork can be determined from:

$$pf_{eq} = P_{eq} / \sqrt{P_{eq}^{\ 2} + Q_{eq}^{\ 2}} \,, \tag{38}$$

where P_{eq} is the equivalent active power and Q_{eq} is the equivalent reactive power as given by:

$$P_{eq} = \sum_{k=1}^{N_{ld}} (S_k \times pf_k) \,, \tag{39}$$

$$Q_{eq} = \sum_{k=1}^{N_{ld}} S_k \sin(\arccos(pf_k)) \,. \tag{40}$$

where pf_k is the value of power factor for each individual load.

For example, in North American single-phase MV subnetwork of Section 6.1, the calculation can be performed as:

- Coincident equivalent load: $S_{CF} = 0.6\ (1+1/12)\ (265\text{ kVA}) = 172.25$ kVA.
- Equivalent weighted power factor: $pf_{eq} = 248.8 / \sqrt{248.8^2 + 90.2^2} = 0.94$.

10. References

[1] M. Szechtman, T. Wess, C. V. Thio: Premier modèle de référence destiné à des études portant sur le contrôle-commande de réseaux CCHT. ELECTRA, no. 135, 1991.

[2] K. Strunz, H. Louie: Cache energy control for storage: Power system integration and education based on analogies derived from computer engineering. IEEE Transactions on Power Systems, vol. 24, no. 1, 2009.

[3] K. Strunz, E. K. Brock: Stochastic energy source access management: infrastructure-integrative modular plant for sustainable hydrogen-electric co-generation. International Journal of Hydrogen Energy, vol. 31, no. 9, 2006.

[4] S. Jiang, U. D. Annakkage, A. M. Gole: A platform for validation of FACTS models. IEEE Transactions on Power Delivery, vol. 21, no. 1, 2006.

[5] Aluminum Association: Aluminum Electrical Conductor Handbook. 1982.

[6] Southwire Company: Overhead Conductor Manual, second Edition. 2007.

[7] International Electrotechnical Commission (IEC): International Standard 61089, Round wire concentric lay overhead electrical stranded conductors. 1991.

[8] International Electrotechnical Commission (IEC): Technical Report (Type 3) 61597, Overhead electrical conductors – calculation methods for stranded bare conductors. 1995.

[9] O. Anaya-Lara, E. Acha: Modeling and analysis of custom power systems by PSCAD/EMTDC. IEEE Transactions on Power Delivery, vol. 17, no. 1, 2002.

[10] R. Peña, J. C. Clare, G. M. Asher: Doubly fed induction generator using back-to-back PWM converters and its application to variable-speed wind-energy generation. IEE Proceedings Electric Power Applications, vol. 143, no. 3, 1996.

[11] USA Federal Energy Regulatory Commission: Interconnection for wind energy. Docket No. RM05-4-000.

[12] L. Heinhold, R. Stubbe: Power cables and their applications: part 2. Wiley-VCH, 1993.

[13] CIGRE TF C6.04.01: Connection criteria at the distribution network for distributed generation. Technical Brochure, ref. 313, 2007.

[14] International Electrotechnical Commission (IEC): International Standard 60364-1, Low-voltage electrical installations. 2005.

[15] B. Lacroix, R. Calvas: Earthing systems in LV. Cahier Technique No. 172, Schneider Electric, 2000.

[16] T. A. Short: Electric power distribution handbook. CRC Press, 2004.

[17] Sixth Framework Project of the European Union: MICROGRIDS. Contract no. ENK5-CT-2002-00610, website: http://www.microgrids.eu/, 2003.

[18] N. Mohan, T. M. Undeland, W. Robbins: Power electronics: converters, applications, and design. Wiley-VCH, 2002.

[19] S. Barsali, G. Celli, M. Ceraolo, R. Giglioli, P. Pelacchi, F. Pilo: Operating and planning issues of distribution grids containing diffuse generation. CIRED 16th International Conference and Exhibition on Electricity Distribution, Amsterdam, 2001.

[20] S. Barsali, M. Ceraolo, P. Pelacchi, D. Poli: Control techniques of dispersed generators to improve the continuity of electricity supply. IEEE PES Winter Meeting, New York, 2002.

[21] M. C. Chandorkar, D. M. Divan, R. Adapa: Control of parallel connected inverters in standalone ac supply systems. IEEE Transactions on Industry Applications, vol. 29, no. 1, 1993.

[22] M. C. Chandorkar, D. M. Divan, B. Banerjee: Control of distributed UPS systems. IEEE Power Electronics Specialists Conference, Taipei, 1994.

[23] A. Tuladhar, H. Jin, T. Unger, K. Mauch: Parallel operation of single phase inverter modules with no control interconnections. IEEE Applied Power Electronics Conference and Exposition, Atlanta, 1997.

[24] F. Katiraei, M. R. Iravani, P. W. Lehn: Micro-grid autonomous operation during and subsequent to islanding process. IEEE Transactions on Power Delivery, vol. 20, no. 1, 2005.

[25] F. Katiraei, M. R. Iravani: Power management strategies for a microgrid with multiple distributed generation units. IEEE Transactions on Power Systems, vol. 21, no. 4, 2006.

[26] A. L. Dimeas, N. D. Hatziargyriou: Operation of a multiagent system for microgrid control. IEEE Transactions on Power Systems, vol. 20, no. 3, 2005.

[27] Y. Li, D. Mahinda Vilathgamuwa, P. C. Loh: Design, analysis, and real-time testing of a controller for multibus microgrid system. IEEE Transactions on Power Electronics, vol. 19, no. 5, 2004.

[28] C. Abbey, G. Joos: Supercapacitor energy storage for wind energy applications. IEEE Transactions on Industry Applications, vol. 43, no. 3, 2007.

[29] T. Kinjo, T. Senjyu, N. Urasaki, H. Fujita: Output levelling of renewable energy by electric double-layer capacitor applied for energy storage system. IEEE Transactions on Energy Conversion, vol. 21, no. 1, 2006.

[30] L. Ran, J. R. Bumby, P. J. Tavner: Use of turbine inertia for power smoothing of wind turbines with a DFIG. 11th IEEE International Conference on Harmonics and Quality of Power, Lake Placid, 2004.

[31] Risø National Laboratory for Sustainable Energy, Technical University of Denmark: Database on wind characteristics. Website: http://www.winddata.com/, 2006.

[32] H.V. Nguyen, J. J. Burke, S. Benchluch: Rural distribution system design comparison. IEEE PES Winter Meeting, Las Vegas, 2000.

[33] J. Carr, L. V. McCall: Divergent evolution and resulting characteristics among the world's distribution systems. IEEE Transactions on Power Delivery, vol. 7, no. 3, 1992.

[34] W. Kersting: Distribution system modeling and analysis. CRC Press, 2007.

[35] R. H. Fletcher, K. Strunz: Optimal distribution system horizon planning–Part I: Formulation. IEEE Transactions on Power Systems, vol. 22, no. 2, 2007.